CONTACT MECHANICS OF A GRADED SURFACE WITH ELASTIC GRADATION IN LATERAL DIRECTION

A THESIS SUBMITTED TO
THE GRADUATE SCHOOL OF NATURAL AND APPLIED SCIENCES
OF
THE MIDDLE EAST TECHNICAL UNIVERSITY

BY

A. CİHAN ÖZATAĞ

IN PARTIAL FULFILLMENT OF THE REQUIREMENTS FOR THE DEGREE OF
MASTER OF SCIENCE
IN
THE DEPARTMENT OF MECHANICAL ENGINEERING

AUGUST 2003

Approval of the Graduate School of Natural and Applied Sciences

_____

Prof. Dr. Canan ÖZGEN

Director

I certify that this thesis satisfies all the requirements as a thesis for the degree of Master of Science.

_____

Prof. Dr. S.Kemal İDER

Head of Department

This is to certify that we have read this thesis and that in our opinion it is fully adequate, in scope and quality, as a thesis for the degree of Master of Science.

_____

Asst. Prof. Dr. Serkan DAĞ

Supervisor

Examining Committee Members

Prof. Dr. Bülent DOYUM _____

Assoc. Prof. Dr. Müfit GÜLGEÇ _____

Assoc. Prof. Dr. Suat KADIOĞLU _____

Asst. Prof. Dr. Serkan DAĞ _____

Asst. Prof. Dr. Bora YILDIRIM _____

ABSTRACT

CONTACT MECHANICS OF A GRADED SURFACE WITH ELASTIC GRADATION IN LATERAL DIRECTION

Özatağ, A.Cihan

M.S., Department of Mechanical Engineering

Supervisor: Asst. Prof. Dr. Serkan Dağ

August 2003, 109 pages

Today, nonhomogeneous materials are used in many technological applications. Nonhomogeneity can be introduced intentionally in order to improve the thermomechanical performance of material systems. The concept of functionally graded materials (FGMs) is an example of such an application. Nonhomogeneity can also be an intrinsic property of some of the natural materials such as natural soil. The main interest in this study is on the contact mechanics of nonhomogeneous surfaces. There is an extensive volume of literature on the contact mechanics of nonhomogeneous materials. In most of these studies, the elastic gradation is assumed to exist in depth direction. But, it is known that elastic gradation may also exist laterally. This may either occur naturally as in the case of natural soil or may be induced as a result of the applied processing technique as in the case of FGMs. The main objective in this study is therefore to examine the effect of the lateral nonhomogeneities on the contact stress distribution at the surface of an elastically graded material. In the model developed to examine this problem, a laterally graded surface is assumed to be in sliding contact with a rigid stamp of arbitrary profile. The problem is formulated using the theory of elasticity and reduced to a singular integral equation. The integral equation is solved numerically using a collocation

approach. By carrying out parametric studies, the effects of the nonhomogeneity constants, coefficient of friction and stamp location on the contact stress distribution and on the required contact forces are studied.

Keywords: Contact mechanics, Sliding Contact, Laterally Nonhomogeneous Medium, Functionally Graded Materials, Singular Integral Equations.

ÖZ

YANAL YÖNDE ELASTİK DERECELENMİŞ BİR YÜZEYİN TEMAS MEKANİĞİ

Özatağ, A. Cihan
Yüksek Lisans, Makina Mühendisliği Bölümü
Tez Yöneticisi: Y. Doç. Dr. Serkan Dağ

Ağustos 2003, 109 sayfa

Günümüzde, homojen olmayan malzemeler, pek çok teknolojik uygulamada kullanılmaktadır.Homojen olmama özelliği, malzemelerin termomekanik performanslarını geliştirmek amacıyla bilinçli olarak sonradan kazandırılabilir. Fonksiyonel olarak derecelenmiş malzemeler bu tür bir uygulamanın örneğidir. Homojen olmama özelliği, toprak gibi bazı doğal malzemelerin esas özelliği olabilmektedir. Bu çalışmanın esas ilgi alanı, homojen olmayan yüzeylerin kontak mekaniği üzerinedir. Literatürde, homojen olmayan yüzeylerin temas mekaniği üzerine birçok çalışma vardır. Bu çalışmaların çoğunda elastik derecelenmenin derinlik yönünde olduğu varsayılmıştır. Fakat, elastik derecelenme yanal yönde varolabilir. Bu özellik toprakta olduğu gibi doğal olarak ya da fonksiyonel olarak derecelendirilmiş malzemelerde olduğu gibi sonradan kazandırılabilir. Bu yüzden, bu çalışmadaki ana hedef, yanal yöndeki homojen olmama özelliklerinin elastik olarak derecelenmiş malzemelerin yüzeyindeki temas gerilmesi dağılımı üzerindeki etkisini incelemektir. Bu problemi incelemek için geliştirilen modelde, yanal yönde derecelenmiş bir yüzeyin rijit bir zımba ile kayma temasında olduğu varsayılmıştır. Problem, elastisite teorisi kullanılarak formüle edilmiş ve tekil bir integral denklemine indirgenmiştir. İntegral denklemi sayısal olarak çözülmüş ve parametrik

çalışmalar yürütülerek, homojen olmama sabitlerinin, sürtünme katsayısının ve zımba konumunun temas gerilmesi dağılımı ve gerekli temas kuvvetleri üzerindeki etkileri incelenmiştir

Anahtar kelimeler: Temas mekaniği, Kaymalı Temas, Yanal Yönde Homojen Olmayan Ortam, Fonksiyonel Olarak Derecelenmiş Malzemeler, Tekil İntegral Denklemleri.

To my Parents

ACKNOWLEDGEMENTS

I would like to express my sincere appreciation to my thesis supervisor Asst.Prof. Dr. Serkan DAĞ for his continuous supervision, guidance throughout my study, sharing his experience and giving me the chance of meeting contact mechanics. And also, i would like to thank Asst. Prof. Dr. Bora YILDIRIM for providing FEA results.

And lastly, I would like to thank to my family, my best friends and my colleagues for supporting me.

TABLE OF CONTENTS

LIST OF TABLES

TABLE

LIST OF FIGURES

FIGURE

LIST OF SYMBOLS

μ	: Shear modulus
γ	: Nonhomogeneity parameter
ν	: Poisson's ratio
κ	: (3-4ν) for plane strain, (3-ν)/(1+ν) for plane stress
P	: Normal force
η	: Coefficient of friction
a,b	: End points of the contact area
u,v	: Displacement components in x- and y- directions
σ_{ij}	: Stres components (i,j = x,y)
s_i	: Roots of the chracteristic equations (j = 1,2,3,4)
ρ	: Fourier Transform variable
A_{1i}	: Integration cut-off points (i = 1,2,3,4)
γ^*, γ^{**}	: Normalized nonhomonegeity parameters
$P_n^{(\beta 1,\beta 2)}$	: Jacobi polynomials
β_1, β_2	: Strengths of the singularity
N	: Number of terms retalned in the series expansion
m	: Slope of the triangular stamp
R	: Radius of the circular stamp
δ	: Rigid body displacement for the circular stamp
c	: Location of the centerline for the circular stamp

CHAPTER I

INTRODUCTION

Contact mechanics of nonhomogeneous elastic materials has been studied by many researchers in the past. Selvadurai and Lan [1] classifies the contact mechanics problem of nonhomogeneous materials as a nonclassical problem in the theory of elasticity. Largely because of the applications in soil mechanics, there is an extensive literature on the contact mechanics problems for nonhomogeneous elastic half space. In these problems, the elastic constants are assumed to be functions of the spatial variables. Recently, there has been a renewed intereset on the contact mechanics of nonhomogeneous elastic materials, this time within the context of functionally graded materials (FGMs). In most of the studies mentioned above, the elastic nonhomogeneity is assumed to exist in depth direction at the surface of the nonhomogeneous medium. But, it is well known that nonhomogeneities may exist in directions other than the depth direction in both soil mechanics applications and in materials which are processed using the FGM concept.

The main objective in this study is to develop a method to examine the contact mechanics problem for a nonhomogeneous elastic medium by assuming that there is a material nonhomogeneity in lateral direction instead of the depth or thickness direction. Main interest in this study is therefore on the effect of the lateral material nonhomogeneity on the contact stress distribution. In this section, we will first give a brief literature review of the contact mechanics problems in nonhomogeneous media. Then, the scope of this study will be described by giving the problem definition and the techniques used in the solution of the problem.

1.1.Previous Work on Contact Mechanics of Nonhomogeneous Media

Contact mechanics is one of the central problems of solid mechanics, since the load transfer between different components in an engineering structure can take place through a contact region. In most of the cases, the highest stresses occur in the contact area which may lead to the failure of a component through any of the mechanisms of wear, surface cracking, spallation or surface fatigue. The analysis of stress and displacement fields induced due to contact loading is the main field of study in contact mechanics. Generally, it is accepted that studies in contact mechanics originated with Hertz's work [2]. This work gives the solution of the frictionless contact problem of two elastic bodies of ellipsoidal profile. A brief review of the development of the field of contact mechanics since the work of Hertz and the state of art can be found in the review article of Barber and Ciavarella [3].

Because of the applications in soil mechanics, there was a great deal of interest in the contact mechanics of nonhomogeneous materials, especially in the 60's and the 70's. There are a number of articles which review the work that belong to that era. For a detailed literature review, the reader may refer to [4] or [5]. Early studies related to the contact mechanics of nonhomogeneous materials were aimed to provide Flamant's solution for these materials. Several studies investigating the stress and displacement fields within and on the bounding surface of a half – plane, which is subjected to point or distributed loads were published. These works were mainly motivated by the need to understand the settlement of structures founded on large mass of soil. It is known that the rigidity of natural soil increases with overburden pressure and such media were analyzed within the framework of linear elasticity. An elastic and incompressible half – plane with a linear variation in elastic modulus is considered in several studies. Gibson [6] and Calladine and Greenwood [7] solved this problem for line and point loads on the bounding surface of the half – plane. Awojobi and Gibson [8] presented results for an axisymmetric half – space. Gibson and Sills [9] considered a nonhomogeneous orthotropic elastic semi – infinite medium. Brown and Gibson [10] released the assumption of

incompressibility and Poisson's ratio was assumed to have a constant value between zero and one – half. In all the studies cited above, primary focus is on the settlement of foundations and elastic modulus varies linearly in depth direction.

Contact of nonhomogeneous surfaces with rigid stamps are also considered by many researchers within the context of soil mechanics. Kassir [11] considered the indentation of an elastic half – space by stamps with arbitrary profiles. Shear modulus is assumed to have a power – law type variation in the depth direction. Contact is assumed to be frictionless and normal stress distributions beneath the stamp are presented for various nonhomogeneity parameters. Bakırtaş [12] examined frictionless planar stamp problems. Elastic modulus is assumed to vary exponentially in depth direction. Contact stresses for flat ended and circular stamps are given for different values of the nonhomogeneity constants. In the stamp problems quoted above, Poisson's ratio is assumed to be constant. Fabrikant and Sankar [13] studied axisymmetric contact problems for a nonhomogeneous half – space whose elastic modulus is a power function of the depth coordinate. The contact region is assumed to be in the shape of a circle. Selvadurai and coworkers have a series of studies [1,5,14] dealing with axisymmetric stamp problems for a nonhomogeneous half – space with elastic nonhomogeneity in the depth direction.

Graded materials, also known as *functionally graded materials* (FGMs) are generally multi – phase composites with continuously varying thermomechanical properties. The important property of FGMs from mechanics point of view is their macroscopic nonhomogeneity. These material systems were originally proposed to be used as protective coatings in high temperature applications, e.g. as thermal barrier coatings in aircraft engines. An excellent up – to – date review of the FGM subject can be found in [15]. In recent years, functionally graded materials are also proposed to be used as coatings or bulk materials to enhance the resistance of structural components to tribological damage [15]. For example, graded coatings for the cutting edges of the cutting tools have been developed [16]. The coating material in these applications is most of the time ceramic and carbide or nitride content is varied from the substrate interface to the surface. The cutting behavior and wear resistance of the graded ceramic tools were observed to be better than the conventional ceramic ones. Suresh *et al*. [17] showed that gradients in elastic

modulus at a surface may enhance the resistance against cracking due to sliding contact. In their experiment, these researchers processed a functionally graded alumina–aluminosilicate glass FGM using the infiltration technique. Aluminosilicate glass penetrates into the grain boundaries of alumina at high temperatures. In the indentation and scratch tests using the processed FGM specimens, it was seen that controlled gradients in elastic modulus alone can lead to a marked increase in the resistance of a surface to frictional sliding contact. The findings of this study show that FGMs can be utilized as protective coatings against wear and specifically against frictional contact related cracking.

Due to the promising results obtained in these studies, recently a number of research papers are published on the contact mechanics of functionally graded materials. Indentation of a graded half – space by a point force is examined by Giannakopoulos and Suresh [18]. Again, in another study by the same authors [19], analytical and computational results are given for stress and displacement fields in a graded elastic half – space due to indentation from a rigid axisymmetric indentor. A review of the analytical, computational and experimental results on the spherical indentation of a graded elastic half space is given by Giannakopoulos [20]. Two dimensional sliding contact problems for an elastic graded half – plane is considered by Giannakopoulos and Pallot [21]. In this study, for the sake of mathematical expediency, the authors used a power – law variation for the elastic modulus. The drawback in this assumption is that, the elastic modulus becomes zero at the contact surface which is physically unrealistic. Two dimensional contact problems for elastic FGM coatings bonded to homogeneous substrates are examined by Güler [22]. In this study, a more realistic exponential variation in elastic modulus for the FGM coating is assumed. The sliding contact problems for rigid stamps, and for two contacting FGM coatings are reduced to singular integral equations which are solved using a collocation method. Extensive results are given on the influence of the material nonhomogeneity in thickness direction and friction on the contact stress distribution at the contacting surfaces.

An important failure mode related to contact loading is the fretting fatigue which is essentially the initiation and propagation of surface cracks due to oscillatory contact loading at the contact surfaces. The analysis of this problem requires the

examination of coupled crack and contact problems. For an elastically graded surface this problem is solved by Dağ [23]. Some of the details and extensive results related to this problem can also be found in the studies by Dağ and Erdoğan [24] and Erdoğan and Dağ [25].

1.2.Motivation and Scope of the Study

In all the studies mentioned above the elastic nonhomogeneity is assumed to exist in depth direction and Poisson's ratio is assumed to have a constant value. The confinement of the direction of the nonhomogeneity to the depth direction is most of the time a consequence of mathematical tractability. Actually, in soil mechanics it is a well known fact that the earth surface may also have nonhomogeneities in lateral direction. The effect of lateral nonhomogeneity seemed to be taken into account in some studies on seismic wave propagation [26,27]. Contact mechanics analyses of a surface that has lateral nonhomogeneities are very few in the literature. In one study, Singh *et al.* [28] examined the distribution of stresses induced in a semi – infinite solid when a rigid punch penetrates its plane boundary. The shear modulus is assumed to be a function of the spatial coordinates in perpendicular and lateral directions. But, no numerical parametric analyses are given on the effect of material nonhomogeneities on the stress distribution. As mentioned in the previous section, Suresh *et al.* [17] processed an alumina – aluminosilicate glass FGM surface using the infiltration technique. At high temperatures, (about 1700 ^{0}C) aluminosilicate glass penetrates into the grain boundaries of alumina and a graded ceramic FGM can be obtained. The indentation and scratch tests and theoretical analyses show that this graded surface is perfectly suitable for applications that require wear and cracking resistance. But, in addition to the thickness direction, the processed material contains nonhomogeneities in lateral direction which is not taken into account in the analytical and computational analyses.The main objective in this study is to develop a technique to study the effect of the lateral nonhomogeneities on the contact stress distribution for a graded surface. Depending on the nature of the effect of the lateral nonhomogeneity, the

processing of an FGM surface with elastic gradation in lateral direction can also be suggested. In order to study the effect of the material nonhomogeneity, a contact mechanics model as shown in Figure 1 is considered. As can be seen in the Figure, the forces transferred by the contact are P and ηP, where η is the coefficient of friction. An FGM half – plane is in sliding contact with a rigid circular indentor. We assume that Coulomb's friction model applies to our case, and tangential force transferred by the contact is sufficiently large and is equal to friction coefficient multiplied by the normal force *P*. In this model, shear modulus is assumed to vary exponentially in lateral direction. The graded surface is assumed to be isotropic, hence shear modulus variation is mathematically expressed as, $\mu(y) = \mu_0 \exp(\gamma y)$. This type of exponential variation is used in most of the analytical and computational studies related to the fracture and contact mechanics of FGMs [23]. In this equation μ_0 is the shear modulus at $y = 0$ and γ is a nonhomogeneity constant which has a unit of 1/length and which can be used for curve – fit purposes. Partial differential equations resulting from this type of variation in shear modulus proved to be tractable [23-25]. Poisson's ratio, on the other hand is assumed to have a constant value. This is another assumption whose validity is verified by almost all the studies in the literature. The main unknown in this problem is the contact stress distribution at the contact surface between $y = a$ and $y = b$. The material is assumed to be under a condition of plane stress or plane strain.

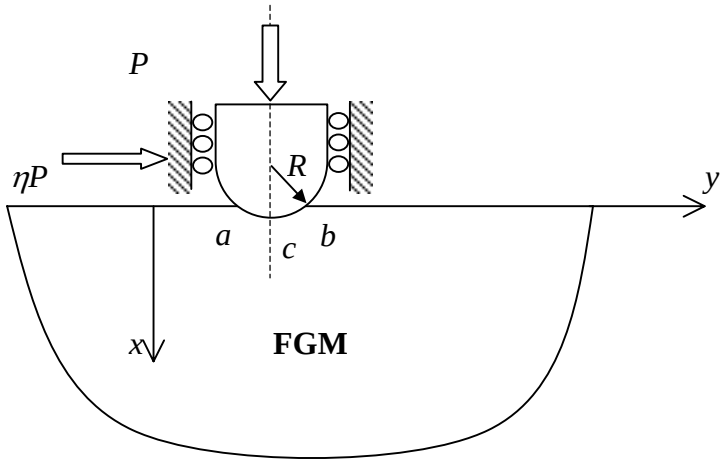

Figure 1: Contact mechanics model for a laterally nonhomogeneous FGM surface

This problem can be categorized as a mixed boundary value problem in mechanics. A convenient technique of solution of these types of problems is to formulate them using singular integral equations. The integral equations can be solved using the properties of orthogonal polynomials. The theory of singular integral equations applied to the mixed boundary value problems in mechanics is laid down by Erdoğan [29]. The solution technique developed in this study is mainly based upon the methods in given in [29]. Also, we note that the solution methods developed in this study can be used for any type of stamp profile. The stamp profile that can be considered is not necessarily confined to a circular shape as shown in Figure 1.

In Chapter 2, the sliding contact problem for the laterally nonhomogeneous medium is formulated using Fourier Transformations and the problem is reduced to a singular integral equation. Normal contact stress is used as the unknown function in the formulation of the problem. In Chapter 3, the singular behavior of the unknown function at the end points of its domain of definition is taken into account and bounded part of the function is expanded into a series of Jacobi polynomials. The problem is then solved numerically using a collocation technique. A computer program is developed using Visual Fortran 90 language to implement the developed numerical solution technique. In the numerical solution, flat – ended, triangular and circular stamp profiles are considered. Numerical results are presented in Chapter 4. Some of the numerical results obtained in this study are compared to the results obtained by a finite element model of the same problem which are provided by Yıldırım [30]. A good agreement is observed between the results computed using the semi – analytical technique developed in this study and the results obtained using the finite element model. The discussion of the results and the suggestions for future work are given in Chapter 5.

CHAPTER II

FORMULATION

The contact problem for a non-homogeneous half-plane considered in this study is described in Figure 2. The half plane is in sliding contact with a rigid stamp of arbitrary profile. The normal and tangential forces transferred by the contact are P and ηP, respectively where η is the coefficient of friction and contact area extends from $y=a$ to $y=b$.

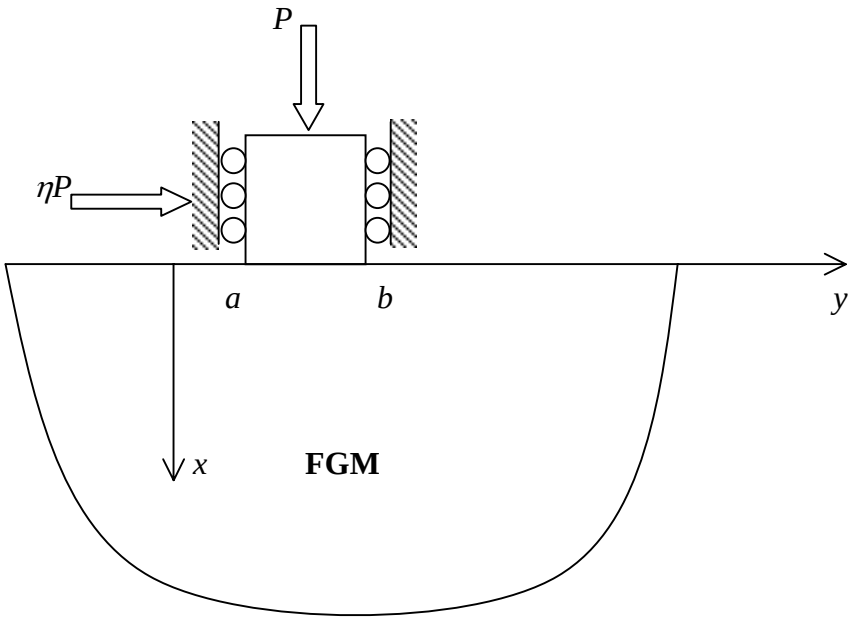

Figure 2: The general description of the contact problem in a graded medium.

In this study, we will formulate the problem and reduce it to a singular integral equation. Solving the integral equation numerically, we will examine the effects of

material non-homogeneity and friction on contact stresses and singularities at the ends of the contact region. It will be assumed that the elastic parameters of the graded medium may be approximated by;

$$\mu(y) = \mu_0 e^{\gamma y} \quad , \qquad \kappa = \text{constant} \tag{1a,b}$$

where μ is the shear modulus , γ is the non-homogeneity parameter, κ =3-4ν for plane strain and κ = (3-ν) / (1+ν) for generalized plane stress, ν being the Poisson's ratio. Equations of equilibrium can be written in the following form:

$$\frac{\partial \sigma_{yy}}{\partial y} + \frac{\partial \sigma_{xy}}{\partial x} = 0 \tag{2a}$$

$$\frac{\partial \sigma_{xx}}{\partial x} + \frac{\partial \sigma_{xy}}{\partial y} = 0 \tag{2b}$$

Assuming plane stress or plane strain and small deformations for the isotropic linear elastic medium considered, Hooke's law becomes:

$$\sigma_{xx}(x,y) = \frac{\mu(y)}{\kappa - 1}\left((\kappa + 1)\frac{\partial u}{\partial x} + (3 - \kappa)\frac{\partial v}{\partial y} \right) \tag{3a}$$

$$\sigma_{yy}(x,y) = \frac{\mu(y)}{\kappa - 1}\left((\kappa + 1)\frac{\partial v}{\partial y} + (3 - \kappa)\frac{\partial u}{\partial x} \right) \tag{3b}$$

$$\sigma_{xy}(x,y) = \mu(y)\left(\frac{\partial u}{\partial y} + \frac{\partial v}{\partial x} \right) \tag{3c}$$

Substituting equations (3) in (2); governing equations for the displacements can be obtained as follows,

$$(\kappa + 1)\frac{\partial^2 u}{\partial x^2} + (\kappa - 1)\frac{\partial^2 u}{\partial y^2} + 2\frac{\partial^2 v}{\partial x \partial y} + \gamma(\kappa - 1)\frac{\partial u}{\partial y} + \gamma(\kappa - 1)\frac{\partial v}{\partial x} = 0 \tag{4a}$$

$$(\kappa + 1)\frac{\partial^2 v}{\partial y^2} + (\kappa - 1)\frac{\partial^2 v}{\partial x^2} + 2\frac{\partial^2 u}{\partial x \partial y} + \gamma(\kappa + 1)\frac{\partial v}{\partial y} + \gamma(3 - \kappa)\frac{\partial u}{\partial x} = 0 \tag{4b}$$

In the previous studies [23], it was shown that the contact stresses in graded materials are not significantly influenced by the variation in ν. Therefore in this study the Poisson's ratio will be assumed to be constant. Considering Figure 2, the following boundary conditions must be satisfied in the solution of the problem.

$$\sigma_{xx}(0,y)=0\ , \qquad \sigma_{xy}(0,y)=0 \quad , \quad -\infty<y<a\ , \quad b<y<\infty \tag{5a,b}$$

$$\sigma_{xy}(0,y)=\eta f(y)\,, \qquad \sigma_{xx}(0,y)=f(y) \qquad , \quad a<y<b \tag{6a,b}$$

$$\int_a^b \sigma_{xx}(0,y)=-P \qquad (\text{ equilibrium equation }) \tag{7}$$

where η is the coefficient of friction for sliding contact. Considering Fourier Transformation in y-direction, u and v can be represented in the following form,

$$u(x,y)=\frac{1}{2\pi}\int_{-\infty}^{\infty}U(x,\rho)\exp(i\rho y)d\rho \tag{8a}$$

$$v(x,y)=\frac{1}{2\pi}\int_{-\infty}^{\infty}V(x,\rho)\exp(i\rho y)d\rho \tag{8b}$$

where $i=\sqrt{-1}$ and $U(x,\rho)$ and $V(x,\rho)$ are Fourier transforms of $u(x,y)$ and $v(x,y)$ in y, respectively. Substituting 8a, 8b in 4a, 4b, following ordinary differential equations are obtained,

$$(\kappa+1)\frac{d^2U}{dx^2}+(\kappa-1)(-\rho^2)U+2i\rho\frac{dV}{dx}+\gamma(\kappa-1)(i\rho)U+\gamma(\kappa-1)\frac{dV}{dx}=0 \tag{9a}$$

$$(\kappa+1)(-\rho^2)V+(\kappa-1)\frac{d^2V}{dx^2}+2i\rho\frac{dU}{dx}+\gamma(\kappa+1)(i\rho)V+\gamma(3-\kappa)\frac{dU}{dx}=0 \tag{9b}$$

Assuming a solution of the form $\exp(sx)$, we obtain the characteristic equation,

$$\left[s^2-\rho(\rho+i\gamma)\right]^2-\left[\gamma^2\left(\frac{3-\kappa}{\kappa+1}\right)\right]s^2=0 \tag{10}$$

The roots of the characteristic equation are,

$$s_1 = -\frac{1}{2}\gamma\sqrt{\frac{3-\kappa}{\kappa+1}} - \frac{1}{2}\sqrt{4\rho^2 + 4i\gamma\rho + \gamma^2\left(\frac{3-\kappa}{\kappa+1}\right)} \qquad \mathrm{Re}\{s_1\}<0 \qquad (11a)$$

$$s_2 = \frac{1}{2}\gamma\sqrt{\frac{3-\kappa}{\kappa+1}} - \frac{1}{2}\sqrt{4\rho^2 + 4i\gamma\rho + \gamma^2\left(\frac{3-\kappa}{\kappa+1}\right)} \qquad \mathrm{Re}\{s_2\}<0 \qquad (11b)$$

$$s_3 = -\frac{1}{2}\gamma\sqrt{\frac{3-\kappa}{\kappa+1}} + \frac{1}{2}\sqrt{4\rho^2 + 4i\gamma\rho + \gamma^2\left(\frac{3-\kappa}{\kappa+1}\right)} \qquad \mathrm{Re}\{s_3\}>0 \qquad (11c)$$

$$s_4 = \frac{1}{2}\gamma\sqrt{\frac{3-\kappa}{\kappa+1}} + \frac{1}{2}\sqrt{4\rho^2 + 4i\gamma\rho + \gamma^2\left(\frac{3-\kappa}{\kappa+1}\right)} \qquad \mathrm{Re}\{s_4\}>0 \qquad (11d)$$

After solving the equations (9a,b), the displacement components *u* and *v* can be written as:

$$u(x.y) = \frac{1}{2\pi}\int_{-\infty}^{\infty}\sum_{j=1}^{2} M_j \exp(s_j x + i\rho y)d\rho \qquad (12a)$$

$$v(x.y) = \frac{1}{2\pi}\int_{-\infty}^{\infty}\sum_{j=1}^{2} M_j N_j \exp(s_j x + i\rho y)d\rho \qquad (12b)$$

where M_j are unknown functions of ρ and,

$$N_j(\rho) = \frac{-\left[(\kappa+1)s^2{}_j + \gamma(\kappa-1)i\rho + \rho^2(1-\kappa)\right]}{2i\rho.s_j + \gamma(\kappa-1)s_j} \qquad (13)$$

Note that only the roots whose real parts are less than zero are used in the solution. Using Hooke's Law, stresses and the displacement derivative can be written as follows;

$$\sigma_{xx}(x.y) = \frac{\mu(y)}{(\kappa-1)}\frac{1}{2\pi}\int_{-\infty}^{\infty}\sum_{j=1}^{2}\left[(\kappa+1)s_j + (3-\kappa)i\rho N_j\right]M_j \exp(s_j x + i\rho y)d\rho \qquad (14a)$$

$$\sigma_{yy}(x.y)=\frac{\mu(y)}{(\kappa-1)}\frac{1}{2\pi}\int_{-\infty}^{\infty}\sum_{j=1}^{2}\left[(3-\kappa)s_j+(\kappa+1)i\rho N_j\right]M_j\exp(s_jx+i\rho y)d\rho \quad (14b)$$

$$\sigma_{xy}(x.y)=\mu(y)\frac{1}{2\pi}\int_{-\infty}^{\infty}\sum_{j=1}^{2}(i\rho+N_js_j)M_j\exp(s_jx+i\rho y)d\rho \quad (14c)$$

$$\frac{\partial u}{\partial y}(x,y)=\frac{1}{2\pi}\int_{-\infty}^{\infty}i\rho\sum_{j=1}^{2}M_j\exp(s_jx+i\rho y)d\rho \quad (14d)$$

Using the boundary conditions given by equations (5),(6) and (14), we can write;

$$\frac{\mu(y)}{(\kappa-1)}\frac{1}{2\pi}\int_{-\infty}^{\infty}\sum_{j=1}^{2}\left[(\kappa+1)s_j+(3-\kappa)i\rho N_j\right]M_j\exp(i\rho y)d\rho=$$

$$=\begin{cases}f(y) & a<y<b\\ 0 & -\infty<y<a,b<y<\infty\end{cases} \quad (15a)$$

$$\mu(y)\frac{1}{2\pi}\int_{-\infty}^{\infty}\sum_{j=1}^{2}(i\rho+N_js_j)M_j\exp(i\rho y)d\rho=$$

$$=\begin{cases}\eta f(y) & a<y<b\\ 0 & -\infty<y<a,b<y<\infty\end{cases} \quad (15b)$$

After taking Fourier Transforms of both sides, we obtain the following equation system to determine the unknown constants,

$$\sum_{j=1}^{2}\left(s_j(\kappa+1)+i\rho(3-\kappa)\right)M_j=\int_a^b\frac{\kappa-1}{\mu(t)}f(t)\exp(-i\rho t)dt \quad (16)$$

$$\sum_{j=1}^{2}\left(i\rho+N_js_j\right)M_j=\int_a^b\frac{1}{\mu(t)}\eta f(t)\exp(-i\rho t)dt \quad (17)$$

So, $M_j(\rho)$, $(j=1,2)$ can be expressed as,

$$M_j(\rho)=\frac{1}{\mu_0}\left[\phi_j(\rho)\int_a^b f(t)\exp(-t(i\rho+\gamma))dt+\varphi_j(\rho)\int_a^b\eta f(t)\exp(-t(i\rho+\gamma))dt\right] \quad (18)$$

Here, the functions $\phi_j(\rho)$ and $\varphi_j(\rho)$, $(j=1,2)$ can be easily determined using a symbolic manipulator. Stresses and displacement derivative for the stamp loading can now be obtained using equations (14), (16) and (18).Substituting (18) in (14d), normal displacement derivative can be written as:

$$\frac{\partial u}{\partial y}=\frac{1}{\mu_0}\left\{\int_a^b \exp(-\gamma t)\,f(t)dt\,\frac{1}{2\pi}\int_{-\infty}^{\infty}(i\rho\sum_{j=1}^{2}\phi_j\exp(s_j x))\exp(i\rho(y-t))d\rho\right.$$

$$\left.+\int_a^b \exp(-\gamma t)\eta f(t)dt\,\frac{1}{2\pi}\int_{-\infty}^{\infty}(i\rho\sum_{j=1}^{2}\varphi_j\exp(s_j x))\exp(i\rho(y-t))d\rho\right\} \qquad (19)$$

Now, we define two functions $H_{11}(\rho,x)$ and $H_{12}(\rho,x)$ as:

$$H_{11}(\rho,x)=i\rho\sum_{j=1}^{2}\phi_j\exp(s_j x) \qquad (20a)$$

$$H_{12}(\rho,x)=i\rho\sum_{j=1}^{2}\varphi_j\exp(s_j x) \qquad (20b)$$

So, *du/dy* becomes;

$$\frac{du}{dy}=\frac{1}{\mu_0}\left\{\int_a^b \exp(-\gamma t)\,f(t)dt\,\frac{1}{2\pi}\int_{-\infty}^{\infty}H_{11}\exp(i\rho(y-t))d\rho\right.$$

$$\left.+\int_a^b \exp(-\gamma t)\eta f(t)dt\,\frac{1}{2\pi}\int_{-\infty}^{\infty}H_{12}\exp(i\rho(y-t))d\rho\right\} \qquad (21)$$

In the numerical solution, it will be easier to deal with (0,∞) integrals instead of the (-∞,∞) integrals. Here, we convert the (-∞,∞) integrals to (0, ∞) integrals as follows:

$$\int_{-\infty}^{\infty}H_{11}(\rho,x)\exp(i\rho(y-t))d\rho=\int_0^{\infty}\left[H_{11}(-\rho.x)+H_{11}(\rho,x)\right]\cos(\rho(y-t))d\rho$$

$$+\int_0^{\infty}i\left[H_{11}(\rho.x)-H_{11}(-\rho,x)\right]\sin(\rho(y-t))d\rho \qquad (22a)$$

$$\int_{-\infty}^{\infty} H_{12}(\rho,x)\exp(i\rho(y-t))d\rho = \int_{0}^{\infty}\left[H_{12}(-\rho.x)+H_{12}(\rho,x)\right]\cos(\rho(y-t))d\rho$$

$$+\int_{0}^{\infty} i\left[H_{12}(\rho.x)-H_{12}(-\rho,x)\right]\sin(\rho(y-t))d\rho \tag{22b}$$

We rename some of the terms in these equations as;

$$K_{11}(\rho.x) = H_{11}(-\rho.x)+H_{11}(\rho,x) \tag{23a}$$

$$K_{12}(\rho.x) = i\left[H_{11}(\rho.x)-H_{11}(-\rho,x)\right] \tag{23b}$$

$$K_{13}(\rho.x) = H_{12}(-\rho.x)+H_{12}(\rho,x) \tag{23c}$$

$$K_{14}(\rho.x) = i\left[H_{12}(\rho.x)-H_{12}(-\rho,x)\right] \tag{23d}$$

Therefore, *du/dy* takes the following form;

$$\frac{\partial u}{\partial y} = \frac{1}{\mu_0}\left\{\int_a^b \exp(-\gamma t)\,f(t)dt\,\frac{1}{2\pi}\left[\int_0^{\infty} K_{11}(\rho,x)\cos(\rho(y-t)d\rho\right]\right.$$

$$+\int_a^b \exp(-\gamma t)\,f(t)dt\,\frac{1}{2\pi}\left[\int_0^{\infty} K_{12}(\rho,x)\sin(\rho(y-t)d\rho\right]$$

$$+\int_a^b \exp(-\gamma t)\eta f(t)dt\,\frac{1}{2\pi}\left[\int_0^{\infty} K_{13}(\rho,x)\cos(\rho(y-t)d\rho\right]$$

$$\left.+\int_a^b \exp(-\gamma t)\eta f(t)dt\,\frac{1}{2\pi}\left[\int_0^{\infty} K_{14}(\rho,x)\sin(\rho(y-t)d\rho\right]\right\} \tag{24}$$

It is well known that [23] in order to extract the singular terms, asymptotic analyses of the functions K_{11}, K_{12}, K_{13} and K_{14} are required as $\rho \to \infty$. By using the symbolic manipulator MAPLE it can be shown that,

$$s_1,\ s_2 = -\rho \text{ as } \rho \to \infty \tag{25a}$$

Using this result, asymptotic expressions for the mentioned functions can be written as,

$$K_{11}^{\infty}(\rho,x)=i\rho\left(\phi_1(\rho)+\phi_2(\rho)-\phi_1(-\rho)-\phi_2(-\rho)\right)\exp(-\rho x) \tag{25b}$$

$$K_{12}^{\infty}(\rho,x)=-\rho\left(\phi_1(\rho)+\phi_2(\rho)+\phi_1(-\rho)+\phi_2(-\rho)\right)\exp(-\rho x) \tag{25c}$$

$$K_{13}^{\infty}(\rho,x)=i\rho\left(\varphi_1(\rho)+\varphi_2(\rho)-\varphi_1(-\rho)-\varphi_2(-\rho)\right)\exp(-\rho x) \tag{25d}$$

$$K_{14}^{\infty}(\rho,x)=-\rho\left(\varphi_1(\rho)+\varphi_2(\rho)+\varphi_1(-\rho)+\varphi_2(-\rho)\right)\exp(-\rho x) \tag{25e}$$

Now, in order to complete the asymptotic analyses the terms preceding the exponential term can be expanded into Taylor series as $\rho\to\infty$. Using MAPLE, following results are obtained for the asymptotic expansions,

$$K_{11}^{\infty}=\left\{a_1+\frac{a_2}{\rho}+\frac{a_3}{\rho^2}+\frac{a_4}{\rho^3}+\ldots+\frac{a_8}{\rho^7}\right\}\exp(-\rho x) \tag{26}$$

where;

$$a_1=a_3=a_5=a_7=0 \tag{27a}$$

$$a_2=-\frac{\gamma(-5-3\kappa+2\kappa^2)}{4} \tag{27b}$$

$$a_4=\frac{\gamma^3(\kappa^4-5\kappa^3+9\kappa^2-3\kappa-13)}{8} \tag{27c}$$

$$a_6=-\frac{\gamma^5(\kappa^7-6\kappa^6+13\kappa^5-12\kappa^4+\kappa^3+30\kappa^2-60\kappa-54)}{32(\kappa+1)} \tag{27d}$$

$$a_8=\left(\frac{\gamma^7(\kappa^{10}-7\kappa^9+18\kappa^8-18\kappa^7-6\kappa^6+30\kappa^5)}{128(\kappa+1)^2}\right.$$

$$\left.+\frac{\gamma^7\left(-26\kappa^4+98\kappa^3-114\kappa^2-451\kappa-216\right)}{128(\kappa+1)^2}\right) \tag{27e}$$

$$K_{12}^{\infty}=\left\{b_1+\frac{b_2}{\rho}+\frac{b_3}{\rho^2}+\frac{b_4}{\rho^3}+\ldots+\frac{b_8}{\rho^7}\right\}\exp(-\rho x) \tag{28}$$

where;

$$b_2 = b_4 = b_6 = b_8 = 0 \tag{29a}$$

$$b_1 = \frac{\kappa + 1}{2} \tag{29b}$$

$$b_3 = -\frac{\gamma^2(\kappa^3 - 4\kappa^2 + 2\kappa + 6)}{4} \tag{29c}$$

$$b_5 = \frac{\gamma^4(\kappa^6 - 5\kappa^5 + 8\kappa^4 - 4\kappa^3 - 15\kappa^2 + 30\kappa + 26)}{16(\kappa + 1)} \tag{29d}$$

$$b_7 = -\left(\frac{\gamma^6(\kappa^9 - 6\kappa^8 + 12\kappa^7 - 6\kappa^6 - 12\kappa^5)}{64(\kappa + 1)^2} + \frac{\gamma^6\left(18\kappa^4 - 56\kappa^3 + 53\kappa^2 + 221\kappa + 105\right)}{64\left(\kappa + 1\right)^2} \right) \tag{29e}$$

$$K_{13}^{\infty} = \left\{ c_1 + \frac{c_2}{\rho} + \frac{c_3}{\rho^2} + \frac{c_4}{\rho^3} + \ldots + \frac{c_8}{\rho^7} \right\} \exp(-\rho x) \tag{30}$$

where;

$$c_2 = c_4 = c_6 = c_8 = 0 \tag{31a}$$

$$c_1 = \frac{1 - \kappa}{2} \tag{31b}$$

$$c_3 = \frac{\gamma^2(\kappa^3 - 2\kappa^2 - 1)}{4} \tag{31c}$$

$$c_5 = -\frac{\gamma^4(\kappa^5 - 4\kappa^4 + 6\kappa^3 - 4\kappa^2 - 3\kappa - 4)}{16} \tag{31d}$$

$$c_7 = \frac{\gamma^6(\kappa^7 - 6\kappa^6 + 15\kappa^5 - 20\kappa^4 + 15\kappa^3 - 6\kappa^2 - 15\kappa - 16)}{64} \tag{31e}$$

$$K_{14}^{\infty} = \left\{ d_1 + \frac{d_2}{\rho} + \frac{d_3}{\rho^2} + \frac{d_4}{\rho^3} + \ldots + \frac{d_8}{\rho^7} \right\} \exp(-\rho x) \tag{32}$$

where;

$$d_1 = d_3 = d_5 = d_7 = 0 \tag{33a}$$

$$d_2 = -\frac{\gamma(-1 - 3\kappa + 2\kappa^2)}{4} \tag{33b}$$

$$d_4 = \frac{\gamma^3(\kappa^4 - 3\kappa^3 + 3\kappa^2 - 3\kappa - 2)}{8} \tag{33c}$$

$$d_6 = -\frac{\gamma^5(\kappa^6 - 5\kappa^5 + 10\kappa^4 - 10\kappa^3 + 5\kappa^2 - 9\kappa - 8)}{32} \tag{33d}$$

$$d_8 = \frac{\gamma^7(\kappa^8 - 7\kappa^7 + 21\kappa^6 - 35\kappa^5 + 35\kappa^4 - 21\kappa^3 + 7\kappa^2 - 33\kappa - 32)}{128} \tag{33e}$$

By subtracting and adding the first terms of the asymptotic expansions, we can determine the dominant singular terms,

$$\frac{\partial u}{\partial y} = \frac{1}{\mu_0}\left\{\int_a^b f(t)\exp(-\gamma t)dt \frac{1}{2\pi}\left[\int_0^\infty K_{11}(\rho, x)\cos(\rho(y-t)d\rho\right.\right.$$

$$\left. + \int_0^\infty (K_{12}(\rho, x) - b_1\exp(-\rho x))\sin(\rho(y-t))d\rho + \int_0^\infty b_1\exp(-\rho x)\sin\rho(y-t))d\rho\right]$$

$$+ \int_a^b \eta f(t)\exp(-\gamma t)dt \frac{1}{2\pi}\left[\int_0^\infty (K_{13}(\rho, x) - c_1\exp(-\rho x))\cos(\rho(y-t)d\rho\right.$$

$$\left.\left. + \int_0^\infty c_1\exp(-\rho x)\cos(\rho(y-t))d\rho + \int_0^\infty K_{14}(\rho, x)\sin(\rho(y-t))d\rho\right]\right\} \tag{34}$$

The integrals that occur after adding the leading terms can be evaluated in closed form using the equations given below,

$$\int_0^\infty \exp(-\rho x)\cos(\rho(y-t))d\rho = \frac{x}{x^2 + (y-t)^2} \tag{35a}$$

$$\int_0^\infty \exp(-\rho x)\sin(\rho(y-t))d\rho = \frac{y-t}{x^2 + (y-t)^2} \tag{35b}$$

Now, we make following definitions,

$$P_1(t) = f(t)\exp(-\gamma t) \tag{36}$$

$$Q_1(t) = \eta f(t)\exp(-\gamma t) \tag{37}$$

Substituting in (34), and taking the limit as $x \to 0$, we get:

$$\frac{\partial u(0,y)}{\partial y} = \frac{1}{2\pi\mu_0}\left\{\frac{\kappa+1}{2}\int_a^b \frac{P_1(t)}{(y-t)}dt + \int_a^b P_1(t)dt\left(\int_0^\infty K_{11}(\rho,0)\cos(\rho(y-t))d\rho\right.\right.$$

$$\left.+\int_0^\infty (K_{12}(\rho,0)-b_1)\sin(\rho(y-t))d\rho\right)$$

$$-\frac{\kappa-1}{2}\pi Q_1(y) + \int_a^b Q_1(t)dt\left(\int_0^\infty (K_{13}(\rho,0)-c_1)\cos(\rho(y-t)d\rho\right.$$

$$\left.\left.+\int_0^\infty K_{14}(\rho,0)\sin(\rho(y-t))d\rho\right)\right\} \qquad (38)$$

Multiplying both sides of equation (38) by $(4\mu_0 / \kappa+1)$,we obtain the standard form for the displacement derivative:

$$\left(\frac{4\mu_0}{\kappa+1}\right)\frac{\partial u(0,y)}{\partial y} = \frac{1}{\pi}\int_a^b \frac{P_1(t)}{(y-t)}dt - \left(\frac{\kappa-1}{\kappa+1}\right)Q_1(y)$$

$$+$$

$$\int_a^b P_1(t)dt\left(\frac{2}{\pi(\kappa+1)}\right)\left(\int_0^\infty K_{11}(\rho,0)\cos(\rho(y-t))d\rho + \int_0^\infty (K_{12}(\rho,0)-b_1)\sin(\rho(y-t))d\rho\right)$$

$$+\int_a^b Q_1(t)dt\left(\frac{2}{\pi(\kappa+1)}\right)\left(\int_0^\infty (K_{13}(\rho,0)-c_1)\cos(\rho(y-t))d\rho\right.$$

$$\left.+\int_0^\infty (K_{14}(\rho,0)\sin(\rho(y-t))d\rho\right) \qquad (39)$$

Note that, we have the Cauchy singularity and the free term in equation (39). Remaining terms exist because of the elastic gradation. Now, we rename some terms in equation (39) as,

$$\int_0^\infty K_{11}(\rho,0)\cos(\rho(y-t))d\rho = h_{11}(y,t) \qquad (40a)$$

$$\int_0^{\infty}(K_{12}(\rho,0)-b_1)\sin(\rho(y-t))d\rho = h_{12}(y,t) \tag{40b}$$

$$\int_0^{\infty}(K_{13}(\rho,0)-c_1)\cos(\rho(y-t))d\rho = h_{13}(y,t) \tag{40c}$$

$$\int_0^{\infty}(K_{14}(\rho,0)\sin(\rho(y-t))d\rho = h_{14}(y,t) \tag{40d}$$

In the computations, Gauss-Legendre quadrature and integration cut-off points are used to evaluate the functions $h_{11}(y,t)$, $h_{12}(y,t)$, $h_{13}(y,t)$ and $h_{14}(y,t)$. Using integration cut-off points these terms can be rearranged to give:

$$h_{11}(y,t) = \int_0^{A_{11}} K_{11}(\rho,0)\cos(\rho(y-t))d\rho + \int_{A_{11}}^{\infty}\left(K_{11}(\rho,0) - \frac{a_2}{\rho} - \ldots - \frac{a_8}{\rho^7}\right)\cos(\rho(y-t))d\rho$$

$$+ \int_{A_{11}}^{\infty}\left(\frac{a_2}{\rho} + \frac{a_3}{\rho^2} + \ldots + \frac{a_8}{\rho^7}\right)\cos(\rho(y-t))d\rho \tag{41a}$$

$$h_{12}(y,t) = \int_0^{A_{12}}(K_{12}(\rho,0)-b_1)\sin(\rho(y-t))d\rho +$$

$$\int_{A_{12}}^{\infty}\left(K_{12}(\rho,0) - b_1 - \frac{b_2}{\rho} - \ldots - \frac{b_8}{\rho^7}\right)\sin(\rho(y-t))d\rho + \int_{A_{12}}^{\infty}\left(\frac{b_2}{\rho} + \ldots + \frac{b_8}{\rho^7}\right)\sin(\rho(y-t))d\rho \tag{41b}$$

$$h_{13}(y,t) = \int_0^{A_{13}}(K_{13}(\rho,0)-c_1)\cos(\rho(y-t))d\rho +$$

$$\int_{A_{13}}^{\infty}\left(K_{13}(\rho,0) - c_1 - \frac{c_2}{\rho} - \ldots - \frac{c_8}{\rho^7}\right)\cos(\rho(y-t))d\rho + \int_{A_{13}}^{\infty}\left(\frac{c_2}{\rho} + \ldots + \frac{c_8}{\rho^7}\right)\cos(\rho(y-t))d\rho \tag{41c}$$

$$h_{14}(y,t) = \int_0^{A_{14}} K_{14}(\rho,0)\sin(\rho(y-t))d\rho + \int_{A_{14}}^{\infty}\left(K_{14}(\rho,0) - \frac{d_2}{\rho} - \ldots - \frac{d_8}{\rho^7}\right)\sin(\rho(y-t))d\rho$$

$$+ \int_{A_{14}}^{\infty}\left(\frac{d_2}{\rho} + \frac{d_3}{\rho^2} + \ldots + \frac{d_8}{\rho^7}\right)\sin(\rho(y-t))d\rho \tag{41d}$$

In these equations, A_{1i}, $(i = 1,..,4)$ are integration cut-off points. A sufficiently large value for these numbers have to be used in order to calculate the integrals accurately. The second terms on the right hand sides of the equations (41a-d) are going to be neglected in the numerical computations. Again, for sufficiently large values of A_{1i}, these terms tend to zero. The third terms can be evaluated in closed form. The expressions used in the evaluation of these terms are given in Appendix A.Finally, normal displacement derivative can be written as:

$$\left(\frac{4\mu_0}{\kappa+1}\right)\frac{\partial u(0,y)}{\partial y} = \frac{1}{\pi}\int_a^b \frac{P_1(t)}{(y-t)}dt - \left(\frac{\kappa-1}{\kappa+1}\right)Q_1(y)$$

$$+\left(\frac{2}{\pi(\kappa+1)}\right)\left\{\int_a^b P_1(t)\left[h_{11}(y,t)+h_{12}(y,t)\right]dt + \int_a^b Q_1(t)\left[h_{13}(y,t)+h_{14}(y,t)dt\right]\right\} \quad (42)$$

2.1.Normalization

The expression given above by equation (42) can be normalized. With the normalized form, parametric analyses can be more easily done. The interval of integration can be normalized by defining:

$$y = \frac{(b-a)}{2}s + \frac{(b+a)}{2} \quad (43a)$$

$$t = \frac{(b-a)}{2}r + \frac{(b+a)}{2} \quad (43b)$$

Normalized unknown functions are defined as:

$$P_1(y) = P_1\left(\frac{(b-a)}{2}s + \frac{(b+a)}{2}\right) = \overset{)}{P}_1(s) \quad (44a)$$

$$Q_1(y) = Q_1\left(\frac{(b-a)}{2}s + \frac{(b+a)}{2}\right) = \overset{)}{Q}_1(s) \quad (44b)$$

Substituting (43) and (44) in (42), and defining a normalized non-homogeneity parameter γ^* as:

$$\gamma^* = \gamma(b-a)\,, \tag{45}$$

the normalized form of equation (42) is obtained as:

$$\left(\frac{4\mu_0}{\kappa+1}\right)\frac{\partial u(0,y)}{\partial y} = \frac{1}{\pi}\int_{-1}^{1}\frac{P_1(r)}{s-r}\,dr - \left(\frac{\kappa-1}{\kappa+1}\right)Q_1(s)$$
$$+\left(\frac{\gamma^*}{\pi(\kappa+1)}\right)\left\{\int_{-1}^{1}P_1(r)\left[h^*_{11}(s,r)+h^*_{12}(s,r)\right]dr + \int_{-1}^{1}Q_1(r)\left[h^*_{13}(s,r)+h^*_{14}(s,r)\right]dr\right\} \tag{46}$$

In equation (46), it is interesting to note that when $\gamma = 0$, the additional term due to material grading disappears and the expression for a homogeneous half-plane is recovered. The terms $h^*_{1i}(s,r)$, $(i = 1,\mathrm{K},4)$ are also in normalized form. In the normalization of these terms,we use the transformation,

$$\rho = \gamma\alpha\,. \tag{47}$$

Depending on the sign of γ, normalized forms of these terms are given below. For $\gamma > 0$, we have,

$$h^*_{11}(s,r) = \int_{0}^{A^*_{11}} K_{11}(\gamma\alpha,0)\cos(\alpha\frac{\gamma^*}{2}(s-r))d\alpha$$
$$+\int_{A^*_{11}}^{\infty}\left(\frac{a^*_2}{\alpha}+\frac{a^*_3}{\alpha^2}+\ldots+\frac{a^*_8}{\alpha^7}\right)\cos(\alpha\frac{\gamma^*}{2}(s-r))d\alpha \tag{48a}$$

$$\overset{)}{h}^{*}{}_{12}(s,r) = \int_{0}^{A^{*}_{12}} (K_{12}(\gamma\alpha,0) - b_1)\sin(\alpha\frac{\gamma^{*}}{2}(s-r))d\alpha$$

$$+ \int_{A^{*}_{12}}^{\infty} \left(\frac{b_2^{*}}{\alpha} + \frac{b_3^{*}}{\alpha^2} + \ldots + \frac{b_8^{*}}{\alpha^7}\right)\sin(\alpha\frac{\gamma^{*}}{2}(s-r))d\alpha \qquad (48b)$$

$$\overset{)}{h}^{*}{}_{13}(s,r) = \int_{0}^{A^{*}_{13}} (K_{13}(\gamma\alpha,0) - c_1)\cos(\alpha\frac{\gamma^{*}}{2}(s-r))d\alpha$$

$$+ \int_{A^{*}_{13}}^{\infty} \left(\frac{c_2^{*}}{\alpha} + \frac{c_3^{*}}{\alpha^2} + \ldots + \frac{c_8^{*}}{\alpha^7}\right)\cos(\alpha\frac{\gamma^{*}}{2}(s-r))d\alpha \qquad (48c)$$

$$\overset{)}{h}^{*}{}_{14}(s,r) = \int_{0}^{A^{*}_{14}} K_{14}(\gamma\alpha,0)\sin(\alpha\frac{\gamma^{*}}{2}(s-r))d\alpha$$

$$+ \int_{A^{*}_{14}}^{\infty} \left(\frac{d_2^{*}}{\alpha} + \frac{d_3^{*}}{\alpha^2} + \ldots + \frac{d_8^{*}}{\alpha^7}\right)\sin(\alpha\frac{\gamma^{*}}{2}(s-r))d\alpha \qquad (48d)$$

Note that negligibly small terms are omitted. For $\gamma < 0$, the integration cut-off points become negative (see the transformation (47)). In this case, the normalized forms of the terms $\overset{)}{h}^{*}_{1i}(s,r),\ (i = 1,\text{K},4)$ are appropriately modified and are given below:

$$\overset{)}{h}^{*}{}_{11}(s,r) = -\int_{0}^{A^{*}_{11}} K_{11}(\gamma\alpha,0)\cos(\alpha\frac{\gamma^{*}}{2}(s-r))d\alpha$$

$$+ \int_{A^{*}_{11}}^{\infty} \left(\frac{a_2^{*}}{\alpha} + \frac{a_3^{*}}{\alpha^2} + \ldots + \frac{a_8^{*}}{\alpha^7}\right)\cos(\alpha\frac{\gamma^{*}}{2}(s-r))d\alpha \qquad (48e)$$

$$\overset{)}{h}^{*}{}_{12}(s,r) = \int_{0}^{A^{*}_{12}} (K_{12}(-\gamma\alpha,0) - b_1)\sin(\alpha\frac{\gamma^{*}}{2}(s-r))d\alpha$$

$$+ \int_{A^{*}_{12}}^{\infty} \left(\frac{b_2^{*}}{\alpha} + \frac{b_3^{*}}{\alpha^2} + \ldots + \frac{b_8^{*}}{\alpha^7}\right)\sin(\alpha\frac{\gamma^{*}}{2}(s-r))d\alpha \qquad (48f)$$

$$\overset{)}{h}^{*}{}_{13}(s,r) = -\int_{0}^{A^{*}_{13}} (K_{13}(\gamma\alpha,0) - c_1)\cos(\alpha\frac{\gamma^{*}}{2}(s-r))d\alpha$$

$$-\int_{A^{*}_{13}}^{\infty}\left(\frac{c_2^{*}}{\alpha}+\frac{c_3^{*}}{\alpha^2}+...+\frac{c_8^{*}}{\alpha^7}\right)\cos(\alpha\frac{\gamma^{*}}{2}(s-r))d\alpha \qquad (48g)$$

$$\overset{)}{h}^{*}{}_{14}(s,r) = -\int_{0}^{A^{*}_{14}} K_{14}(\gamma\alpha,0)\sin(\alpha\frac{\gamma^{*}}{2}(s-r))d\alpha$$

$$-\int_{A^{*}_{14}}^{\infty}\left(\frac{d_2^{*}}{\alpha}+\frac{d_3^{*}}{\alpha^2}+...+\frac{d_8^{*}}{\alpha^7}\right)\sin(\alpha\frac{\gamma^{*}}{2}(s-r))d\alpha \qquad (48h)$$

In equations (48), the constants $A^{*}{}_{1i}$ (i=1,..,4) are positive. The constants of the asymptotic expansions take the form:

$$a_2^{*}=\frac{a_2}{\gamma},\ a_3^{*}=\frac{a_3}{\gamma^2},\ \ldots,\ a_8^{*}=\frac{a_8}{\gamma^7} \qquad (49a)$$

$$b_2^{*}=\frac{b_2}{\gamma},\ b_3^{*}=\frac{b_3}{\gamma^2},\ \ldots,\ b_8^{*}=\frac{b_8}{\gamma^7} \qquad (49b)$$

$$c_2^{*}=\frac{c_2}{\gamma},\ c_3^{*}=\frac{c_3}{\gamma^2},\ \ldots,\ c_8^{*}=\frac{c_8}{\gamma^7} \qquad (49c)$$

$$d_2^{*}=\frac{d_2}{\gamma},\ d_3^{*}=\frac{d_3}{\gamma^2},\ \ldots,\ d_8^{*}=\frac{d_8}{\gamma^7} \qquad (49d)$$

Note that in all the constants given above, γ dependence is eliminated by normalization. As for the equilibrium equation, substituting (36) in (7), we get:

$$\int_{a}^{b} P_1(y)\exp(\gamma y)dy = -P \qquad (50)$$

At this point, we define another non-homogeneity parameter,

$$\gamma^{**} = \gamma(b+a) \qquad (51)$$

When we use equations (43a), (44a), (45) and (51), we obtain the final form of the normalized equilibrium equation:

$$\int_{-1}^{1} P_1(s)\exp\left(\frac{1}{2}(\gamma^* s+\gamma^{**})\right)ds=\frac{-2P}{b-a} \qquad (52)$$

This compeletes the formulation of the sliding contact problem for a graded half–plane with elastic gradation in lateral direction. Equations (46) and (52) can be used to solve the problem for any type of stamp profile. Before proceeding with the numerical solution of the contact problem, we want to note that, after normalization the required parameters for the solution of the problem are: γ^*, γ^{**} (or γa and γb), η, κ, and the profile of the stamp. In this study, we are mainly interested in the effect of the non-homogeneity parameters γ^* and γ^{**} on the contact stress distribution at the surface. Note that, the first parameter is related to the size of the contact area while the second one is related to the location of the stamp. In Chapter 3, we will give the details of the numerical solution techniques for the flat, triangular and circular stamp problems. The numerical solution is based on a numerical collocation technique where the unknown contact stress is approximated by using a series expansion of Jacobi polynomials.

CHAPTER III

NUMERICAL SOLUTION

3.1.Flat Stamp Problem

The geometry of the flat stamp problem is shown in Figure 3.

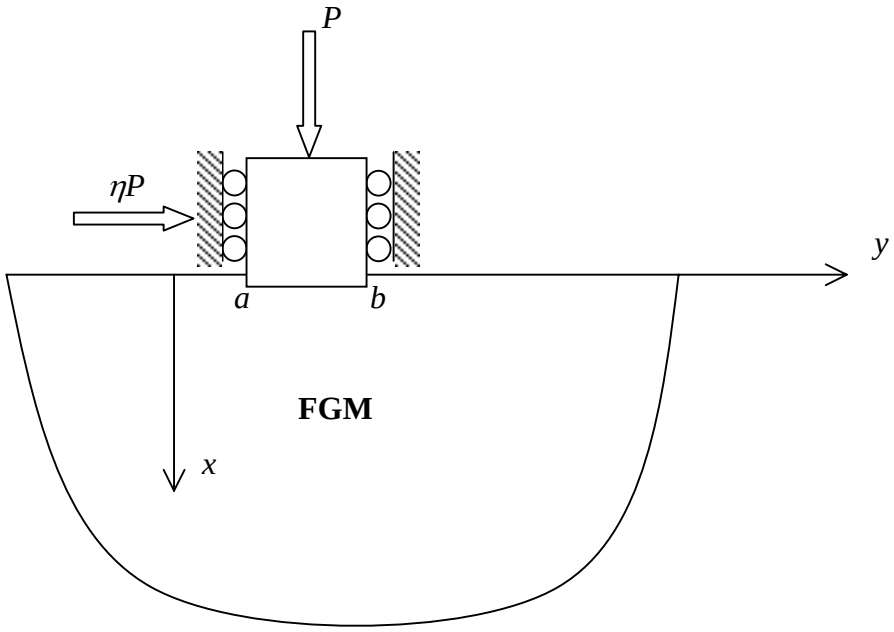

Figure 3: The general description of the contact problem for flat stamp

For the flat stamp, displacement derivative in the contact area is constant. So, we can write:

$$\frac{\partial u(0,y)}{\partial y} = 0\,, \qquad a<y<b \qquad (53)$$

We now normalize the function $P_1'(s)$ by $P/(b-a)$ and define $\overline{P}_1(s)$ as:

$$\overline{P}_1(s) = \frac{P_1'(s)}{P/(b-a)} \tag{54}$$

Substituting equation (54) in (46), we have:

$$\frac{1}{\pi}\int_{-1}^{1}\frac{\overline{P}_1(r)}{s-r}dr - \left(\frac{\kappa-1}{\kappa+1}\right)\eta\overline{P}_1(s)$$
$$+\left(\frac{\gamma^*}{\pi(\kappa+1)}\right)\left\{\int_{-1}^{1}\overline{P}_1(r)\left[h^*_{11}(s,r)+h^*_{12}(s,r)\right]dr + \int_{-1}^{1}\eta\overline{P}_1(r)\left[h^*_{13}(s,r)+h^*_{14}(s,r)\right]dr\right\} = 0$$
$$-1<s<1 \tag{55}$$

Note that (55) is a singular integral equation for the unknown function $\overline{P}_1(s)$ .Substituting (54) in (52), equilibrium equation becomes:

$$\int_{-1}^{1}\overline{P}_1(s)\exp\left(\frac{1}{2}(\gamma^* s+\gamma^{**})\right)ds = -2 \tag{56}$$

There are standard solution methods to solve the equations (55) and (56). A detailed description of the solution techniques using series expansion and collocation approaches can be found in Erdoğan [29]. It is known that, for the flat stamp, the stress $\sigma_{xx}(0,y)$ is singular at the end points of the contact region. In this study, the singular terms obtained for the integral equation (55) are same as those obtained for the homogeneous problem [23]. Hence, the singular behavior of the stresses are exactly the same as those for the homogeneous medium. A material property grading in lateral direction does not effect the singular behavior of the stresses at the ends of the contact region.

The normalized stress is now expressed in the following form:

$$\overline{P}_1(r) = W_1(r)\left(\sum_{n=0}^{\infty} A_n P_n^{(\beta 1,\beta 2)}(r)\right) \tag{57}$$

where, A_n are unknown constants and $P_n^{(\beta 1,\beta 2)}$ are Jacobi polynomials. Other functions and variables are given as:

$$W_1(r) = (1-r)^{\beta 1}(1+r)^{\beta 2} \tag{58}$$

$$\cot(\pi\beta_1) = -\eta\frac{\kappa-1}{\kappa+1} \tag{59a}$$

$$\cot(\pi\beta_2) = \eta\frac{\kappa-1}{\kappa+1} \tag{59b}$$

$$\beta_1 + \beta_2 = -1 \quad , \qquad -1<\beta_1<0 \quad , \qquad -1<\beta_2<0 \tag{60}$$

In the aforementioned equations (57) – (60), the bounded part of the unknown function is expanded into an infinite series of Jacobi polynomials and A_n are the unknown constants. The variables, β_1 and β_2 are the strengths of the singularity at the ends of the contact region for the flat stamp. Using complex function theory, it is possible to derive the equations given by (59). For more details on the derivation of these equations, the reader may refer to Dağ [23]. However, it is interesting to note that the sum of β_1 and β_2 is equal to -1. Substituting (57) in (55), we get:

$$\frac{1}{\pi}\int_{-1}^{1}\frac{W_1(r)}{s-r}\left(\sum_{n=0}^{\infty} A_n P_n^{(\beta 1,\beta 2)}(r)\right)dr - \eta\left(\frac{\kappa-1}{\kappa+1}\right)W_1(s)\left(\sum_{n=0}^{\infty} A_n P_n^{(\beta 1,\beta 2)}(s)\right)$$
$$+\left(\frac{\gamma^*}{\pi(\kappa+1)}\right)\left(\int_{-1}^{1} W_1(r)\left(\sum_{n=0}^{\infty} A_n P_n^{(\beta 1,\beta 2)}(r)\right)\left[h^*_{11}(s,r) + h^*_{12}(s,r)\right]dr\right.$$
$$\left.+\int_{-1}^{1}\eta W_1(r)\left(\sum_{n=0}^{\infty} A_n P_n^{(\beta 1,\beta 2)}(r)\right)\left[h^*_{13}(s,r) + h^*_{14}(s,r)\right]dr\right) = 0 \quad , \ -1< s <1 \tag{61}$$

Now we rearrange equation (61) to get a more useful form,

$$\sum_{0}^{\infty} A_n \left[\frac{1}{\pi} \int_{-1}^{1} \frac{W_1(r) P_n^{(\beta 1, \beta 2)}(r)}{s-r} dr - \eta \frac{\kappa - 1}{\kappa + 1} W_1(s) P_n^{(\beta 1, \beta 2)}(s) \right]$$

$$+ \sum_{0}^{\infty} A_n \left(\frac{\gamma^*}{\pi(\kappa+1)} \right) \left(\int_{-1}^{1} W_1(r) P_n^{(\beta 1, \beta 2)}(r) \left[h^*_{11}(s,r) + h^*_{12}(s,r) \right] dr \right)$$

$$+ \sum_{0}^{\infty} A_n \left(\frac{\gamma^*}{\pi(\kappa+1)} \right) \left(\int_{-1}^{1} \eta W_1(r) P_n^{(\beta 1, \beta 2)}(r) \left[h^*_{13}(s,r) + h^*_{14}(s,r) \right] dr \right) = 0$$

$$-1 < s < 1 \qquad (62)$$

The first integral in equation (62) can be evaluated in closed form using the following identity:

$$\frac{1}{\pi} \int_{-1}^{1} (1-r)^{\alpha} (1+r)^{\beta} P_n^{(\alpha,\beta)}(r) \frac{dr}{s-r} =$$

$$-\cot(\pi\alpha)(1-s)^{\alpha}(1+s)^{\beta} P_n^{(\alpha,\beta)}(s) + \frac{2^{-\chi}}{\sin(\pi\alpha)} P_{n-\chi}^{(-\alpha,-\beta)}(s) \qquad (63)$$

where $\chi = -(\alpha + \beta)$. Note that for this equation to be valid χ has to be equal to 1, -1 or 0 which is the case for all the contact mechanics problems considered in this study. Substituting (63) in (62), we get:

$$\sum_{n=1}^{\infty} A_n \left(\frac{1}{2\sin(\pi\beta_1)} P_{n-1}^{(-\beta 1, -\beta 2)}(s) \right)$$

$$+ \sum_{0}^{\infty} A_n \left(\frac{\gamma^*}{\pi(\kappa+1)} \right) \left(\int_{-1}^{1} W_1(r) P_n^{(\beta 1, \beta 2)}(r) \left[h^*_{11}(s,r) + h^*_{12}(s,r) \right] dr \right)$$

$$+ \sum_{0}^{\infty} A_n \left(\frac{\gamma^*}{\pi(\kappa+1)} \right) \left(\int_{-1}^{1} \eta W_1(r) P_n^{(\beta 1, \beta 2)}(r) \left[h^*_{13}(s,r) + h^*_{14}(s,r) \right] dr \right) = 0$$

$$-1 < s < 1 \qquad (64)$$

Now we define two new functions as:

$$Z_{1n}(s,r) = W_1(r)P_n^{(\beta 1,\beta 2)}(r)\left[h'^*_{11}(s,r) + h'^*_{12}(s,r)\right] \quad (65a)$$

$$Z_{2n}(s,r) = \eta W_1(r)P_n^{(\beta 1,\beta 2)}(r)\left[h'^*_{13}(s,r) + h'^*_{14}(s,r)\right] \quad (65b)$$

Then, equation (64)is written as:

$$\sum_{n=1}^{\infty} A_n\left(\frac{1}{2\sin(\pi\beta_1)}P_{n-1}^{(-\beta 1,-\beta 2)}(s)\right) + \sum_{n=0}^{\infty}\left[A_n\left(\frac{\gamma^*}{\pi(\kappa+1)}\right)\left(\int_{-1}^{1} Z_{1n}(s,r)dr + \int_{-1}^{1} Z_{2n}(s,r)dr\right)\right]$$

$$= 0 \qquad -1< s <1 \quad (66)$$

Again, we rename the two terms of the equation (66):

$$m_{1n}(s) = \frac{1}{2\sin(\pi\beta_1)}P_{n-1}^{(-\beta 1,-\beta 2)}(s) \quad (67a)$$

$$m_{2n}(s) = \left(\frac{\gamma^*}{\pi(\kappa+1)}\right)\left(\int_{-1}^{1} Z_{1n}(s,r)dr + \int_{-1}^{1} Z_{2n}(s,r)dr\right) \quad (67b)$$

To find the final form of the normalized equilibrium equation, we substitute equation (57) in (56):

$$\sum_{n=0}^{\infty}\int_{-1}^{1} W_1(s)A_nP_n^{(\beta 1,\beta 2)}(s)\exp\left(\frac{1}{2}(\gamma^* s + \gamma^{**})\right)ds = -2 \quad (68)$$

We rename the term in equation (68) as:

$$m_{3n} = \int_{-1}^{1} W_1(s)P_n^{(\beta 1,\beta 2)}(s)\exp\left(\frac{1}{2}(\gamma^* s + \gamma^{**})\right)ds \quad (69)$$

When we use equations (67a,b) in (66) and (69) in (68), we finally obtain the following normalized linear equation system:

$$\sum_{n=1}^{N} A_n m_{1n}(s) + \sum_{n=0}^{N} A_n m_{2n}(s) = 0 \tag{70a}$$

$$\sum_{n=0}^{N} A_n m_{3n} = -2 \tag{70b}$$

Note that, the linear equation system is truncated at $n = N$. These functional equations can be solved by using collocation points for equation (70a). In this study, the collocation points for (70a) are selected as the roots of the Chebyshev polynomials as:

$$s_i = \cos\left(\frac{\pi(2i-1)}{N}\right), \qquad i = 1\text{K}\ N. \tag{71}$$

Now collocating equation (70a) at N points using (71) and also using (70b) we have $N+1$ equations for $N+1$ unknowns which are A_n, $(n = 0\text{K}\ N)$. A computer program is written using Visual Fortran 90 language, to solve the equation system and to calculate the normalized contact stress distribution $\overline{P}_1(s)$ for $-1 < s < 1$. Detailed parametric analyses are given in Chapter 4.

3.2.Closed Form Solution Of The Contact Mechanics Problem For The Homogeneous Half-plane (Flat Stamp)

In the previous section, a numerical solution method is developed to solve the frictional contact problem for the graded medium. In this section, we will obtain the closed form solution for the contact stress distribution on the surface of the homogeneous half-plane. The results obtained in this section are going to be used in Chapter 4 for comparison purposes. We assume that the problem definition is same as that given in Section 3.1, except that we now consider a homogeneous half-plane. In this case we have,

$$\gamma = \gamma^{*} = \gamma^{**} = 0. \tag{72}$$

So the governing equations of the problem reduce to:

$$\frac{1}{\pi}\int_{-1}^{1}\frac{\overline{P}_1(r)}{s-r}dr-\eta\frac{\kappa-1}{\kappa+1}\overline{P}_1(s)=0,\qquad -1<s<1, \tag{73a}$$

$$\int_{-1}^{1}\overline{P}_1(s)ds=-2. \tag{73b}$$

$$\overline{P}_1(s)=\frac{\sigma_{xx}\left(0,\frac{b-a}{2}s+\frac{b+a}{2}\right)}{P/(b-a)} \tag{73c}$$

Again we assume a solution of the form:

$$\overline{P}_1(s)=(1-s)^{\beta_1}(1+s)^{\beta_2}\sum_{n=0}^{\infty}A_nP_n^{(\beta_1,\beta_2)}(s) \tag{74}$$

where β_1 and β_2 are given by equation (59). Now substituting (74) in (73a) and integrating in closed form using equation (63), we obtain:

$$\sum_{n=1}^{\infty}A_n\left(\frac{1}{2\sin(\pi\beta_1)}P_{n-1}^{(-\beta_1,-\beta_2)}(s)\right)=0 \tag{75}$$

This equation can be satisfied only if,

$$A_1=A_2=A_3=\mathrm{K}=A_n=0 \tag{76}$$

The only nonzero constant in the expansion is A_0, hence the normalized contact stress takes the form,

$$\overline{P}_1(s)=A_0(1-s)^{\beta_1}(1+s)^{\beta_2} \tag{77}$$

The constant A_0 can be determined by substituting (77) in equation (73b),

$$A_0\int_{-1}^{1}(1-s)^{\beta_1}(1+s)^{\beta_2}ds=-2 \tag{78}$$

The integral can be evaluated in closed form using the expressions given in [29] and A_0 is determined as,

$$A_0 = \frac{2\sin(\pi\beta_2)}{\pi} \tag{79}$$

Finally normalized contact stress distribution for the homogeneous half – plane is expressed as,

$$\overline{P}_1(s) = \frac{2\sin(\pi\beta_2)}{\pi}(1-s)^{\beta_1}(1+s)^{\beta_2}, \qquad -1 < s < 1 \tag{80}$$

Note that β_2 is negative, hence the normalized contact stress is also negative at every point in the contact region. This is an expected result, since the contact stresses are always compressive.

3.3.Triangular Stamp Problem

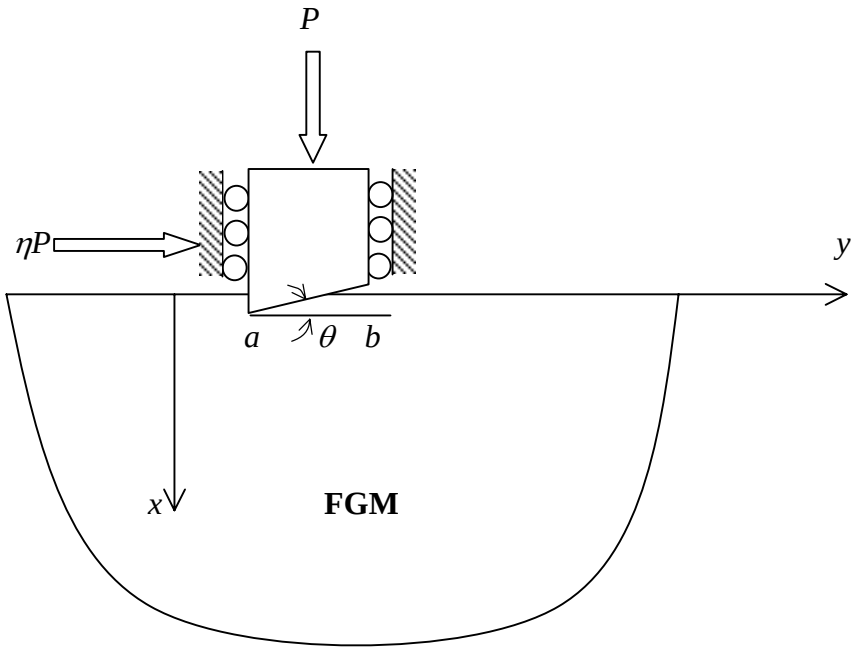

Figure 4: The general description of the contact problem for the triangular stamp.

The geometry of the triangular stamp problem is shown in Figure 4. In this case, the stamp has a constant slope of $\tan(\theta) = m$ in the contact region. The normal displacement decreases as *y* increases in the contact region, hence displacement derivative can be written as:

$$\frac{\partial}{\partial y}u(0,y) = -\tan\theta = -m \qquad a<y<b \qquad (81)$$

Substituting equation (81) in (46) we have:

$$\frac{1}{\pi}\int_{-1}^{1}\frac{\overline{P}_1(r)}{s-r}dr - \left(\frac{\kappa-1}{\kappa+1}\right)\overline{Q}_1(s)$$

$$+\left(\frac{\gamma^*}{\pi(\kappa+1)}\right)\left\{\int_{-1}^{1}\overline{P}_1(r)\left[h^*_{11}(s,r)+h^*_{12}(s,r)\right]dr + \int_{-1}^{1}\overline{Q}_1(r)\left[h^*_{13}(s,r)+h^*_{14}(s,r)\right]dr\right\}$$

$$= -m\left(\frac{4\mu_0}{\kappa+1}\right), \qquad -1< s <1 \qquad (82)$$

We divide both sides by $\mu_0 m$ and let:

$$\frac{\overline{P}_1(r)}{\mu_0 m} = \overline{P}_1(r) \qquad (83a)$$

$$\frac{\overline{Q}_1(r)}{\mu_0 m} = \overline{Q}_1(r) \qquad (83b)$$

Now, equation (82) becomes,

$$\frac{1}{\pi}\int_{-1}^{1}\frac{\overline{P}_1(r)}{s-r}dr - \left(\frac{\kappa-1}{\kappa+1}\right)\eta\overline{P}_1(s)$$

$$+\left(\frac{\gamma^*}{\pi(\kappa+1)}\right)\left\{\int_{-1}^{1}\overline{P}_1(r)\left[h^*_{11}(s,r)+h^*_{12}(s,r)\right]dr + \int_{-1}^{1}\eta\overline{P}_1(r)\left[h^*_{13}(s,r)+h^*_{14}(s,r)\right]dr\right\}$$

$$= -\frac{4}{\kappa+1}, \qquad -1< s <1 \qquad (84)$$

Also, by substituting equation (83a) in (56):

$$\int_{-1}^{1} \overline{P}_1(s) \exp\left(\frac{1}{2}(\gamma^* s + \gamma^{**})\right) ds = -\frac{2P}{\mu_0 m(b-a)} \tag{85}$$

Normalized contact stress is expressed as:

$$\overline{P}_1(s) = (1-s)^{\beta 1}(1+s)^{\beta 2}\left(\sum_{n=0}^{\infty} A_n P_n^{(\beta 1, \beta 2)}(s)\right) \tag{86}$$

In this case, strengths of the singurity are given as:

$$\cot(\pi\beta_1) = -\eta\frac{\kappa-1}{\kappa+1}, \qquad 0 < \beta_1 < 1 \tag{87a}$$

$$\cot(\pi\beta_2) = \eta\frac{\kappa-1}{\kappa+1}, \qquad -1 < \beta_2 < 0 \tag{87b}$$

Note that the contact at $s = 1$ is smooth, hence at this point the exponent is positive and the contact stress is zero. At the other end however there is a sharp corner. Consequently, the exponent at this point is negative and the contact stress tends to infinity. Also, note that $\beta_1 + \beta_2 = 0$. The derivation of the equations (87) using complex function theory can be found in the reference [23]. Substituting equation (86) in (84) and evaluating the Cauchy Principal Value Integral in closed form, using equation (63) we find:

$$\frac{1}{\sin(\pi\beta_1)}\sum_{n=0}^{\infty} A_n\left(P_n^{(-\beta 1, -\beta 2)}(s)\right)$$

$$+\sum_{n=0}^{\infty}\left[A_n\left(\frac{\gamma^*}{\pi(\kappa+1)}\right)\left(\int_{-1}^{1} Z_{1n}(s,r)dr + \int_{-1}^{1} Z_{2n}(s,r)dr\right)\right] = -\frac{4}{\kappa+1},$$

$$-1 < s < 1 \tag{88}$$

where Z_{1n} and Z_{2n} are given by equation (65). We now make the following definitions:

$$q_{1n}(s) = \frac{1}{\sin(\pi\beta_1)} P_n^{(-\beta 1,-\beta 2)}(s) \tag{89a}$$

$$q_{2n}(s) = \left(\frac{\gamma^*}{\pi(\kappa+1)}\right)\left(\int_{-1}^{1} Z_{1n}(s,r)dr + \int_{-1}^{1} Z_{2n}(s,r)dr\right) \tag{89b}$$

Truncating the infinite series at N, the singular integral equation can now be expressed as:

$$\sum_{n=0}^{N} A_n q_{1n}(s) + \sum_{n=0}^{N} A_n q_{2n}(s) = -\frac{4}{\kappa+1} \quad , \qquad -1<s<1 \tag{90}$$

Substituting (86) in (56), we can obtain the equilibrium equation:

$$\sum_{n=0}^{N} \int_{-1}^{1} W_1(s) P_n^{(\beta 1,\beta 2)}(s) \exp\left(\frac{1}{2}(\gamma^* s + \gamma^{**})\right) ds = -\frac{2P}{\mu_0 m(b-a)} \tag{91}$$

We define q_{3n} as:

$$q_{3n} = \int_{-1}^{1} W_1(s) P_n^{(\beta 1,\beta 2)}(s) \exp\left(\frac{1}{2}(\gamma^* s + \gamma^{**})\right) ds \tag{92}$$

So, the equilibrium equation takes the final form as:

$$\sum_{n=0}^{N} A_n q_{3n} = -\frac{2P}{\mu_0 m(b-a)} \tag{93}$$

Equations (90) and (93) can be used to solve the contact mechanics problem for the triangular stamp. But, in this case the solution approach is going to be slightly different. Technically, triangular stamp problem is defined as an incomplete contact

mechanics problem where the size of the contact region is a function of the applied force. So, in the numerical solution first, the contact stresses will be computed using equation (90) with $N+1$ collocation points. Then, the computed contact stress distribution will be substituted in equation (93) to calculate the required normalized force. In the triangular stamp problem, for each data set contact stress distribution and required contact force will be the outputs of the numerical analysis. The collocation points for equation (90) are again selected as the following roots of the Chebyshev polynomials,

$$s_i = \cos\left(\frac{\pi(2i-1)}{N+1}\right), \qquad i = 1\text{K}\ N+1. \tag{94}$$

Note that equation (94) gives us $N+1$ equations for $N+1$ unknowns, namely $A_n, (n = 0\text{K}\ N)$.

3.4.Closed Form Solution of the Contact Mechanics Problem for the Homogeneous Half - Plane (Triangular Stamp)

In section 3.3 we laid down the numerical procedure for the solution of the triangular stamp problem for the laterally graded medium. Now, we will derive the closed form expressions for the contact stresses and contact force assuming that the contact is between the triangular stamp and the homogeneous half–plane. The nonhomogeneity constant is zero for the homogeneous half–plane, i.e.,

$$\gamma = \gamma^{*} = \gamma^{**} = 0 \tag{95}$$

Then, the governing equations can be written as:

$$\frac{1}{\pi}\int_{-1}^{1}\frac{\overline{P}_1(r)}{s-r}dr - \eta\frac{\kappa-1}{\kappa+1}\overline{P}_1(s) = -\frac{4}{\kappa+1} \qquad -1 < s < 1 \tag{96a}$$

$$\int_{-1}^{1} \overline{P}_1(s)ds = -\frac{2P}{\mu_0 m(b-a)} \tag{96b}$$

$$\overline{P}_1(s) = \frac{\sigma_{xx}\left(0, \frac{b-a}{2}s + \frac{b+a}{2}\right)}{\mu_0 m} \tag{96c}$$

Again we assume a solution of the form:

$$\overline{P}_1(s) = (1-s)^{\beta_1}(1+s)^{\beta_2}\sum_{n=0}^{\infty} A_n P_n^{(\beta_1,\beta_2)}(s) \tag{97}$$

where β_1 and β_2 are given by equation (87). Now substituting (97) in (96a) and integrating in closed form using equation (63), we obtain:

$$\frac{1}{\sin(\pi\beta_1)}\sum_{n=0}^{\infty} A_n P_n^{(-\beta_1,\beta_2)}(s) = -\frac{4}{\kappa+1} \qquad -1 < s < 1 \tag{98}$$

We can also write this equation in the following form:

$$\frac{1}{\sin(\pi\beta_1)}\sum_{n=0}^{\infty} A_n P_n^{(-\beta_1,\beta_2)}(s) = -\frac{4}{\kappa+1} P_0^{(-\beta_1,-\beta_2)}(s) \qquad -1 < s < 1 \tag{99}$$

Note that, $P_0^{(-\beta_1,-\beta_2)} = 1.$ Equating the coefficients of the polynomials on both sides, we get,

$$A_1 = A_2 = \mathrm{K} = A_n = 0 \tag{100a}$$

$$A_0 = -\frac{4\sin(\pi\beta_1)}{\kappa+1} \tag{100b}$$

Hence, normalized contact stress distribution can be written as,

$$\overline{P}_1(s) = A_0(1-s)^{\beta_1}(1+s)^{\beta_2} \qquad -1 < s < 1 \tag{101}$$

Substituting (101) in (96b) and evaluating the integral in closed form using the expression given in [29], normalized contact force is determined as:

$$\frac{P}{\mu_0 m(b-a)} = -\frac{4\pi\beta_2}{\kappa+1} \tag{102}$$

Note that β_2 is negative and β_1 is positive. Hence, the normalized force given by equation (102) is positive and the contact stress given given by equation (101) is negative, which are as expected.

3.5. Circular Stamp Problem

3.5.1. Geometry of the circular stamp

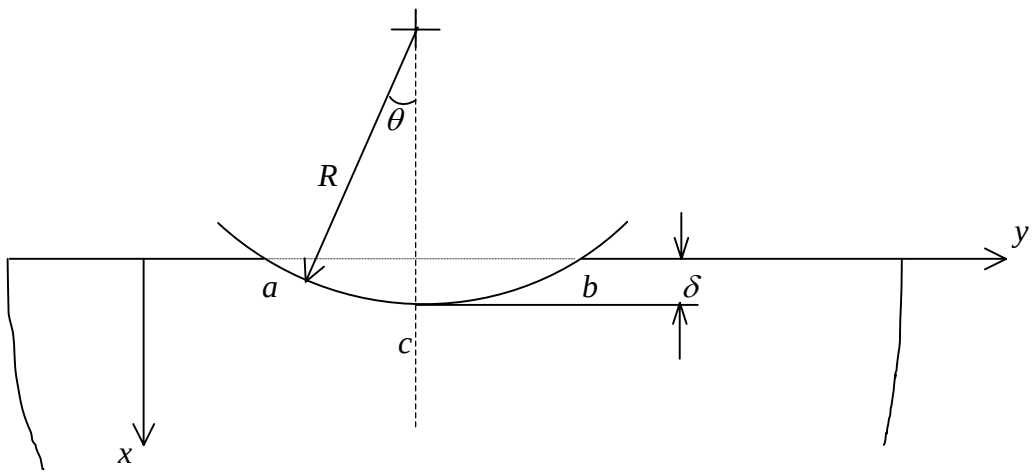

Figure 5: Geometry of the circular stamp

The geometry for a circular stamp is shown in Figure 5. The radius of the stamp is assumed to be equal to R and the centerline of the stamp passes through point $y = c$. δ is the rigid body displacement given to the stamp in x – direction. The normal displacement in the contact area can now be written as,

$$u(0,y) = \delta - R(1 - \cos(\theta(y))), \quad a < y < b, \tag{103}$$

where θ is the angle measured from the axis of symmetry. At this point we make an assumption regarding the geometry of the contact. We assume that, the length of the contact $(b-a)$ is much smaller than the radius of the circular stamp, *R*, i.e.,

$$(b-a) << R\,. \tag{104}$$

Given this assumption, the term $\cos(\theta)$ can be approximated by retaining the first two terms of its Taylor series expansion:

$$\cos(\theta) \approx 1 - \frac{\theta^2}{2} \tag{105}$$

Substituting (105) in (103) we have,

$$u(0,y) = \delta - R\frac{\theta^2}{2}, \quad a < y < b \tag{106}$$

Again, since θ is assumed to be sufficiently small, it can be expressed as,

$$\theta \approx \sin(\theta) = \frac{c-y}{R} \tag{107}$$

Substituting (107) in (106), normal displacement in the contact area is obtained as,

$$u(0,y) = \delta - \frac{(c-y)^2}{2R}, \qquad a < y < b \tag{108}$$

Now, we can easily determine the normal displacement derivative as:

$$\frac{\partial}{\partial y}u(0,y) = \frac{c-y}{R}, \quad a < y < b\,. \tag{109}$$

Equation (109) has to be used as an input to the right hand side of the singular integral equation in the numerical solution.

3.5.2. Numerical Solution

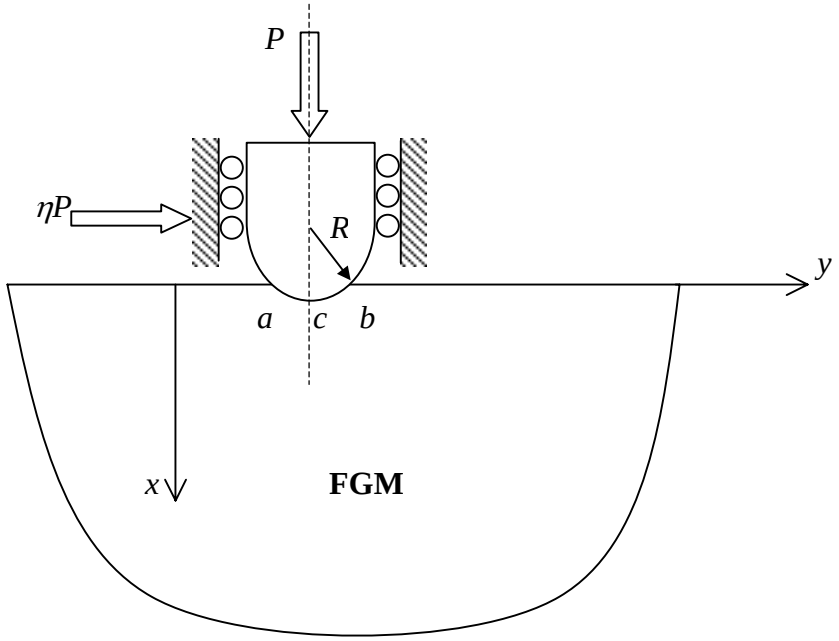

Figure 6: The general description of the contact problem for the circular stamp.

The geometry of the contact problem for the circular stamp is shown in Figure 6. First by substituting equation (107) in equation (46) singular integral equation for the circular stamp problem can be written as,

$$\frac{1}{\pi}\int_{-1}^{1}\frac{P_1(r)}{s-r}dr-\left(\frac{\kappa-1}{\kappa+1}\right)Q_1(s)$$

$$+\left(\frac{\gamma^*}{\pi(\kappa+1)}\right)\left\{\int_{-1}^{1}P_1(r)\left[h^*_{11}(s,r)+h^*_{12}(s,r)\right]dr+\int_{-1}^{1}Q_1(r)\left[h^*_{13}(s,r)+h^*_{14}(s,r)\right]dr\right\}$$

$$=\frac{4\mu_0}{\kappa+1}\left\{\frac{c}{R}-\frac{b-a}{2R}s-\frac{b+a}{2R}\right\},\qquad -1<s<1. \qquad (110)$$

We now divide both sides by μ_0 and and let:

$$\frac{P_1(r)}{\mu_0} = \overline{P}_1(r) \tag{111a}$$

$$\frac{Q_1(r)}{\mu_0} = \overline{Q}_1(r) \tag{111b}$$

Also by substituting (111a) in (56) equilibrium condition is expressed as:

$$\int_{-1}^{1} \overline{P}_1(s) \exp\left(\frac{1}{2}(\gamma^* s + \gamma^{**})\right) ds = -\frac{2P}{\mu_0 (b-a)} \tag{112}$$

Now, we express the normalized contact stress using a series expansion of the Jacobi polynomials,

$$\overline{P}_1(s) = (1-s)^{\beta 1}(1+s)^{\beta 2}\left(\sum_{n=0}^{\infty} A_n P_n^{(\beta 1, \beta 2)}(s)\right) \tag{113}$$

In this case the exponents are given as:

$$\cot(\pi\beta_1) = -\eta\frac{\kappa-1}{\kappa+1}, \qquad 0 < \beta_1 < 1 \tag{114a}$$

$$\cot(\pi\beta_2) = \eta\frac{\kappa-1}{\kappa+1}, \qquad 0 < \beta_2 < 1 \tag{114b}$$

Note that at both ends the contact is smooth, hence contact stress tends to zero at these points. Consequently, there is no singularity and both of the exponents β_1 and β_2 are greater than zero. Also, we notice that $\beta_1 + \beta_2 = 1$. The details of the derivation of equations (114) using complex function theory can be found in [23]. Substituting equation (113) in (110) and evaluating the Cauchy Principal Value Integral in closed form using equation (63), we find:

$$\frac{2}{\sin(\pi\beta_1)}\sum_{n=0}^{\infty} A_n P_{n+1}^{(-\beta_1,-\beta_2)}(s) +$$

$$\frac{\gamma^*}{\pi(\kappa+1)}\sum_{n=0}^{\infty} A_n\left\{\int_{-1}^{1} Z_{1n}(s,r)dr + \int_{-1}^{1} Z_{2n}(s,r)dr\right\} = \frac{4}{\kappa+1}\left\{\frac{c}{R} - \frac{b-a}{2R}s - \frac{b+a}{2R}\right\},$$

$$-1 < s < 1. \qquad (115)$$

where Z_{1n} and Z_{2n} are given by equation (65). We now make the following definitions:

$$p_{1n}(s) = \frac{2}{\sin(\pi\beta_1)} P_{n+1}^{(-\beta_1,-\beta_2)}(s) \qquad (116a)$$

$$p_{2n}(s) = \left(\frac{\gamma^*}{\pi(\kappa+1)}\right)\left(\int_{-1}^{1} Z_{1n}(s,r)dr + \int_{-1}^{1} Z_{2n}(s,r)dr\right) \qquad (116b)$$

Singular integral equation for the circular stamp problem can now be expressed as:

$$\sum_{n=0}^{\infty} A_n p_{1n}(s) + \sum_{n=0}^{\infty} A_n p_{2n}(s) = \frac{4}{\kappa+1}\left\{\frac{c}{R} - \frac{b-a}{2R}s - \frac{b+a}{2R}\right\}, \quad -1 < s < 1. \qquad (117)$$

Now, we will express the right hand hand side of this equation in terms of the Jacobi polynomials. Jacobi polynomial of the first order can be written as:

$$P_1^{(-\beta_1,-\beta_2)}(s) = -\beta_1 + \frac{1}{2} + \frac{s}{2} \qquad (118)$$

Note that equation (118) is valid only if $\beta_1 + \beta_2 = 1$. Solving for s in terms of the first order Jacobi polynomial and then substituting in (117) we have:

$$\sum_{n=0}^{\infty} A_n p_{1n}(s) + \sum_{n=0}^{\infty} A_n p_{2n}(s) =$$
$$= \frac{4}{\kappa+1}\left\{\frac{c}{R} - \frac{b-a}{R}\left(\beta_1 - \frac{1}{2}\right) - \frac{b+a}{2R}\right\} - \frac{4}{\kappa+1}\left(\frac{b-a}{R}\right) P_1^{(-\beta_1,-\beta_2)}(s),$$
$$-1 < s < 1. \qquad (119)$$

In the circular stamp problem, the variables *a*, *b* and *c* are not independent. Only two of these parameters can be independently specified. In order to determine the relationship between *a*, *b* and *c* we first multiply both sides of equation (119) by $(1-s)^{-\beta_1}(1+s)^{-\beta_2}$ and then integrate them from $s=-1$ to $s=1$. Applying this procedure we obtain the following equation:

$$\sum_{n=0}^{\infty} A_n \int_{-1}^{1} p_{1n}(s)(1-s)^{-\beta_1}(1+s)^{-\beta_2} ds + \sum_{n=0}^{\infty} A_n \int_{-1}^{1} p_{2n}(s)(1-s)^{-\beta_2}(1+s)^{-\beta_2} ds$$
$$= \frac{4}{\kappa+1}\left\{\frac{c}{R} - \frac{b-a}{R}\left(\beta_1 - \frac{1}{2}\right) - \frac{b+a}{R}\right\} \int_{-1}^{1} (1-s)^{-\beta_1}(1+s)^{-\beta_2} ds$$
$$- \frac{4}{\kappa+1}\frac{b-a}{R} \int_{-1}^{1} (1-s)^{-\beta_1}(1+s)^{-\beta_2} P_1^{(-\beta_1,-\beta_2)}(s) ds, \qquad -1 < s < 1. \qquad (120)$$

In order to be able to deal with the integrals given in equation (120), we can make use of the integral identities given in Erdoğan [29]. Using these identities we can say that the first integral on the left hand side and the second integral on the right hand side are equal to zero. The first integral on the right hand side of (120) can be determined in closed form using the following identity:

$$\int_{-1}^{1} (1-s)^{-\beta_1}(1+s)^{-\beta_2} ds = \frac{\pi}{\sin(\pi\beta_1)}, \qquad \beta_1 + \beta_2 = 1. \qquad (121)$$

Then, equation (121) is reduced to:

$$\sum_{n=0}^{\infty} A_n \int_{-1}^{1} (1-s)^{-\beta_1}(1+s)^{-\beta_2} p_{2n}(s) ds = \frac{4}{\kappa+1}\left\{\frac{c}{R} - \frac{b-a}{R}\left(\beta_1 - \frac{1}{2}\right) - \frac{b+a}{R}\right\} \frac{\pi}{\sin(\pi\beta_1)} \qquad (122)$$

So, the relationship between *a*, *b* and *c* is expressed as:

$$\frac{4}{\kappa+1}\left\{\frac{c}{R}-\frac{b-a}{R}\left(\beta_1-\frac{1}{2}\right)-\frac{b+a}{R}\right\}=\frac{\sin(\pi\beta_1)}{\pi}\sum_{n=0}^{\infty}A_n\int_{-1}^{1}p_{2n}(s)(1-s)^{-\beta_1}(1+s)^{-\beta_2}\,ds\,. \tag{123}$$

Note that given *a* and *b*, *c* can be calculated using equation (123) if the contact stress distribution is known. We can substitute equation (123) in equation (119) to eliminate *c* dependence in the singular integral equation. Doing so integral equation is reduced to the following form:

$$\sum_{n=0}^{N}A_n p_{1n}(s)+\sum_{n=0}^{N}A_n\left(p_{2n}(s)-M_n\right)=-\frac{4}{\kappa+1}\left(\frac{b-a}{R}\right)P_1^{(-\beta_1,-\beta_2)}(s), \qquad -1<s<1 \tag{124}$$

In this equation the infinite series expansions are truncated at $n=N$ and M_n is given as:

$$M_n=\frac{\sin(\pi\beta_1)}{\pi}\int_{-1}^{1}p_{2n}(s)(1-s)^{-\beta_1}(1+s)^{-\beta_2}\,ds. \tag{125}$$

Equation (125) involves double integrals in *s* and these double integrals will significantly increase the computation time compared to the flat and triangular stamp problems. c/R can be expressed in terms of a/R and b/R using equation (123) as:

$$\frac{c}{R}=\frac{b-a}{R}\left(\beta_1-\frac{1}{2}\right)+\frac{b+a}{2R}+\frac{\kappa+1}{4}\sum_{n=0}^{N}A_nM_n \tag{126}$$

The final equation that has to be considered in the solution of the circular stamp problem is the equilibrium equation. Substituting (113) in (112), this equation is obtained as:

$$\frac{P}{\mu_0(b-a)} = -\frac{1}{2}\sum_{n=0}^{N} A_n m_{3n}, \tag{127}$$

where m_{3n} is given in the following form:

$$m_{3n} = \int_{-1}^{1} (1-s)^{\beta_1} (1+s)^{\beta_2} P_n^{(\beta_1,\beta_2)}(s) \exp\left(\frac{1}{2}\left(\gamma^* s + \gamma^{**}\right)\right) ds\,. \tag{128}$$

The solution approach to the circular stamp problem can now be summarized as follows. First, the geometric parameters, a/R, b/R, the nonhomogeneity constants γ^* and γ^{**}, the friction coefficient η and the Poisson's ratio ν will be specified. Then, the normalized contact stress distribution is going to be computed using equation (124) with $N+1$ collocation points. The collocation points are selected as the following roots of the Chebyshev polynomials:

$$s_i = \cos\left(\frac{\pi(2i-1)}{N+1}\right), \qquad i = 1, \mathrm{K}\ , N+1. \tag{129}$$

Once the contact stress distribution is determined, the corresponding location of the centerline of the circular stamp will be calculated using equation (126) and the normalized contact force will be calculated using equation (127).

3.6. Closed Form Solution of the Contact Mechanics Problem for the Homogeneous Half – Plane (Circular Stamp)

In section 3.5., we laid down the numerical procedure for the solution of the circular stamp problem for the laterally graded medium. Now, we will derive the closed form expressions for the contact stresses and contact force assuming that the contact is between the circular stamp and the homogeneous half – plane. The nonhomogeneity constant is zero for the homogeneous half – plane, i.e.,

$$\gamma = \gamma^* = \gamma^{**} = 0 \tag{130}$$

Then, the governing equations can be written as:

$$\frac{1}{\pi}\int_{-1}^{1}\frac{\overline{P}_1(r)}{s-r}dr-\eta\frac{\kappa-1}{\kappa+1}\overline{P}_1(s)=\frac{4}{\kappa+1}\left\{\frac{c}{R}-\frac{b-a}{2R}s-\frac{b+a}{2R}\right\},$$

$$-1<s<1, \tag{131a}$$

$$\int_{-1}^{1}\overline{P}_1(s)ds=-\frac{2P}{\mu_0(b-a)}, \tag{131b}$$

$$\overline{P}_1(s)=\frac{\sigma_{xx}\left(0,\frac{b-a}{2}s+\frac{b+a}{2}\right)}{\mu_0}. \tag{131c}$$

Again, we assume a solution of the form:

$$\overline{P}_1(s)=(1-s)^{\beta_1}(1+s)^{\beta_2}\sum_{n=0}^{\infty}A_nP_n^{(\beta_1,\beta_2)}(s) \tag{132}$$

where β_1 and β_2 are given by equation (114). Substituting (132) in (131a) and integrating in closed form using equation (63), we obtain:

$$\frac{2}{\sin(\pi\beta_1)}\sum_{n=0}^{\infty}A_nP_{n+1}^{(-\beta_1,-\beta_2)}(s)=\frac{4}{\kappa+1}\left\{\frac{c}{R}-\frac{b-a}{2R}s-\frac{b+a}{2R}\right\}. \tag{133}$$

Right hand side of equation (133) can be expressed in terms of the Jacobi polynomials and then (133) reduces to:

$$\frac{2}{\sin(\pi\beta_1)}\sum_{n=0}^{\infty}A_nP_{n+1}^{(-\beta_1,-\beta_2)}(s)=$$

$$\frac{4}{\kappa+1}\left\{\frac{c}{R}-\frac{b-a}{R}\left(\beta_1-\frac{1}{2}\right)-\frac{b+a}{2R}\right\}-\frac{4}{\kappa+1}\frac{b-a}{R}P_1^{(-\beta_1,-\beta_2)}(s) \tag{134}$$

Now, we multiply this equation by $(1-s)^{-\beta_1}(1+s)^{-\beta_2}$ and integrate from $s=-1$ to $s=1$. Using the integral identities given in Erdoğan [29] following result is obtained:

$$\frac{c}{R}-\frac{b-a}{R}\left(\beta_1-\frac{1}{2}\right)-\frac{b+a}{R}=0. \tag{135}$$

Equation (135) gives the relationship between *c*, *b* and *a*. Now, the integral equation becomes:

$$\frac{2}{\sin(\pi\beta_1)}\sum_{n=0}^{\infty}A_n P_{n+1}^{(-\beta_1,-\beta_2)}(s)=-\frac{4}{\kappa+1}\frac{b-a}{R}P_1^{(-\beta_1,-\beta_2)}(s), \qquad -1<s<1 \tag{136}$$

Equating the coefficients of the Jacobi polynomials on both sides, we get,

$$A_1=A_2=\mathrm{K}=A_n=0 \tag{137a}$$

$$A_0=-\frac{2\sin(\pi\beta_1)}{\kappa+1}\frac{b-a}{R} \tag{137b}$$

Hence, normalized contact stress distribution can be written as

$$\overline{P}_1(s)=-\frac{2\sin(\pi\beta_1)}{\kappa+1}\frac{b-a}{R}(1-s)^{\beta_1}(1+s)^{\beta_2}, \qquad -1<s<1. \tag{138}$$

Substituting (138) in (131b) and evaluating the integral in closed form using the expression given in [29], normalized contact force is determined as:

$$\frac{P}{\mu_0(b-a)}=\frac{2\beta_1(1-\beta_1)\pi}{\kappa+1}\frac{b-a}{R}. \tag{139}$$

Note that, for the homogeneous half-plane, contact force P, is a parabolic function of the size of the contact region (b-a). In order to implement the numerical methods developed in this chapter, a computer program is developed using Visual Fortran language. In the following chapter, we give detailed results of our parametric analyses of the contact mechanics problems considered in this study.

CHAPTER IV

RESULTS

The numerical results obtained are presented in this chapter. In all the numerical results, κ is assumed to be equal to 2. Since we are mainly interested in the effect of the nonhomogeneity constants on the contact stress distribution and also since the effect of the Poisson's ratio is not very significant, we fixed the value of κ as 2. This corresponds to a Poisson's ratio of 0.25 if the problem is considered to be plane strain and to 0.33 if we have a situtation of plane stress. This chapter consists of four subsections. In section 4.1 we give the comparisons of the results for the graded medium with a very small nonhomogeneity constant to the results obtained by using the closed form solutions for the homogeneous half – plane. In section 4.2, our results are compared to the results obtained by a finite element model which are provided by [30]. Detailed parametric studies for flat, triangular and circular stamps are given in sections 4.3, 4.4 and 4.5, respectively. Further comments on the results provided in this section are given in Chapter 5.

4.1.Comparisons of the Results to the Closed Form Solutions

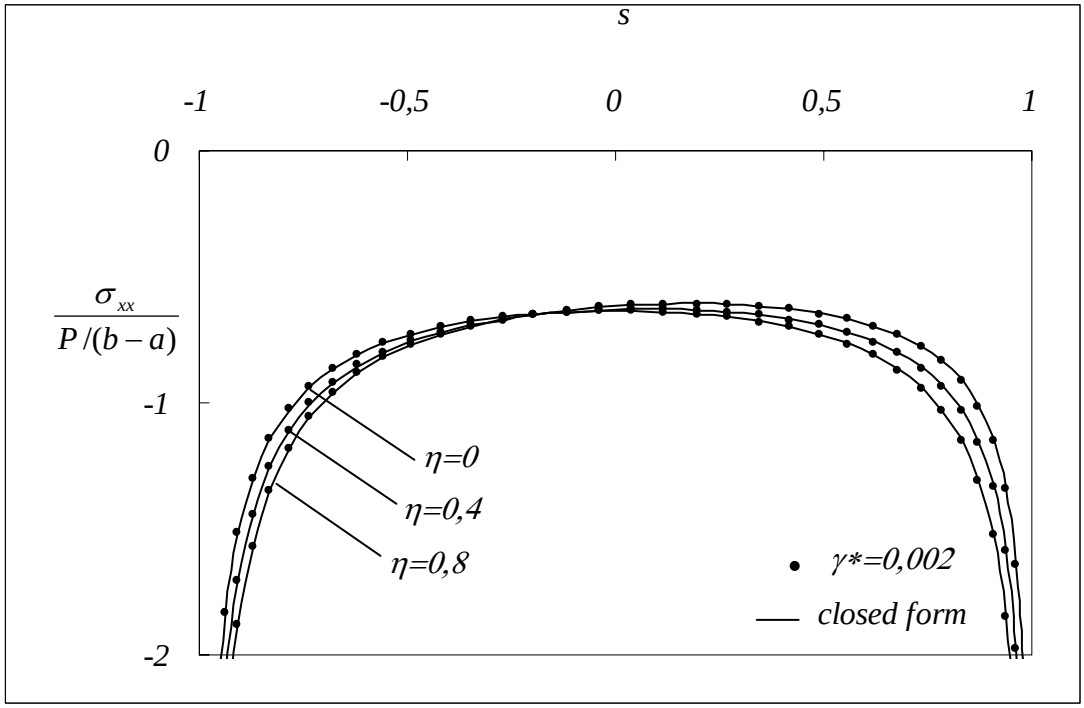

Figure 7: Comparison of the contact stress distribution for various friction coefficients for the flat stamp.

Table 1: Comparison of the results for the normalized force for the triangular stamp.

	Normalized Force ($\frac{P}{\mu_0 m(b-a)}$)	
η	Graded (γ^*=0.002)	Closed form
0	2.0944	2.0934
0.2	2.1832	2.1821
0.4	2.2711	2.2700
0.8	2.4419	2.4405

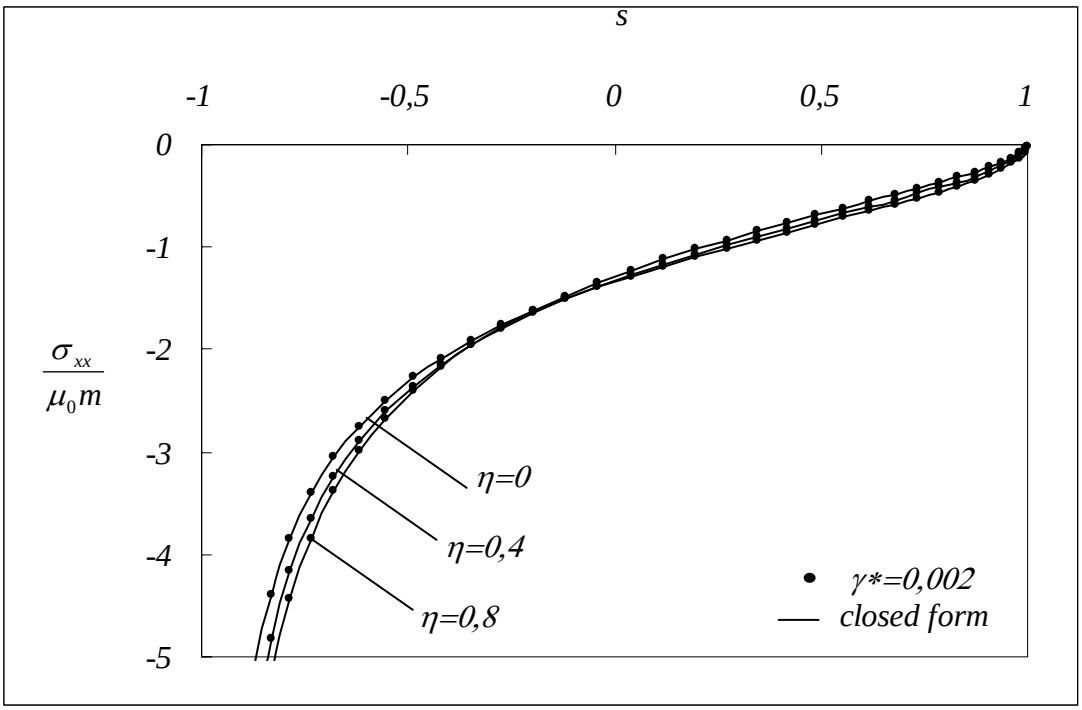

Figure 8: Comparison of the contact stress distribution for various friction coefficients for the triangular stamp.

Table 2: Comparison of the results for the normalized force for the circular stamp. (a/R = -0.05 , b/R = 0.05)

	Normalized Force ($\frac{P}{\mu_0 (b-a)}$)	
η	Graded (γ^*=0.002)	Closed form
0	0.0524	0.0524
0.4	0.0520	0.0520
0.8	0.0509	0.0509

Table 3: Comparison of the results for the location of the centerline for the circular stamp. (a/R = -0.05 , b/R = 0.05)

	Location of the centerline (c/R)	
η	Graded (γ^*=0.002)	Closed form
0	0	0
0.4	0.00421	0.00422
0.8	0.00828	0.00829

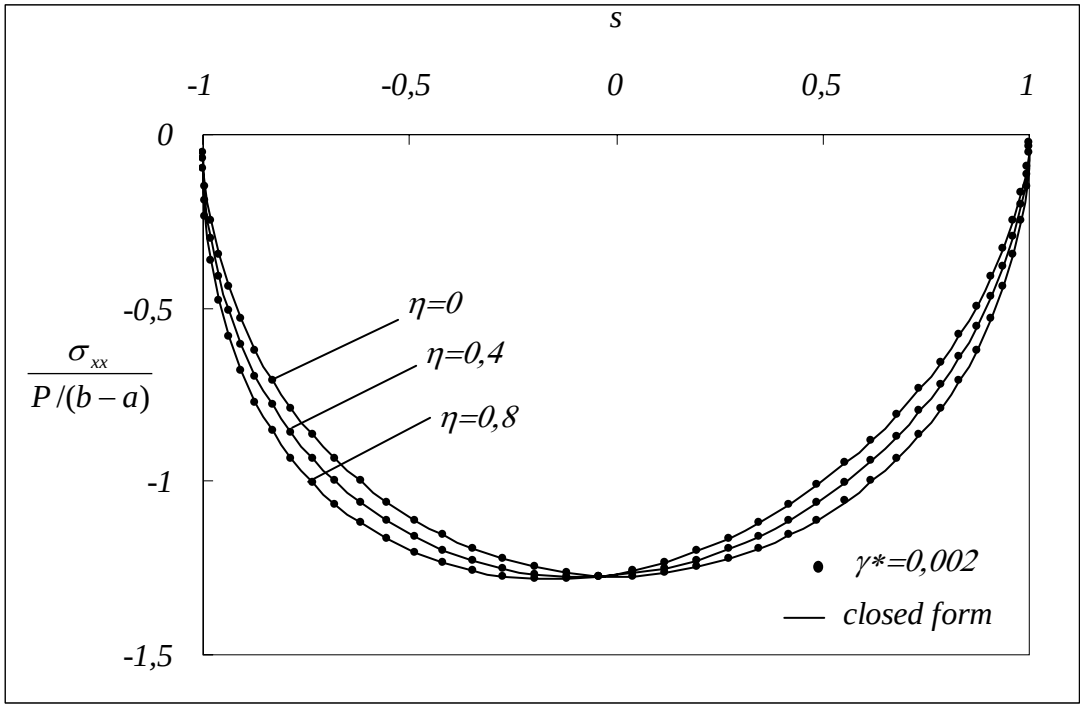

Figure 9: Comparison of the contact stress distribution for various friction coefficients for the circular stamp. (a/R = -0,05 , b/R = 0,05)

4.2.Comparisons to the FEA Results

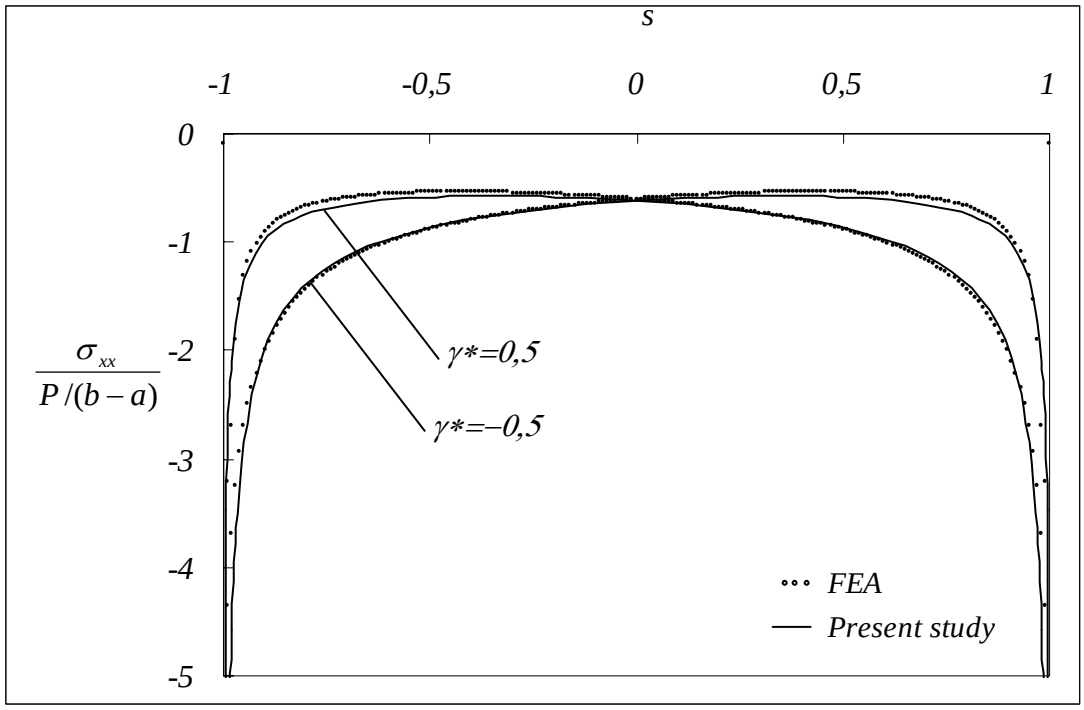

Figure 10: Comparison of the contact stress distribution to FEA results [30] for different values of γ^* for flat stamp. ($\gamma^{**}=0, \eta=0$)

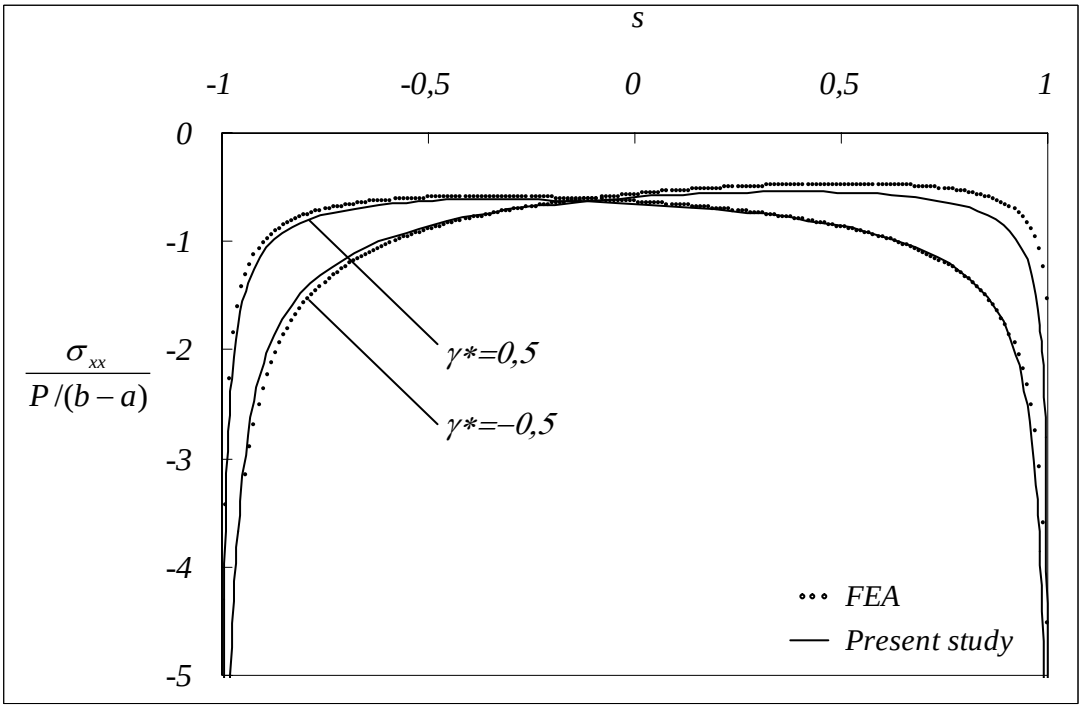

Figure 11: Comparison of the contact stress distribution to FEA results [30] for different values of γ^* for flat stamp. ($\gamma^{**}=0, \eta=0{,}4$)

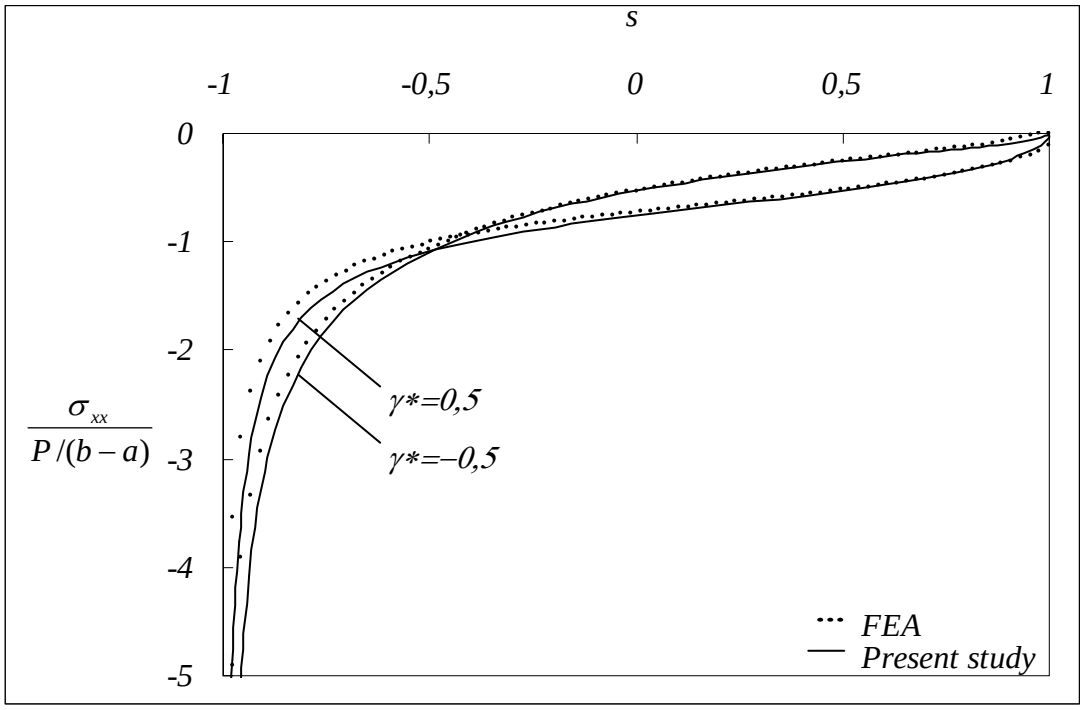

Figure 12: Comparison of the contact stress distribution to FEA results [30] for different values of γ^* for triangular stamp. ($\gamma^{**}=0, \eta=0$)

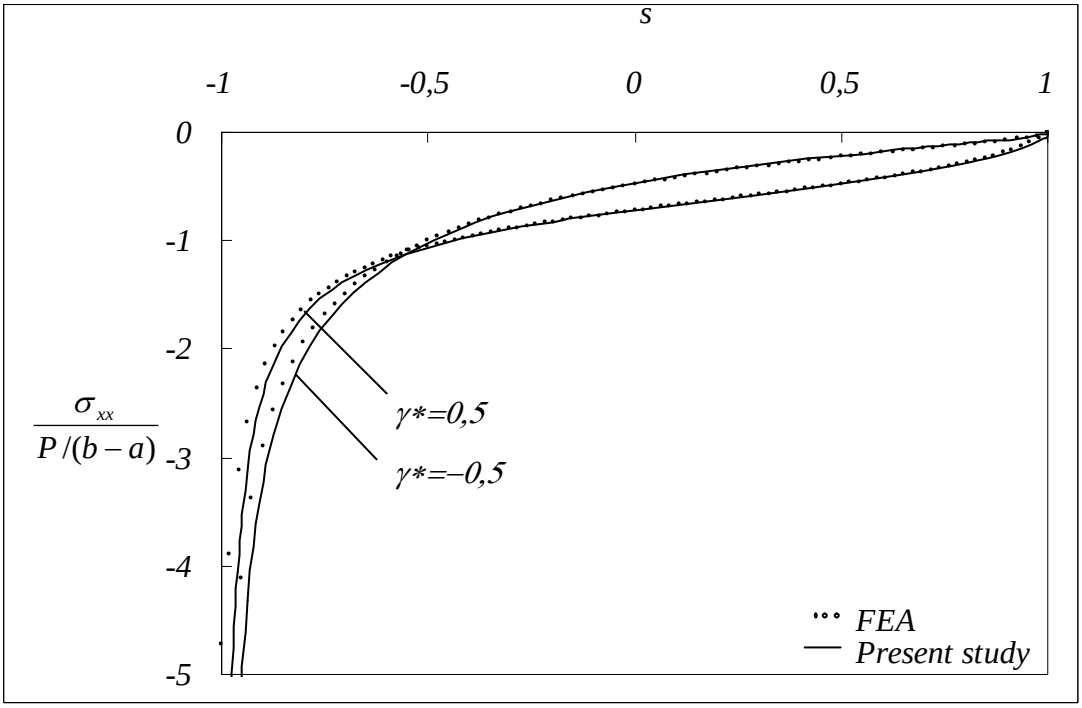

Figure 13: Comparison of the contact stress distribution to FEA results [30] for different values of γ^* for triangular stamp. ($\gamma^{**}=0, \eta=0{,}4$)

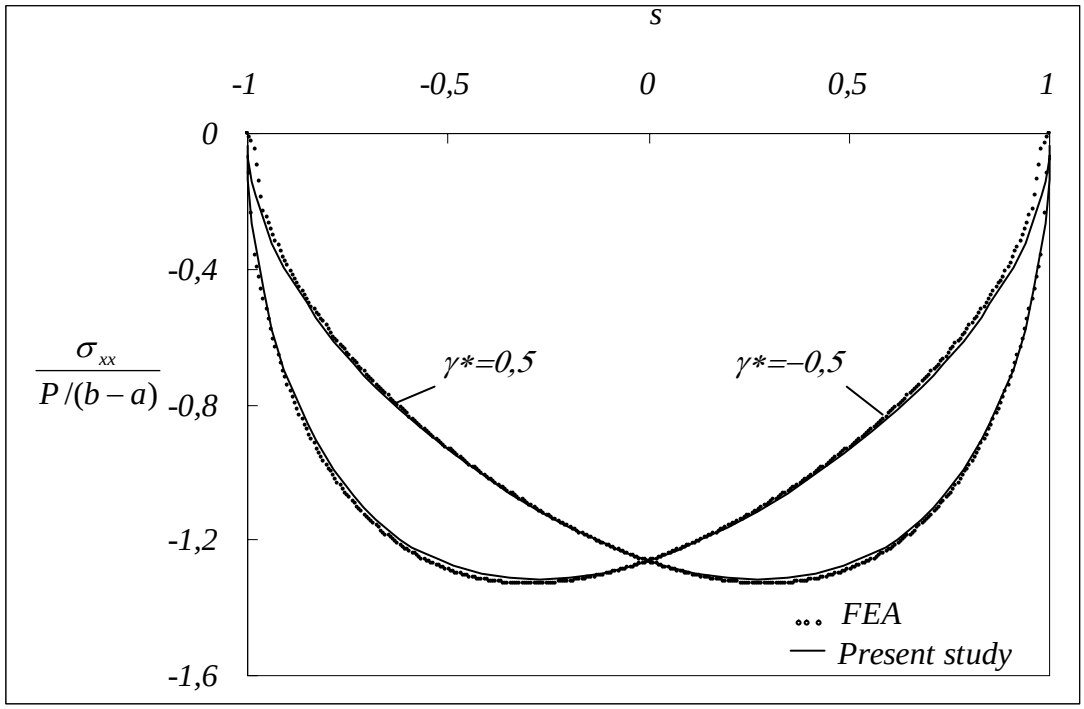

Figure 14: Comparison of the contact stress distribution to FEA results [30] for different values of γ^* for circular stamp. ($\gamma^{**} = 0, \eta = 0$, *a/R* = -0,05 , *b/R* = 0,05)

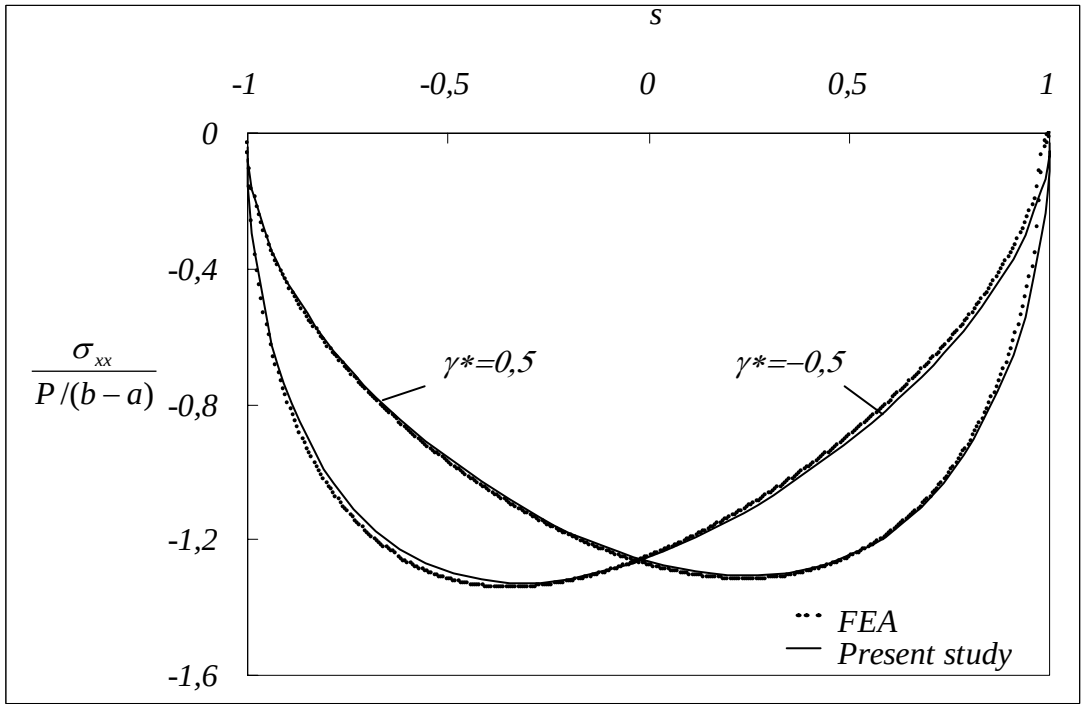

Figure 15: Comparison of the contact stress distribution to FEA results [30] for different values of γ^* for circular stamp.($\gamma^{**} = 0, \eta = 0{,}2$, *a/R* = -0,05,*b/R* = 0,05)

Table 4: Normalized force values for the results given in Figures 12 and 13.

	Normalized Force ($\frac{P}{\mu_0 m(b-a)}$)	
γ^*	$\eta = 0$	$\eta = 0.4$
0.5	1.784	1.920
-0.5	2.712	2.778

Table 5: Normalized force values for the results given in Figures 14 and 15.

	Normalized Force ($\frac{P}{\mu_0 (b-a)}$)	
γ^*	$\eta = 0$	$\eta = 0.2$
0.5	0.0539	0.0543
-0.5	0.0539	0.0534

Table 6: *c/R* values for the results given in Figures 14 and 15.

	Location of the centerline (*c/R*)	
γ^*	$\eta = 0$	$\eta = 0.2$
0.5	-0.00355	-0.00177
-0.5	0.00355	0.00526

4.3.Parametric Studies for the Flat Stamp

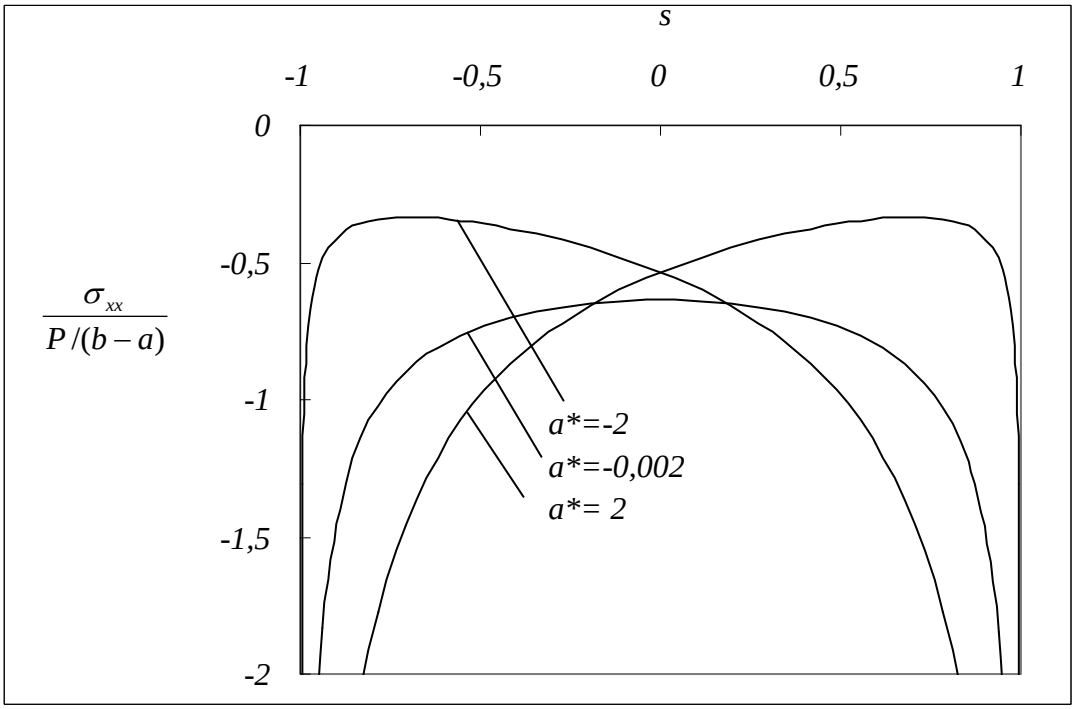

Figure 16: Normalized stress distribution for various values of the nonhomogeneity constant $a^* = \gamma a$. (η=0 and $b^* = \gamma b$ =0)

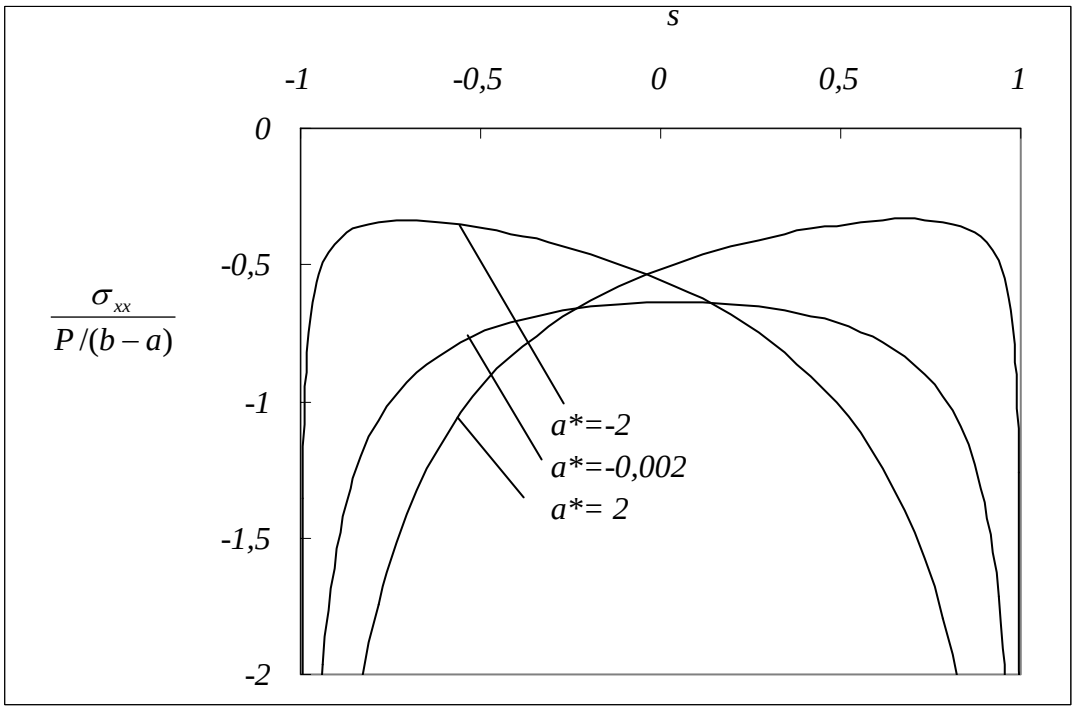

Figure 17: Normalized stress distribution for various values of the nonhomogeneity constant $a^* = \gamma a$. (η=0,2 and $b^* = \gamma b$ =0)

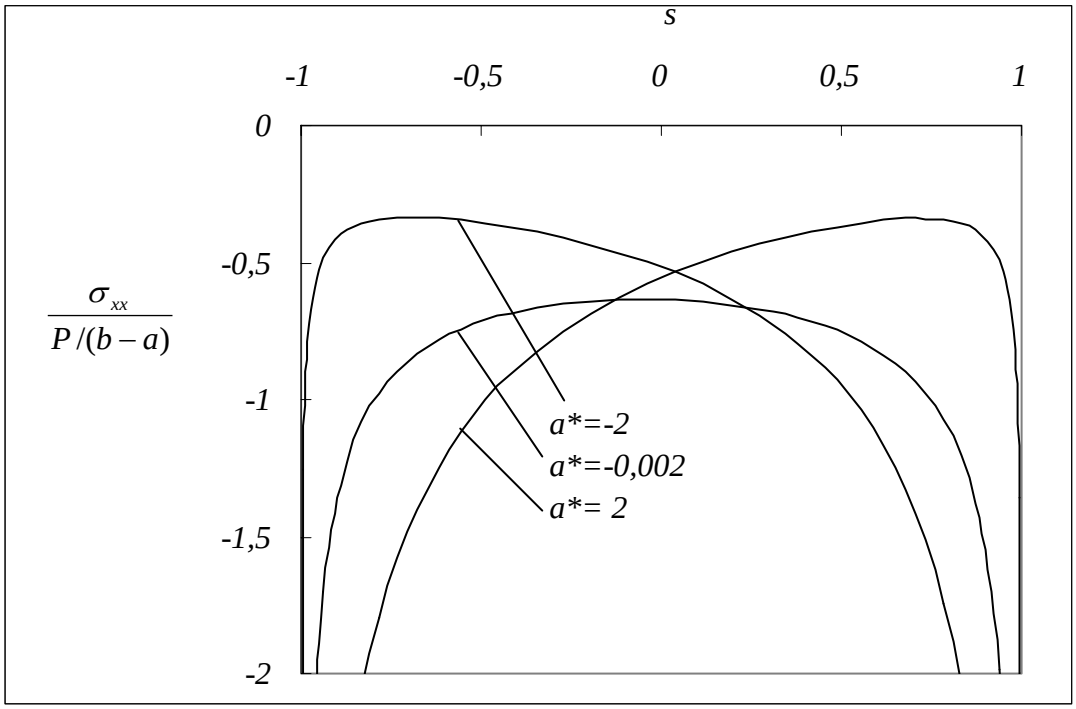

Figure 18: Normalized stress distribution for various values of the nonhomogeneity constant $a^* = \gamma a$. (η= -0,2 and $b^* = \gamma b$ =0)

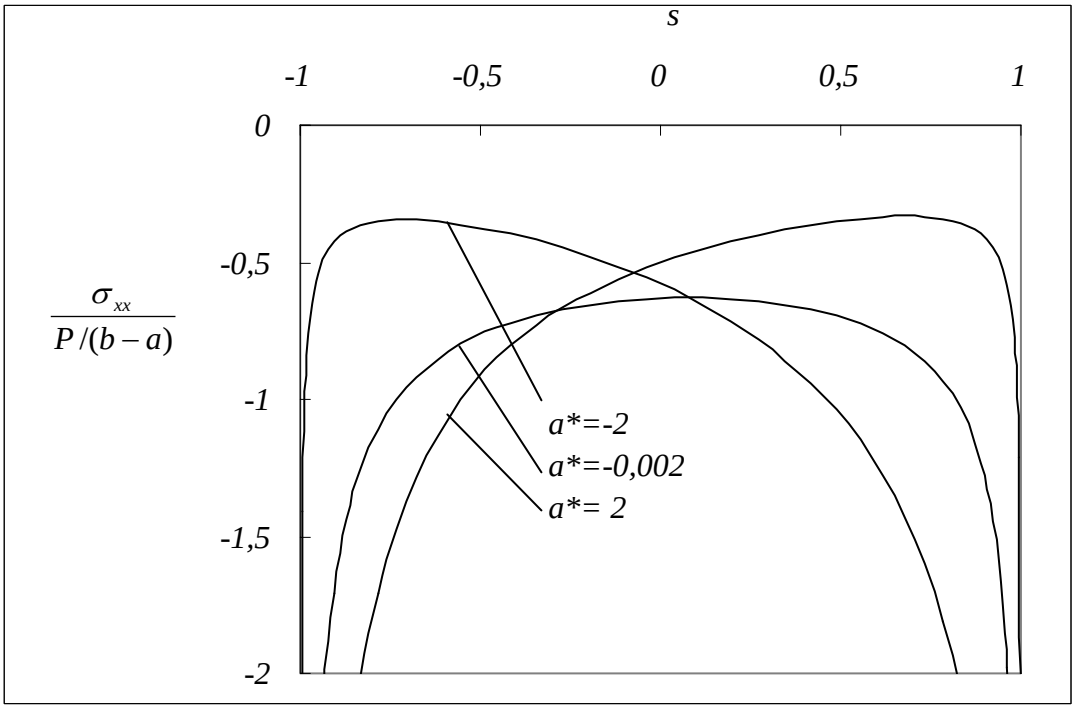

Figure 19: Normalized stress distribution for various values of the nonhomogeneity constant $a^* = \gamma a$. (η= 0,4 and $b^* = \gamma b$ =0)

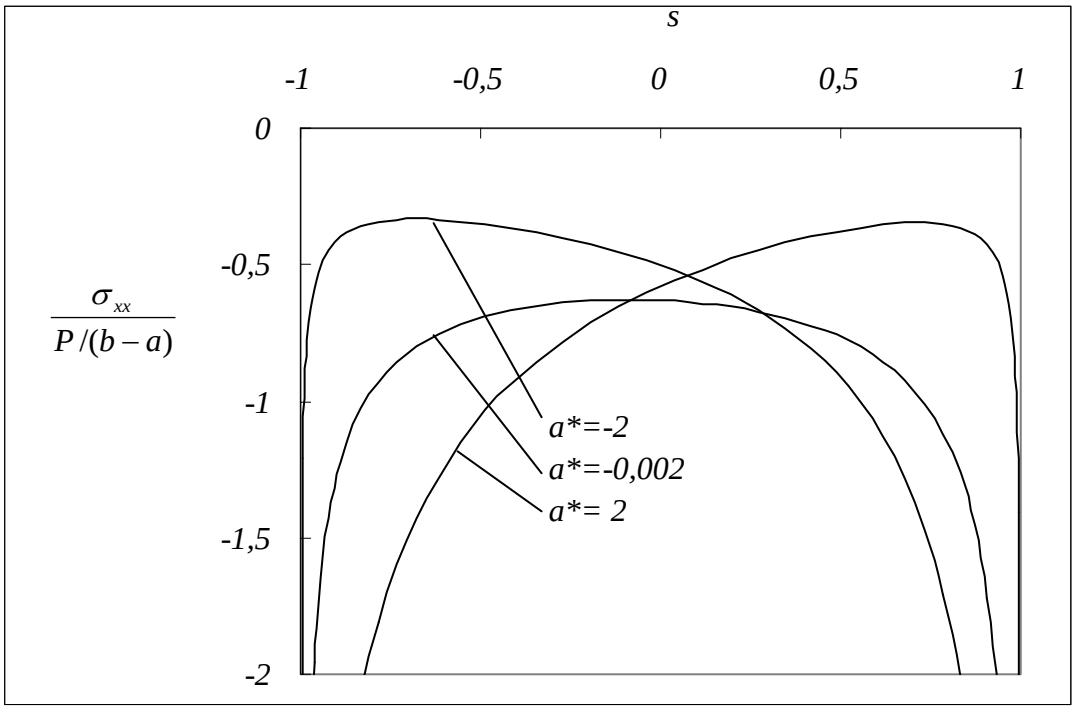

Figure 20: Normalized stress distribution for various values of the nonhomogeneity constant $a^* = \gamma a$. (η= - 0,4 and $b^* = \gamma b$ =0)

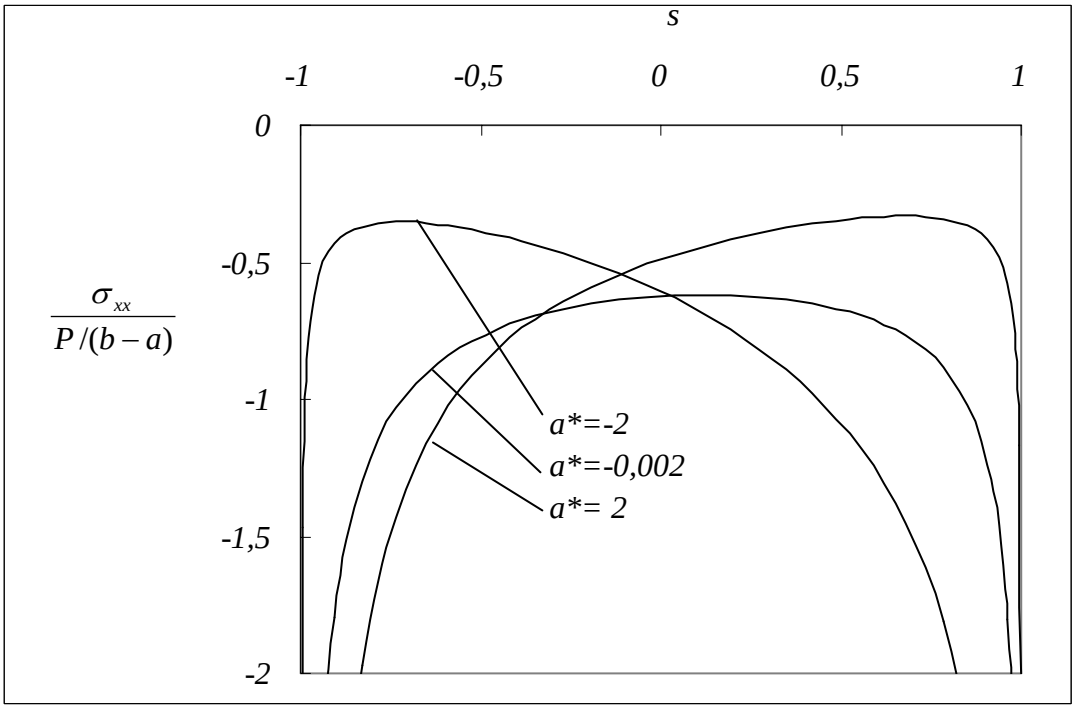

Figure 21: Normalized stress distribution for various values of the nonhomogeneity constant $a^* = \gamma a$. (η= 0,6 and $b^* = \gamma b$ =0)

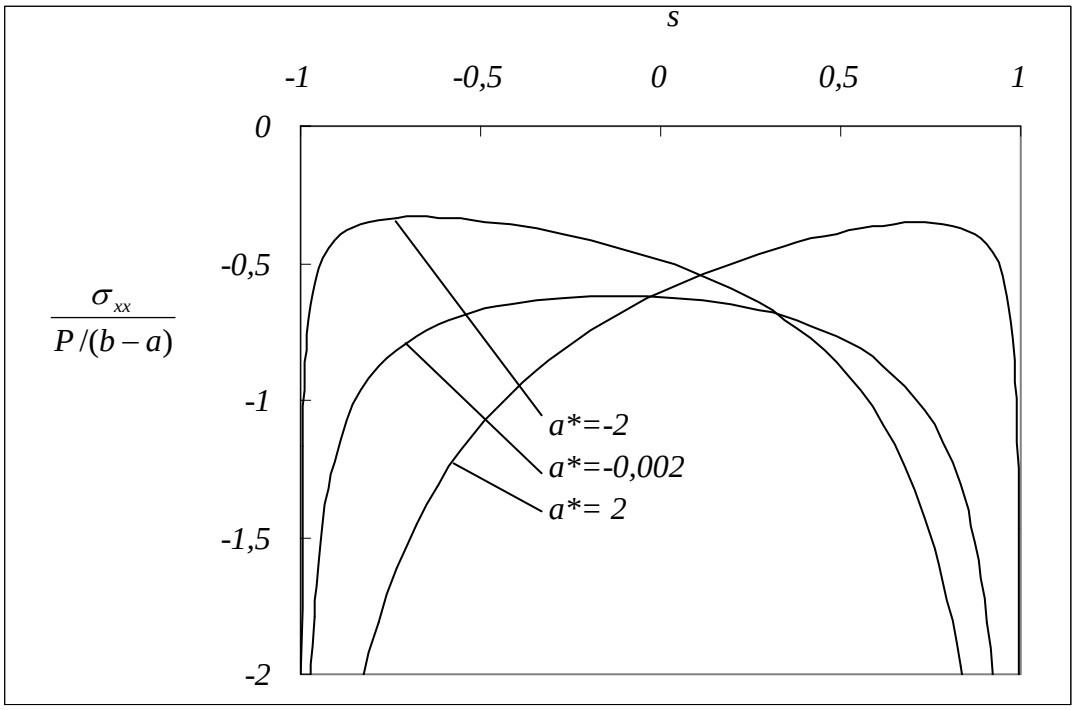

Figure 22: Normalized stress distribution for various values of the nonhomogeneity constant $a^* = \gamma a$. (η= - 0,6 and $b^* = \gamma b$ =0)

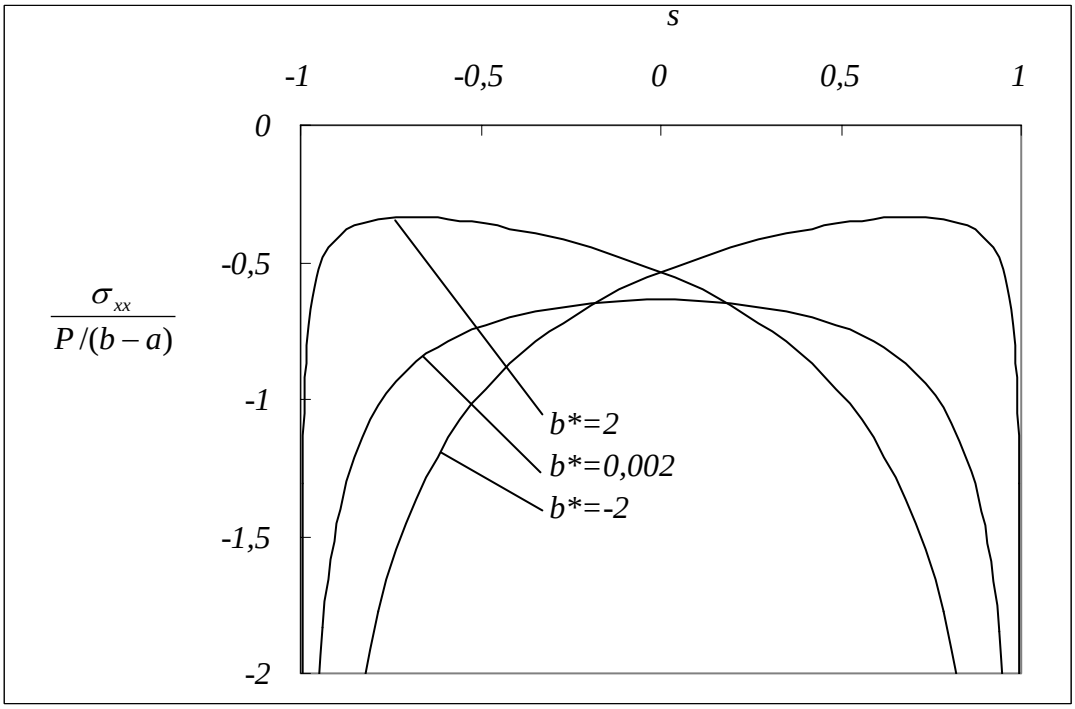

Figure 23: Normalized stress distribution for various values of the nonhomogeneity constant $b^* = \gamma b$. (η= 0 and $a^* = \gamma a$ =0)

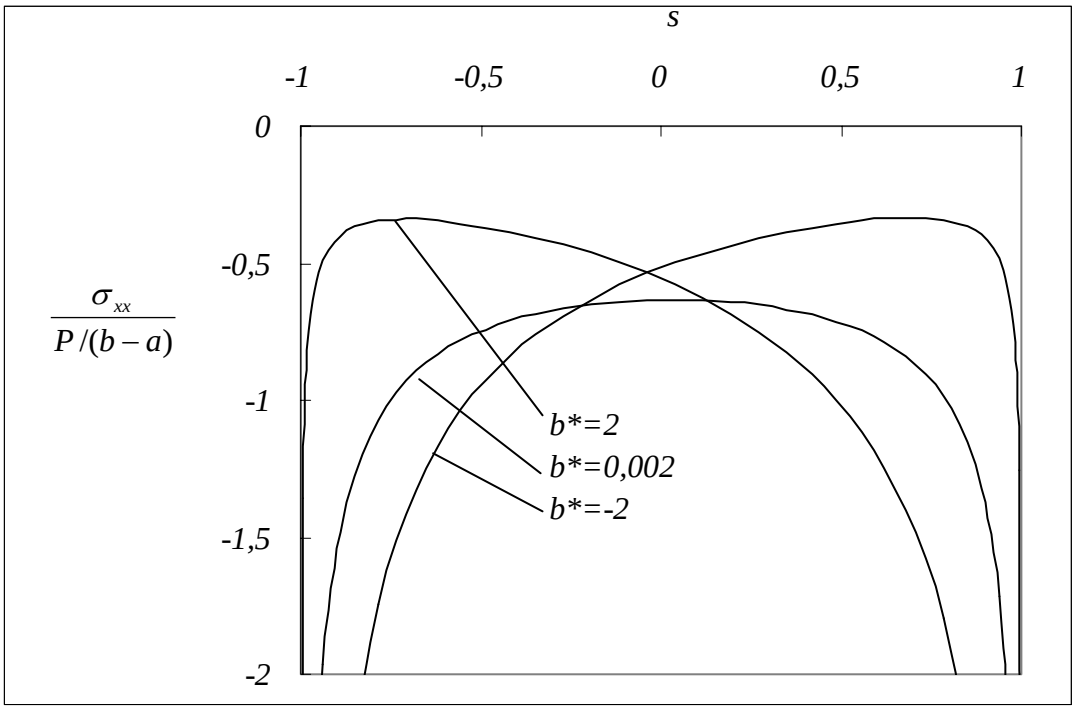

Figure 24: Normalized stress distribution for various values of the nonhomogeneity constant $b^* = \gamma b$. (η= 0,2 and $a^* = \gamma a$ =0)

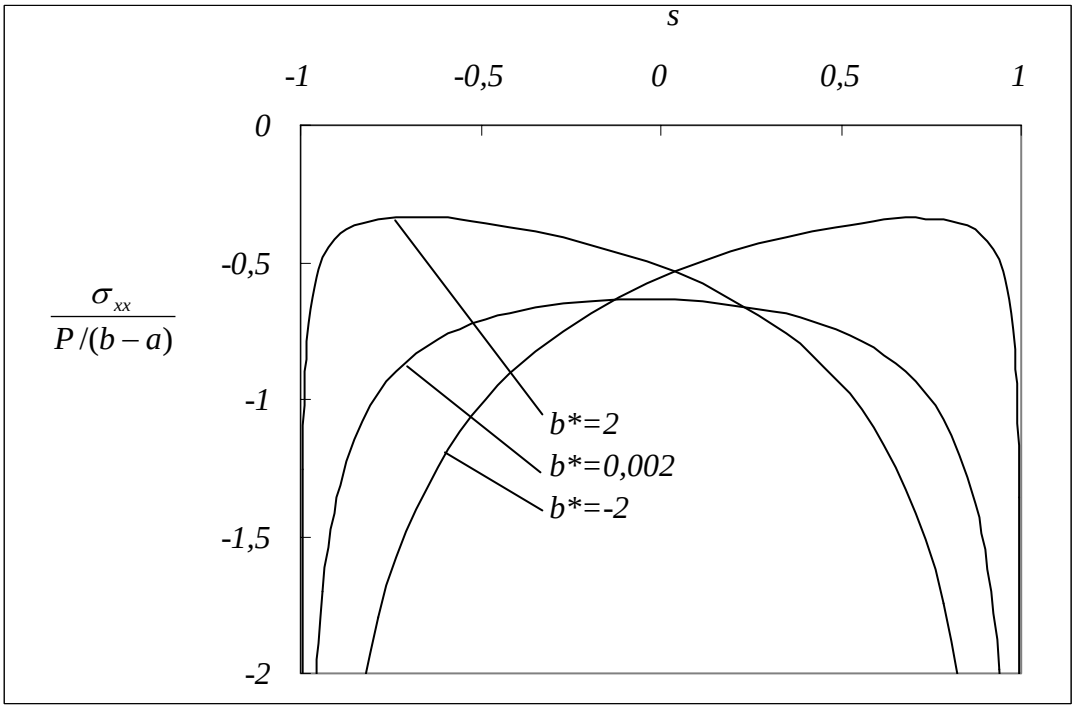

Figure 25: Normalized stress distribution for various values of the nonhomogeneity constant $b^* = \gamma b$. (η= - 0,2 and $a^* = \gamma a$ =0)

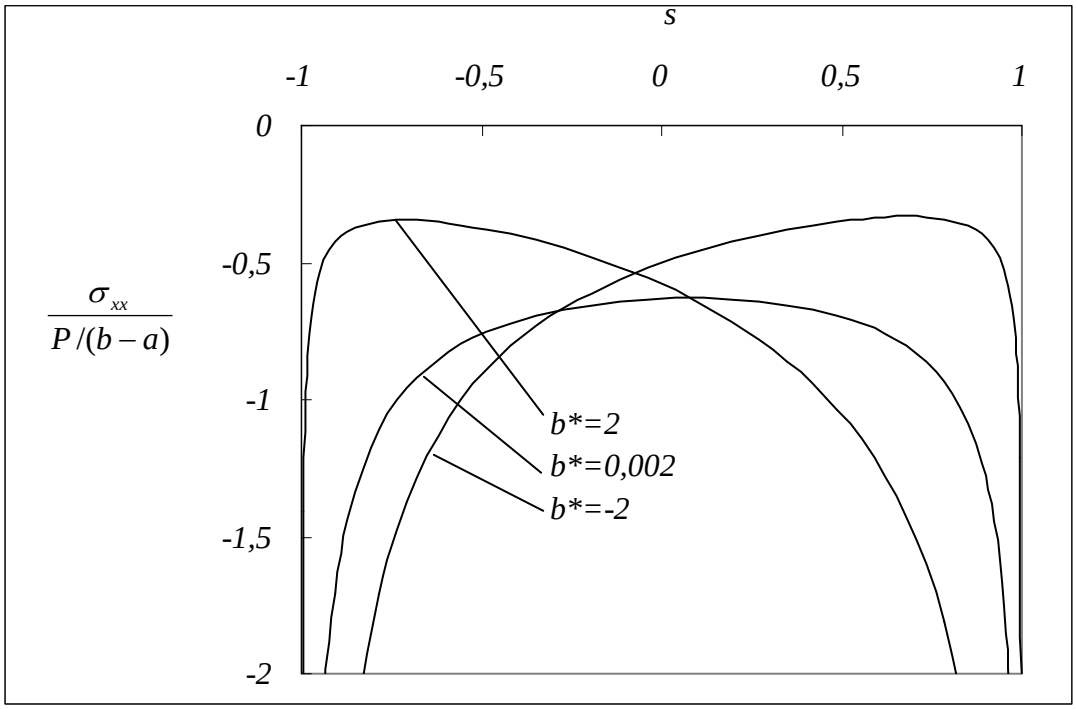

Figure 26: Normalized stress distribution for various values of the nonhomogeneity constant $b^* = \gamma b$. (η= 0,4 and $a^* = \gamma a$ =0)

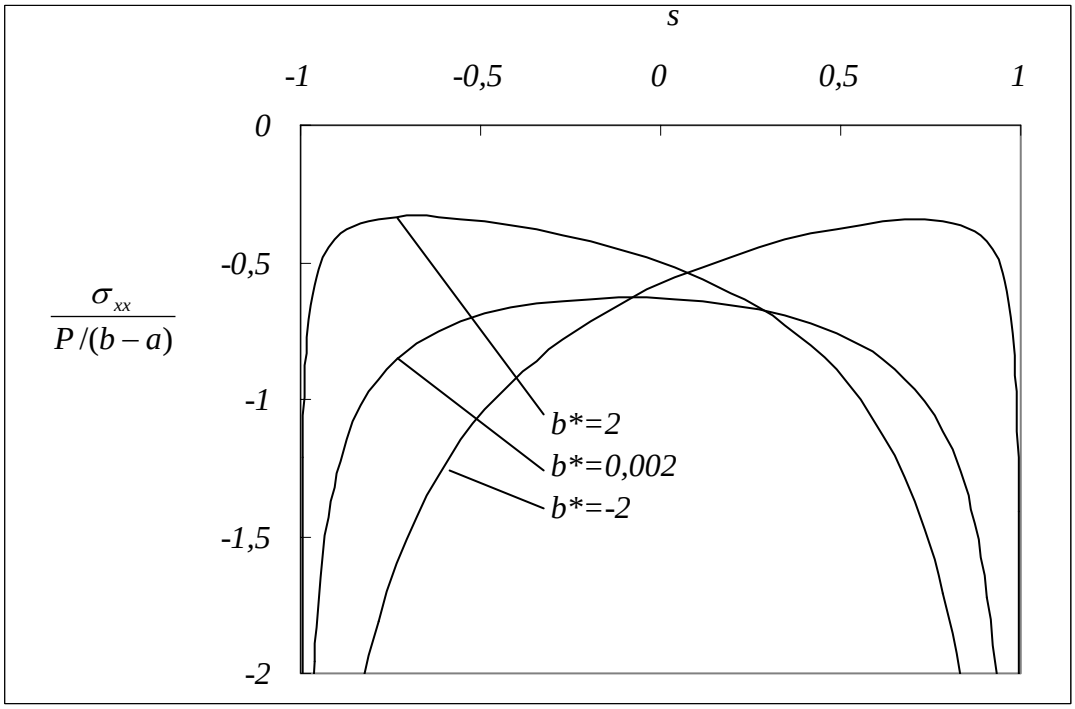

Figure 27: Normalized stress distribution for various values of the nonhomogeneity constant $b^* = \gamma b$. (η= - 0,4 and $a^* = \gamma a$ =0)

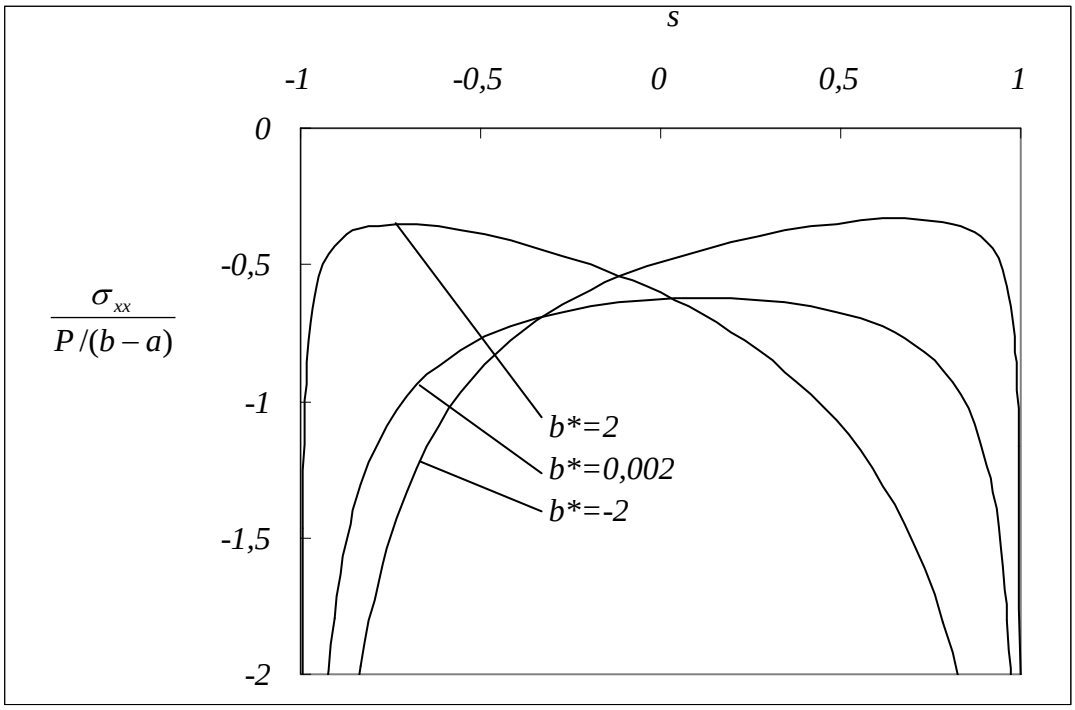

Figure 28: Normalized stress distribution for various values of the nonhomogeneity constant $b^* = \gamma b$. (η= 0,6 and $a^* = \gamma a$ =0)

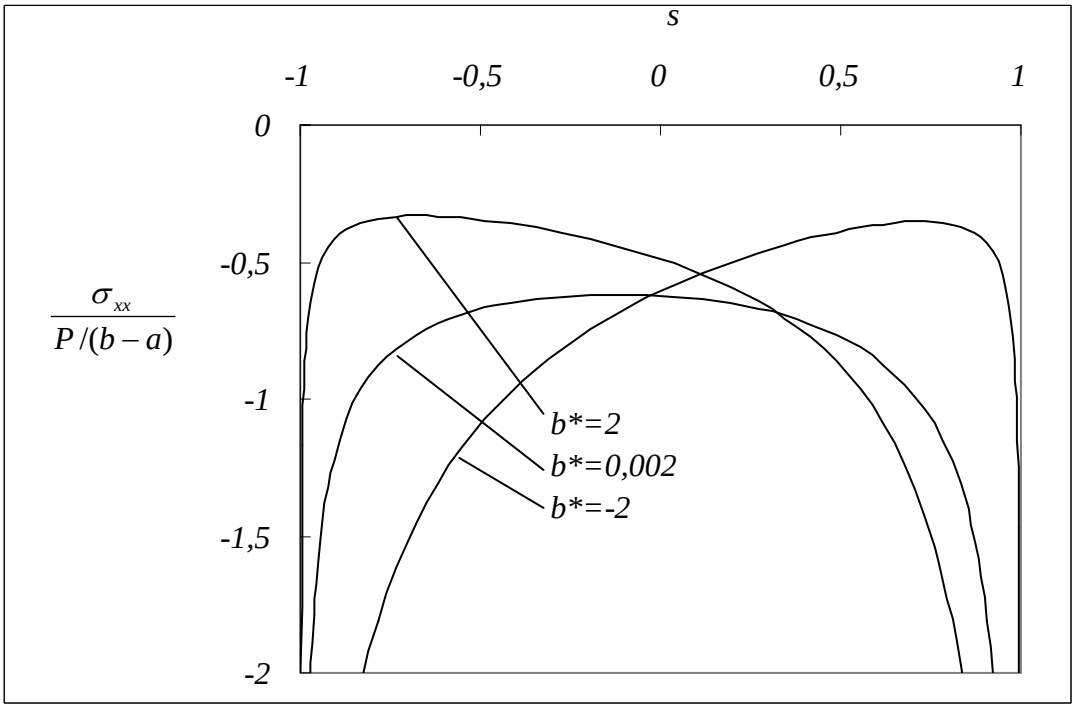

Figure 29: Normalized stress distribution for various values of the nonhomogeneity constant $b^* = \gamma b$. (η= - 0,6 and $a^* = \gamma a$ =0)

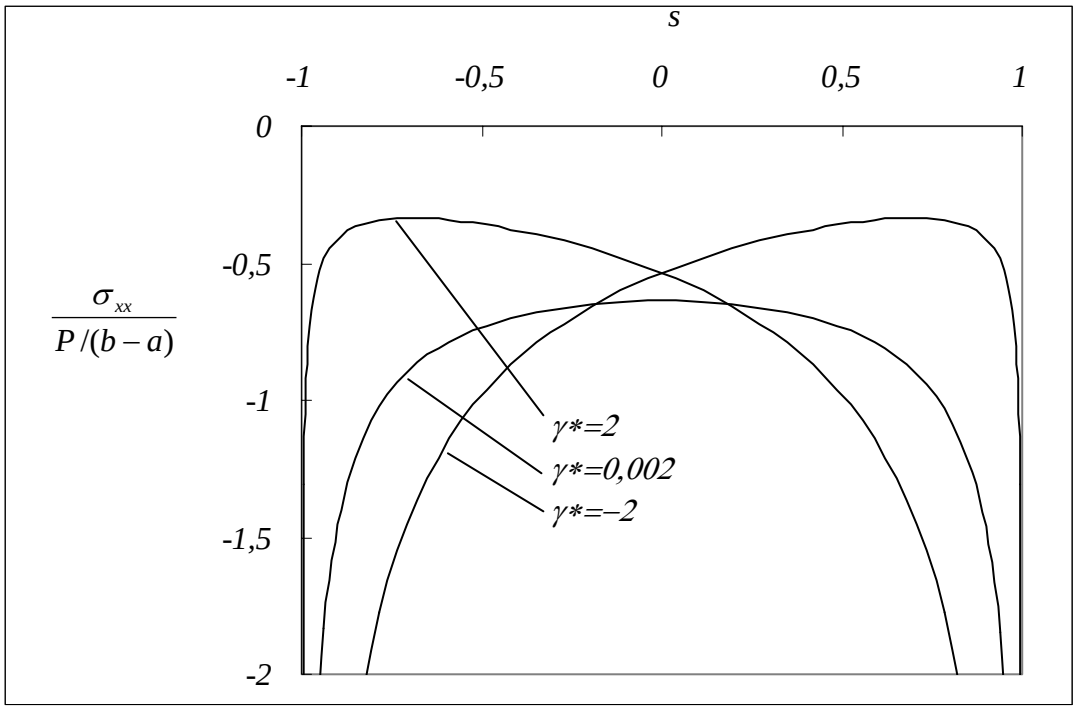

Figure 30: Normalized stress distribution for various values of the nonhomogeneity constant γ^*. (η= 0 and γ**=0)

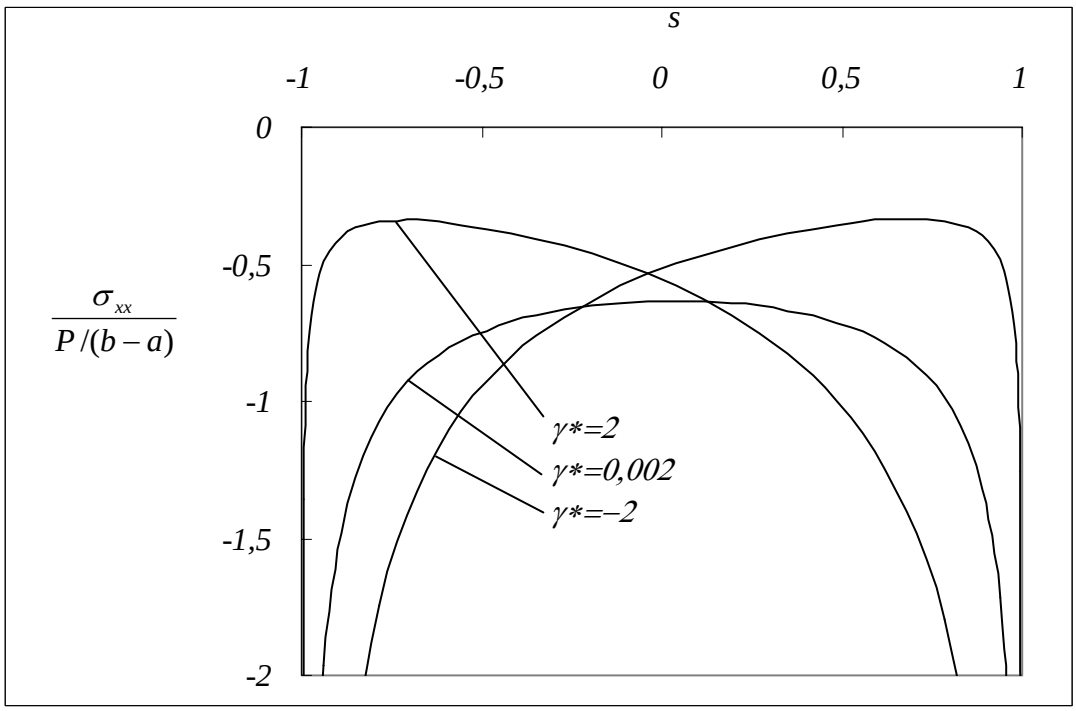

Figure 31: Normalized stress distribution for various values of the nonhomogeneity constant γ^*. (η= 0,2 and γ**=0)

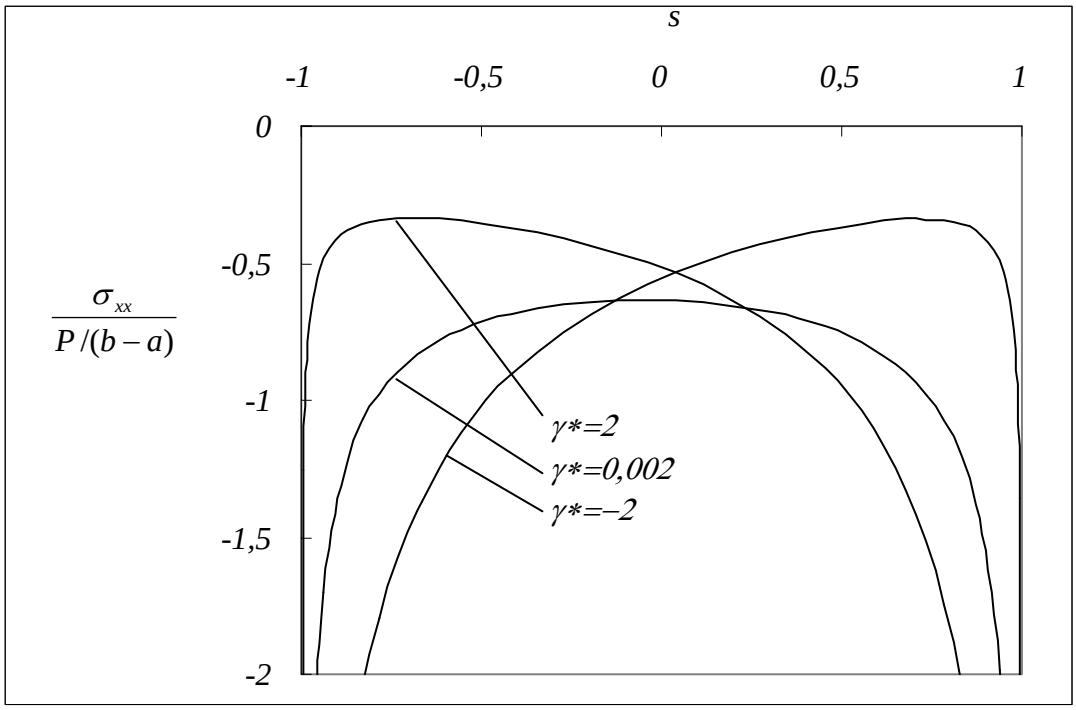

Figure 32: Normalized stress distribution for various values of the nonhomogeneity constant γ^*. (η= - 0,2 and γ^{**}=0)

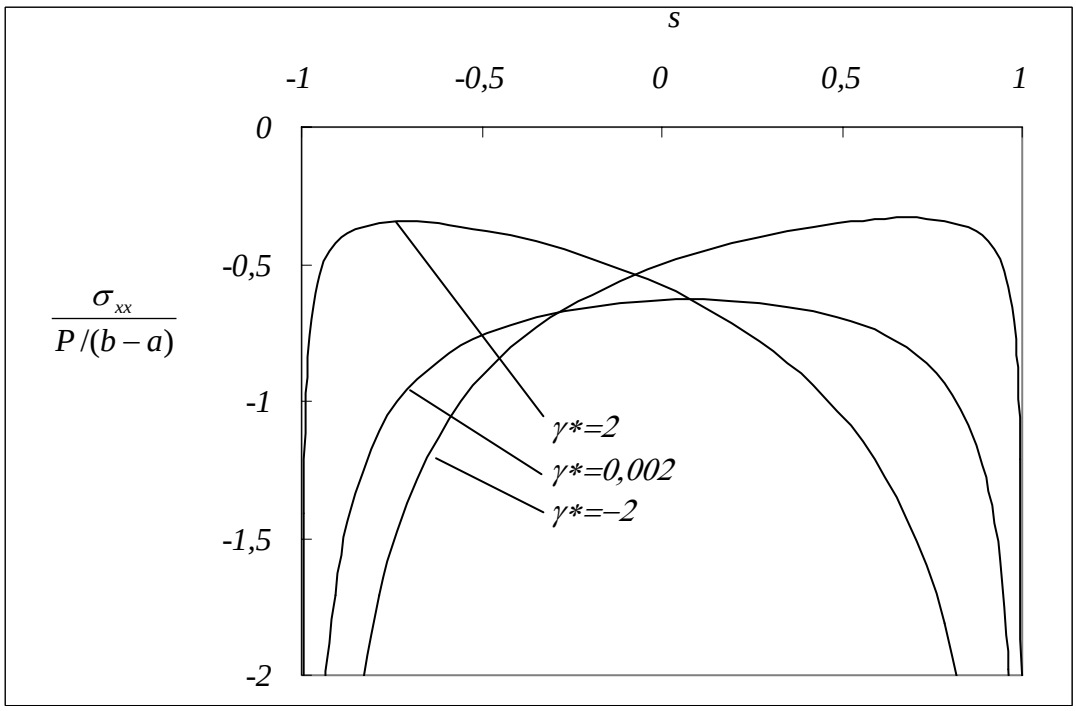

Figure 33: Normalized stress distribution for various values of the nonhomogeneity constant γ^*. (η= 0,4 and γ^{**}=0)

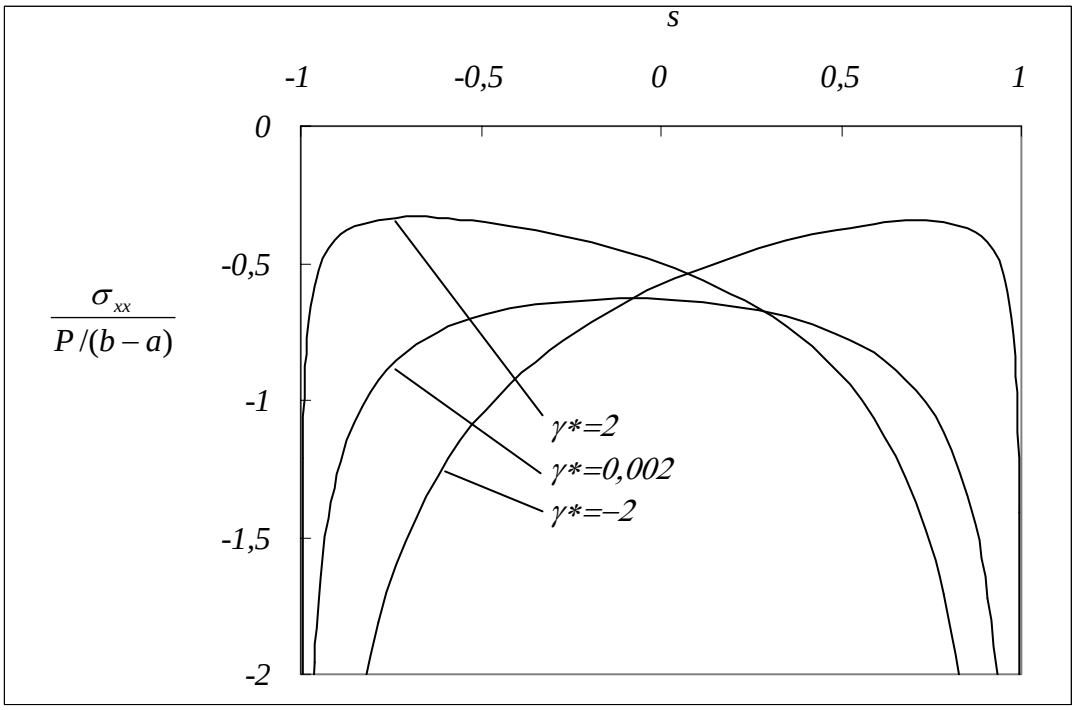

Figure 34: Normalized stress distribution for various values of the nonhomogeneity constant γ^*. (η= - 0,4 and γ^{**}=0)

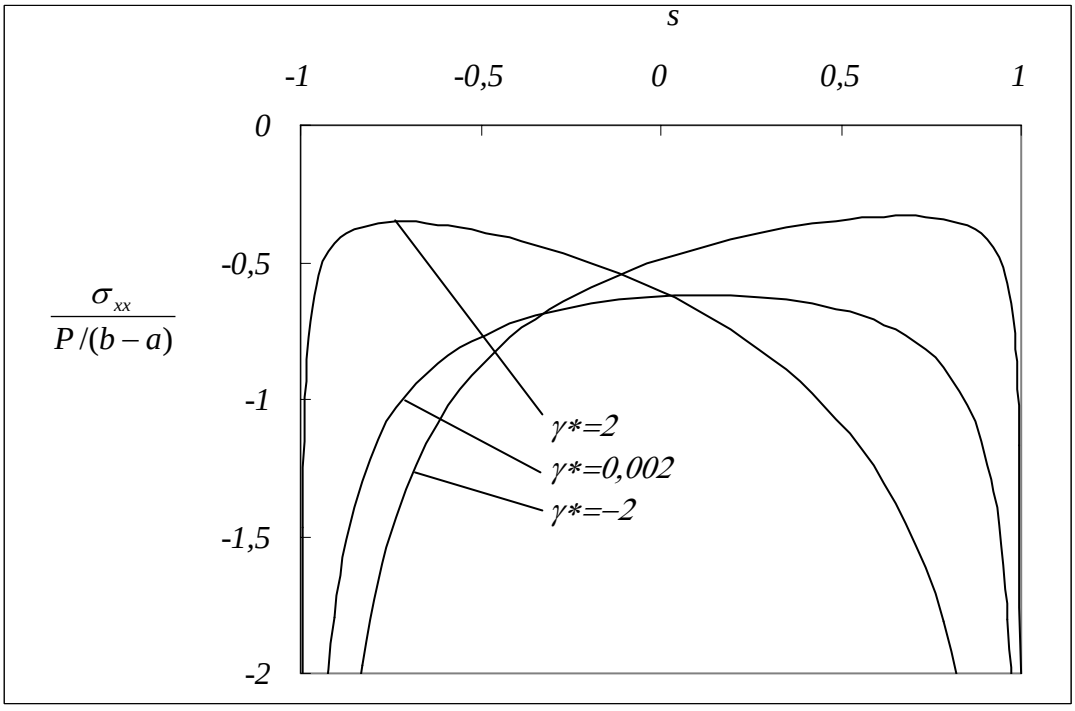

Figure 35: Normalized stress distribution for various values of the nonhomogeneity constant γ^*. (η= 0,6 and γ^{**}=0)

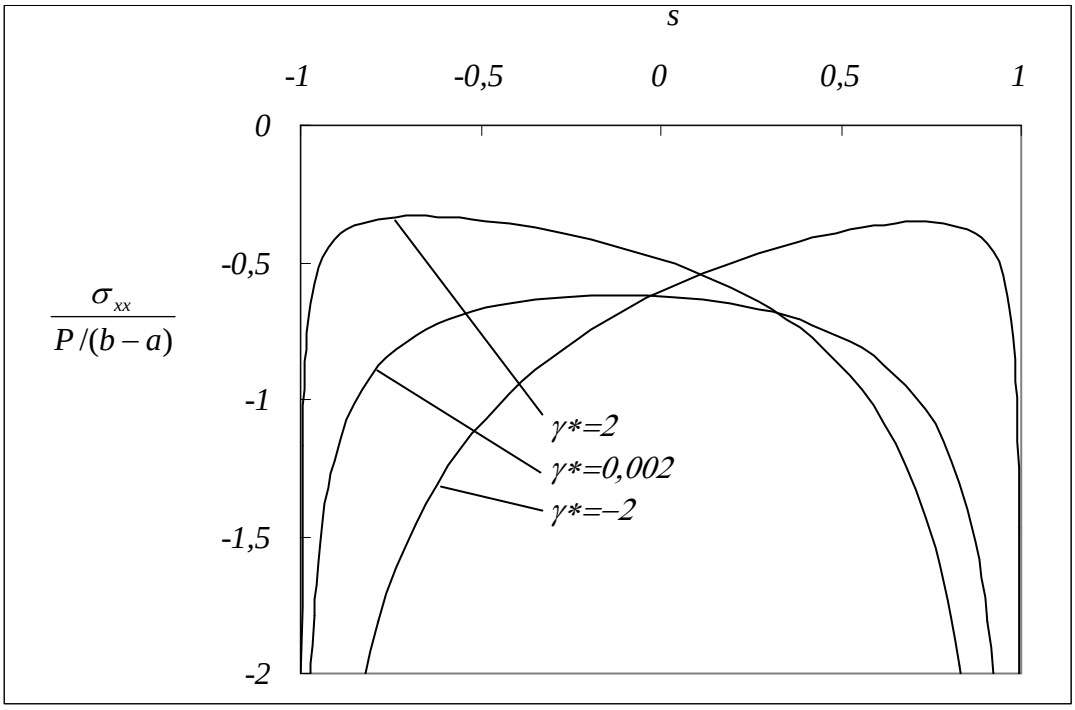

Figure 36: Normalized stress distribution for various values of the nonhomogeneity constant γ^*. (η= - 0,6 and γ^{**}=0)

4.4.Parametric Studies for the Triangular Stamp

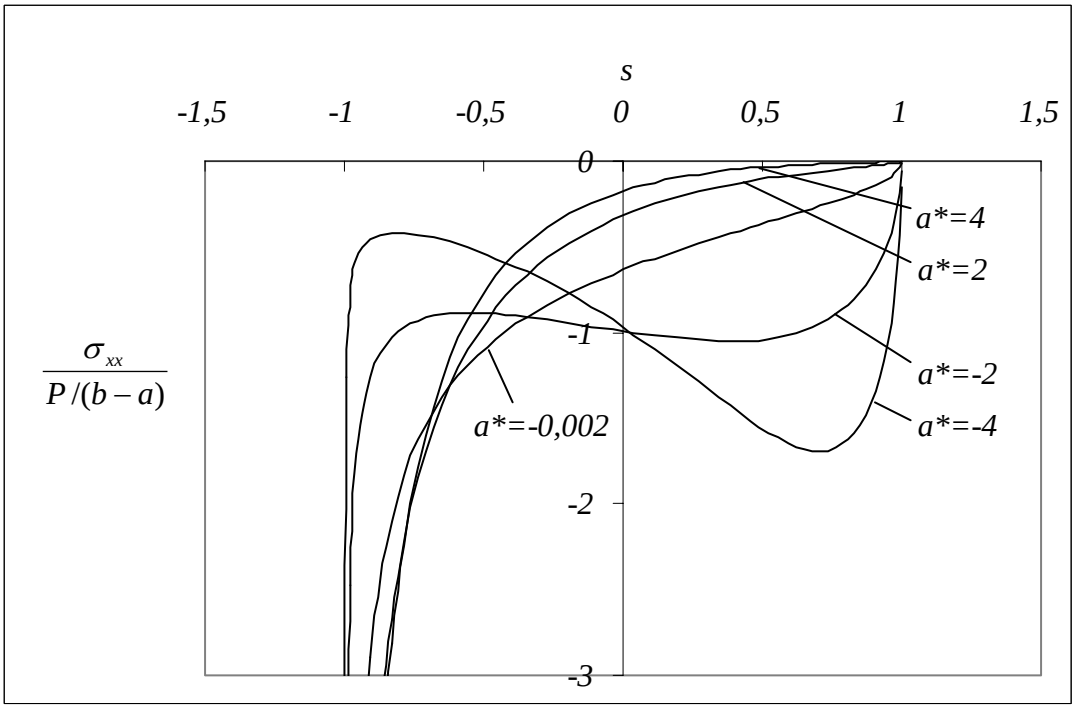

Figure 37: Normalized stress distribution for various values of the nonhomogeneity constant $a^* = \gamma a$. (η=0 and $b^* = \gamma b$ =0)

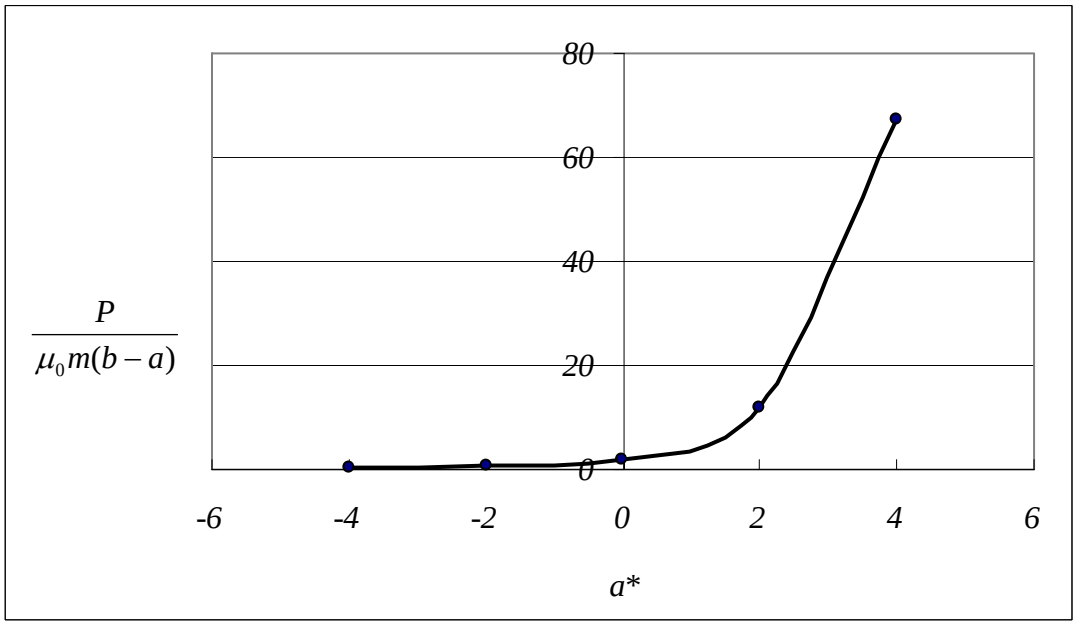

Figure 38: Variation of the normalized force with respect to normalized nonhomogeneity parameter $a^* = \gamma a$. (η=0 and $b^* = \gamma b$ =0)

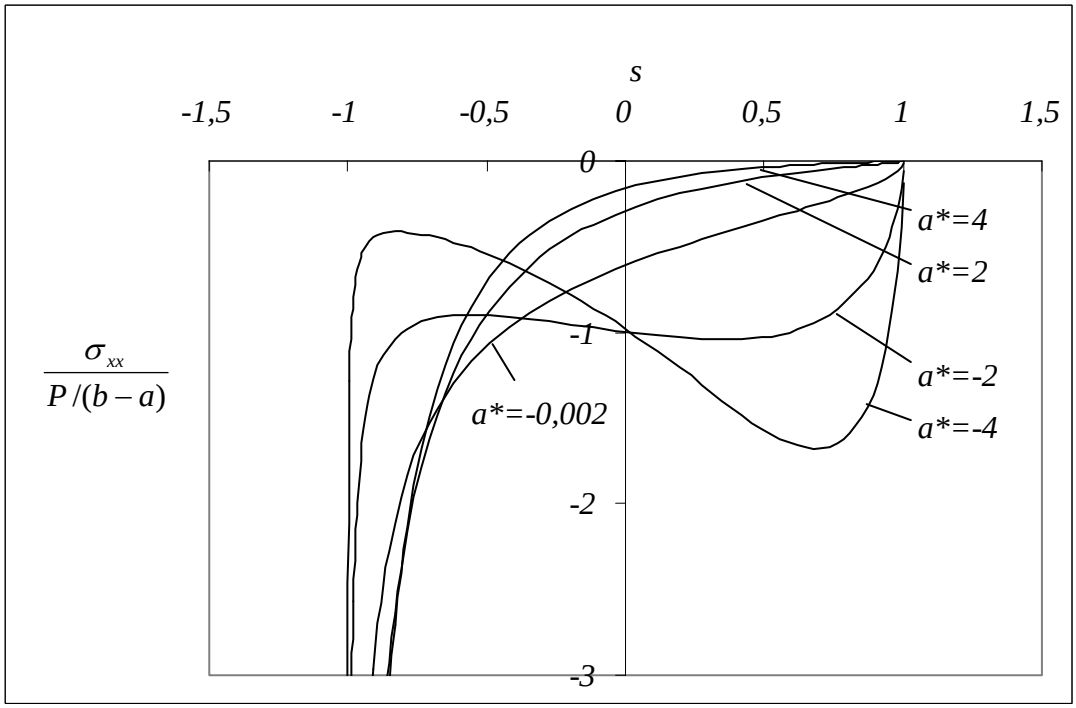

Figure 39: Normalized stress distribution for various values of the nonhomogeneity constant $a^* = \gamma a$. (η=0,2 and $b^* = \gamma b$ =0)

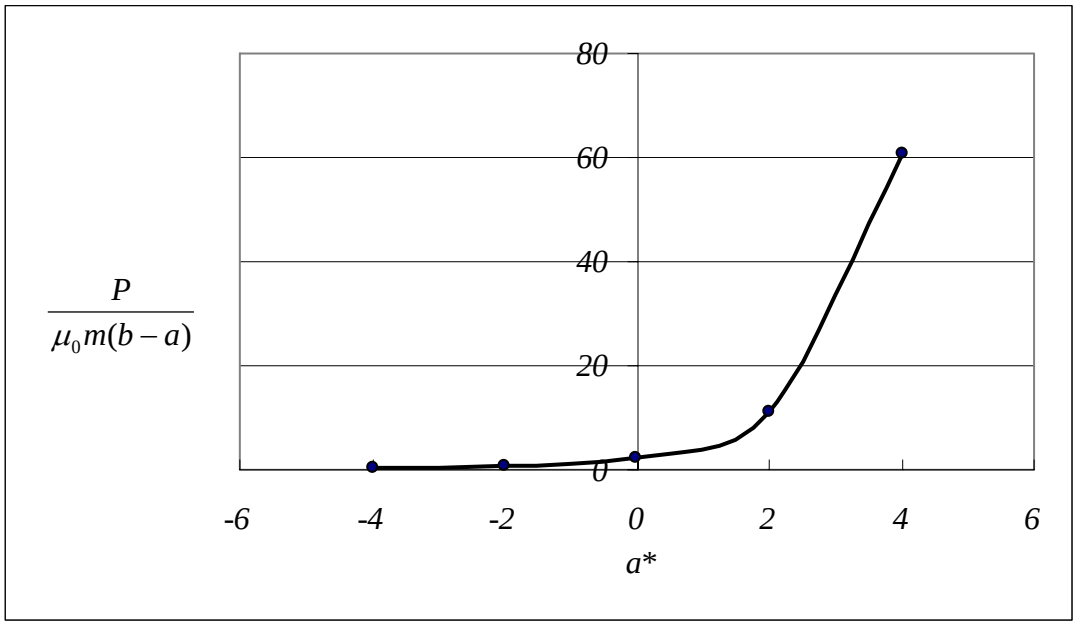

Figure 40: Variation of the normalized force with respect to normalized nonhomogeneity parameter $a^* = \gamma a$. (η=0,2 and $b^* = \gamma b$ =0)

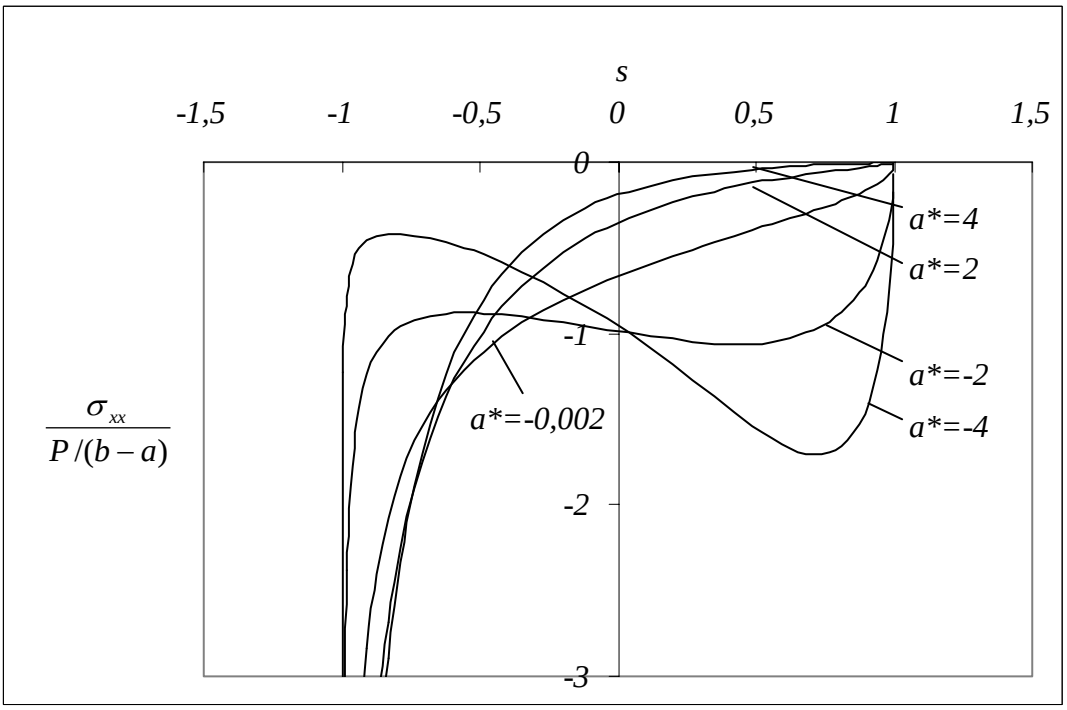

Figure 41: Normalized stress distribution for various values of the nonhomogeneity constant $a^* = \gamma a$. (η= -0,2 and $b^* = \gamma b$ =0)

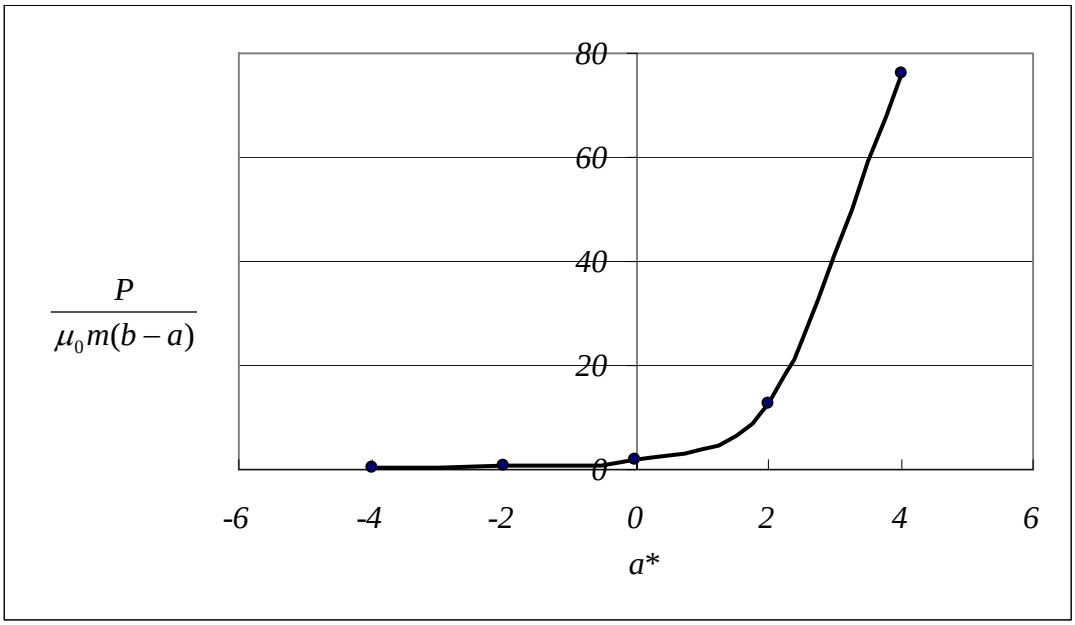

Figure 42: Variation of the normalized force with respect to normalized nonhomogeneity parameter $a^* = \gamma a$. (η= -0,2 and $b^* = \gamma b$ =0)

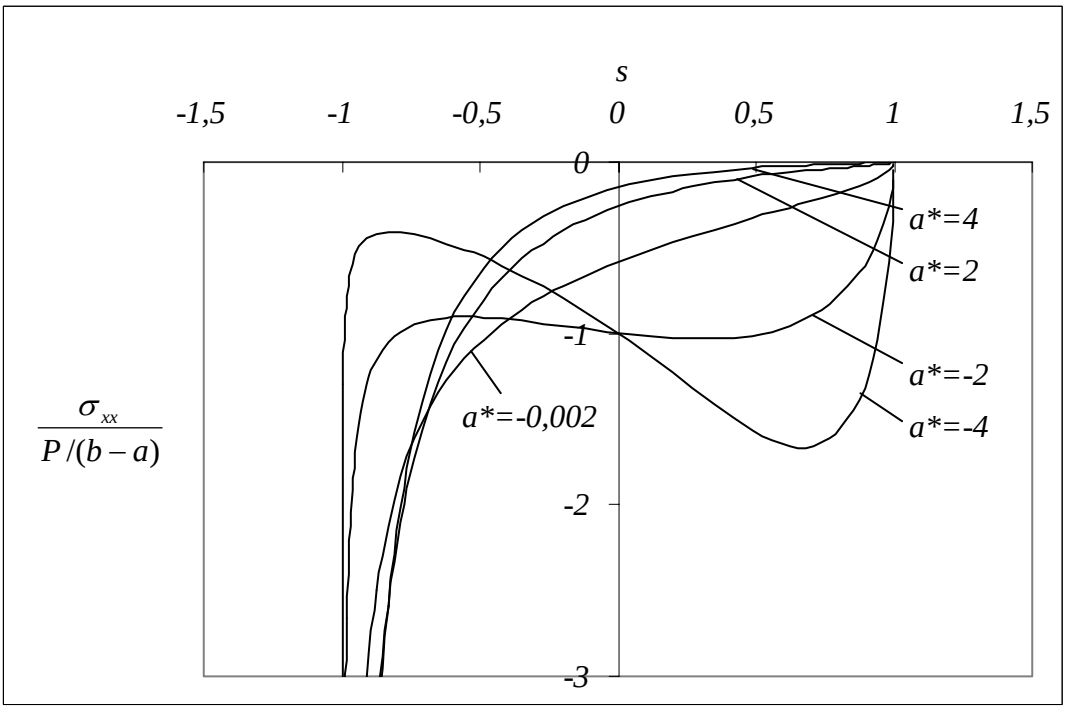

Figure 43: Normalized stress distribution for various values of the nonhomogeneity constant $a^* = \gamma a$. (η= 0,4 and $b^* = \gamma b$ =0)

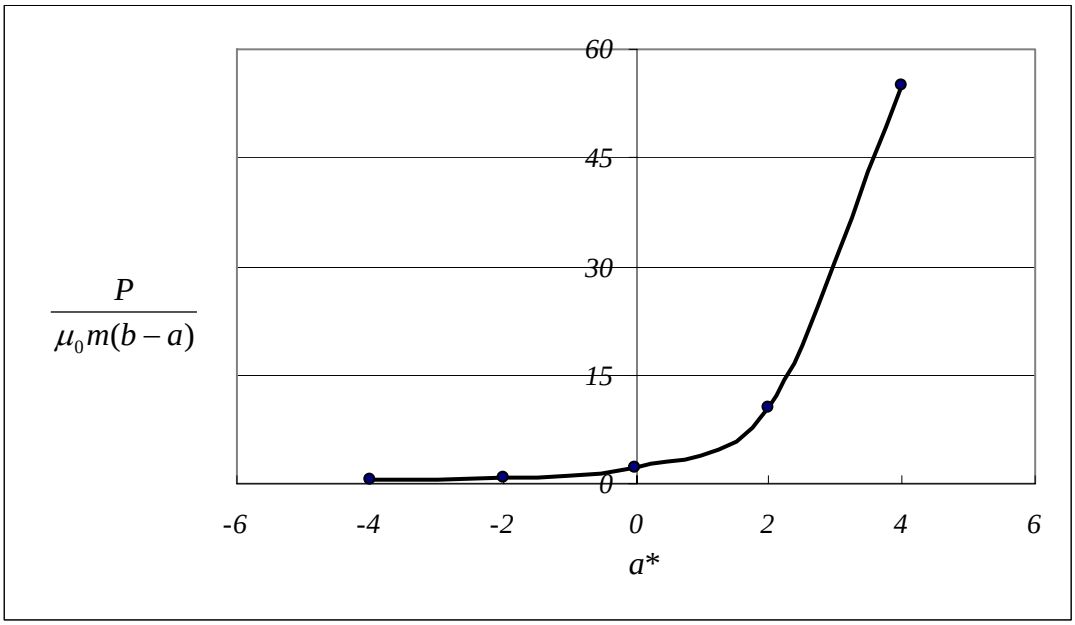

Figure 44: Variation of the normalized force with respect to normalized nonhomogeneity parameter $a^* = \gamma a$. (η= 0,4 and $b^* = \gamma b$ =0)

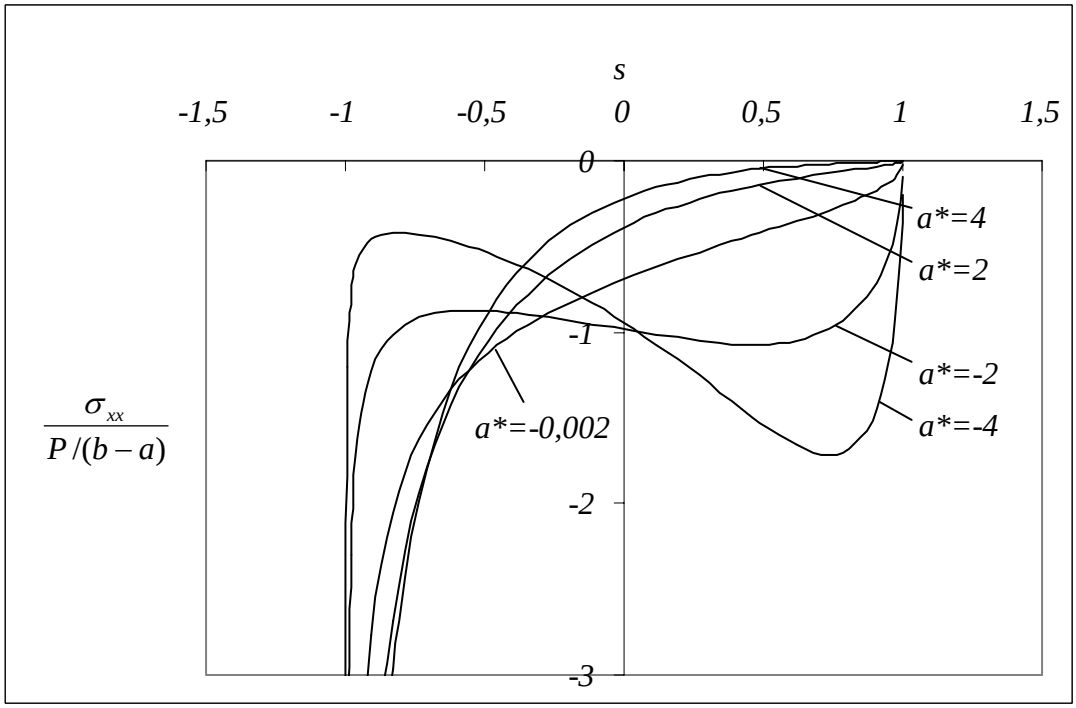

Figure 45: Normalized stress distribution for various values of the nonhomogeneity constant $a^* = \gamma a$. (η= - 0,4 and $b^* = \gamma b$ =0)

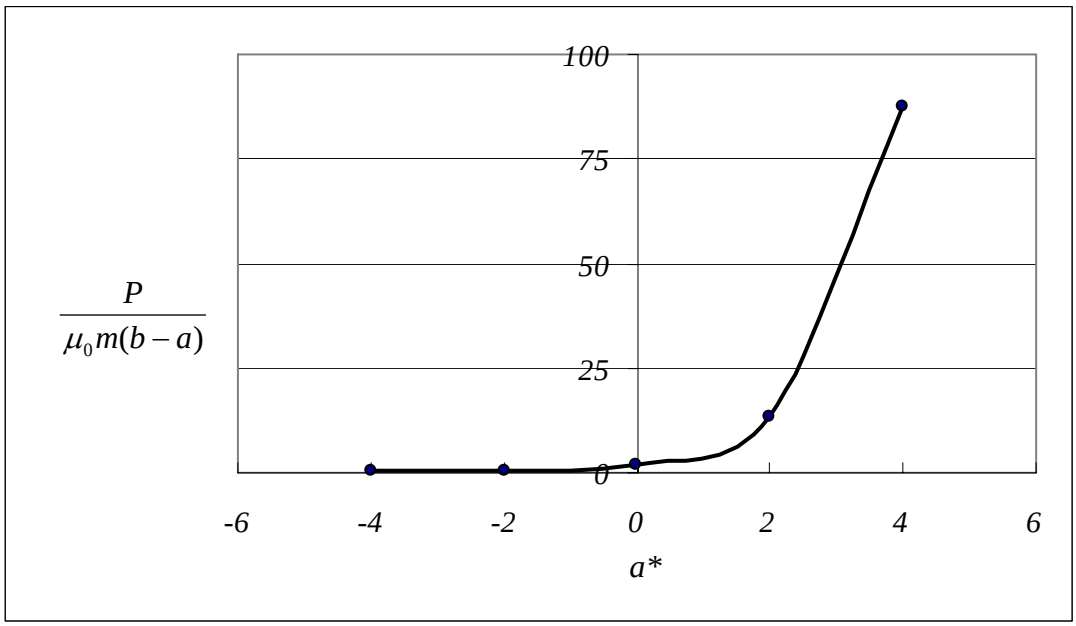

Figure 46: Variation of the normalized force with respect to normalized nonhomogeneity parameter $a^* = \gamma a$. (η= - 0,4 and $b^* = \gamma b$ =0)

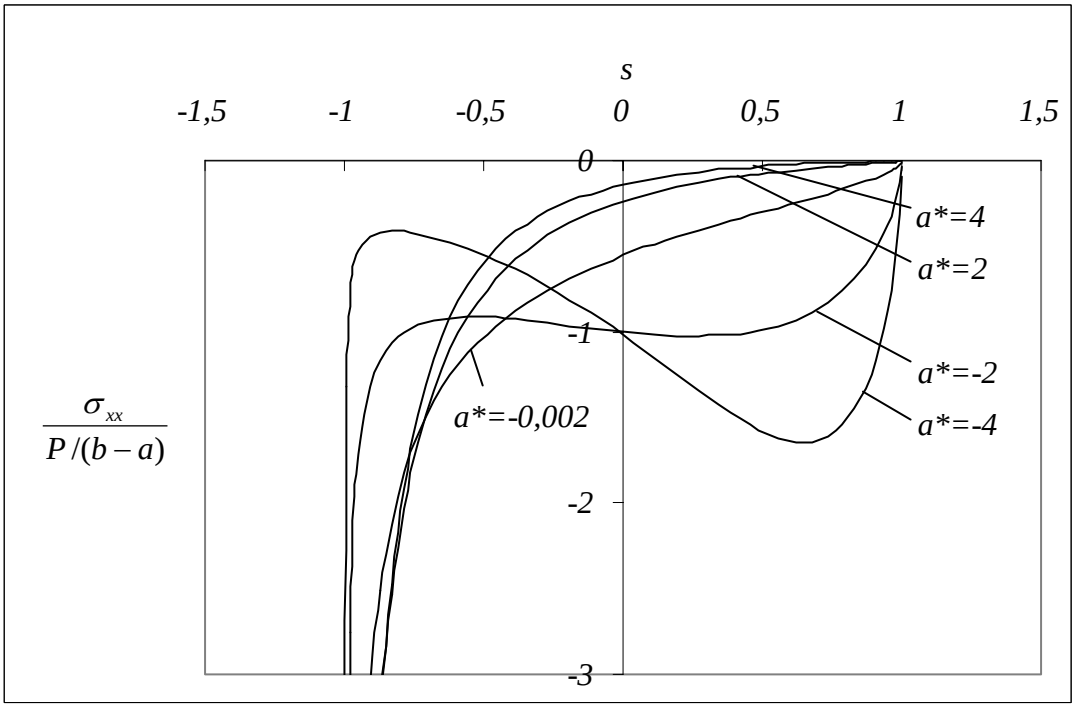

Figure 47: Normalized stress distribution for various values of the nonhomogeneity constant $a^* = \gamma a$. ($\eta = 0{,}6$ and $b^* = \gamma b = 0$)

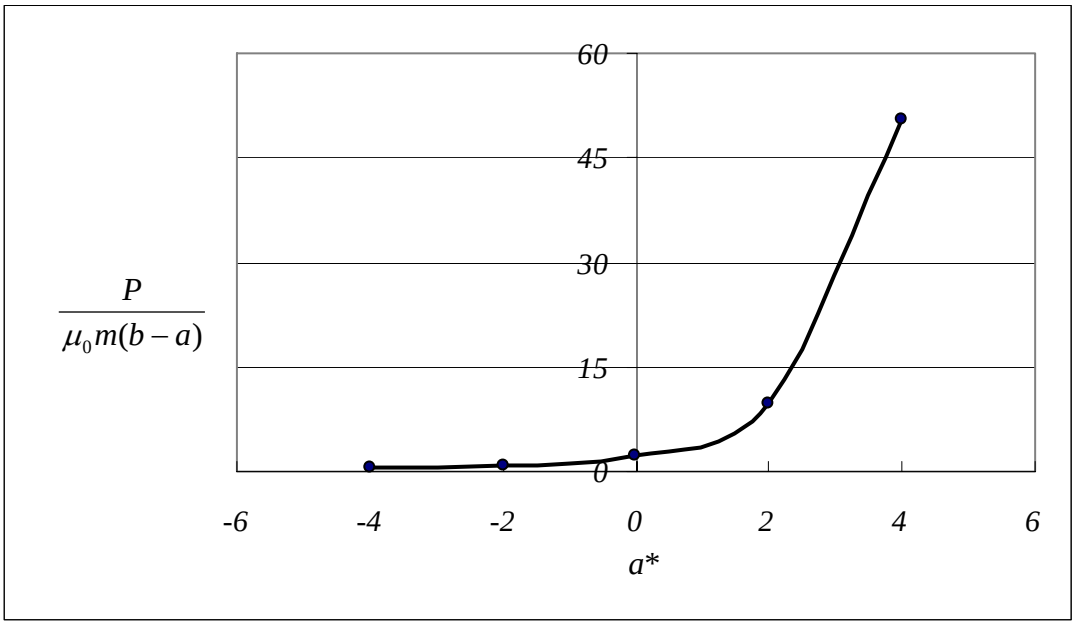

Figure 48: Variation of the normalized force with respect to normalized nonhomogeneity parameter $a^* = \gamma a$. ($\eta = 0{,}6$ and $b^* = \gamma b = 0$)

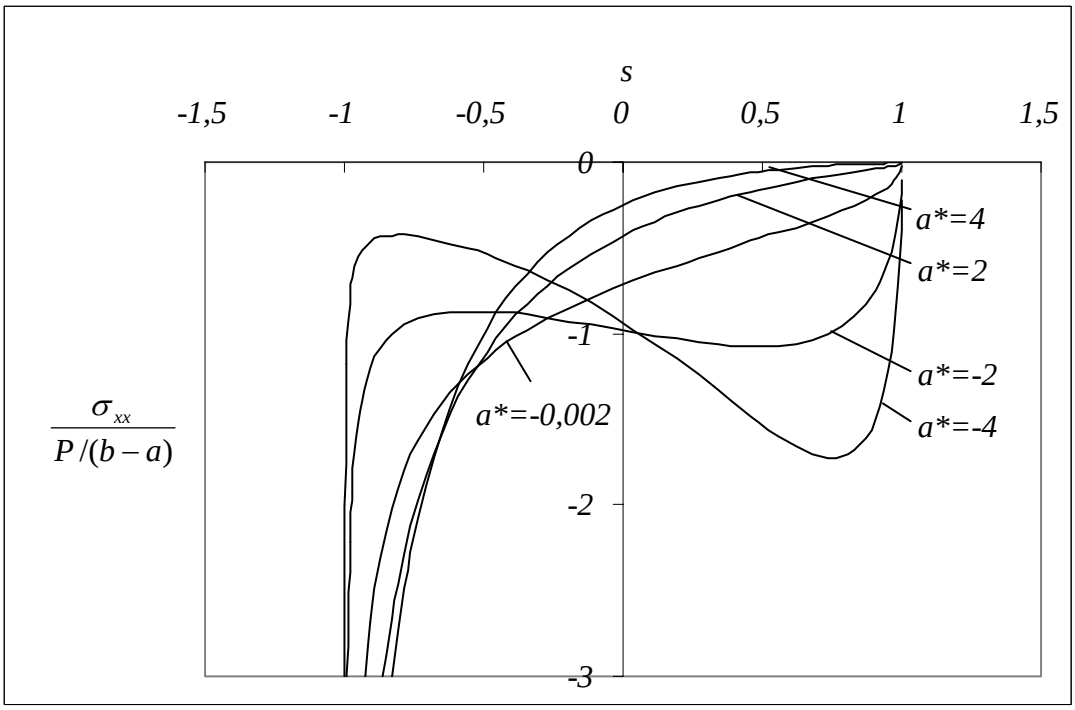

Figure 49: Normalized stress distribution for various values of the nonhomogeneity constant $a^* = \gamma a$. (η= - 0,6 and $b^* = \gamma b$ =0)

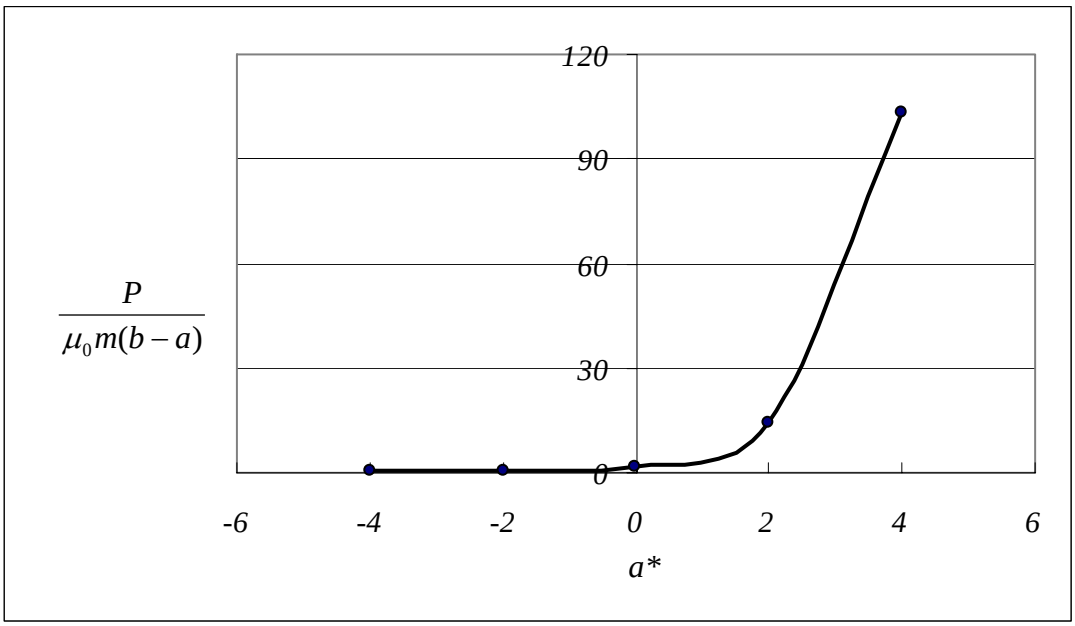

Figure 50: Variation of the normalized force with respect to normalized nonhomogeneity parameter $a^* = \gamma a$. (η= - 0,6 and $b^* = \gamma b$ =0)

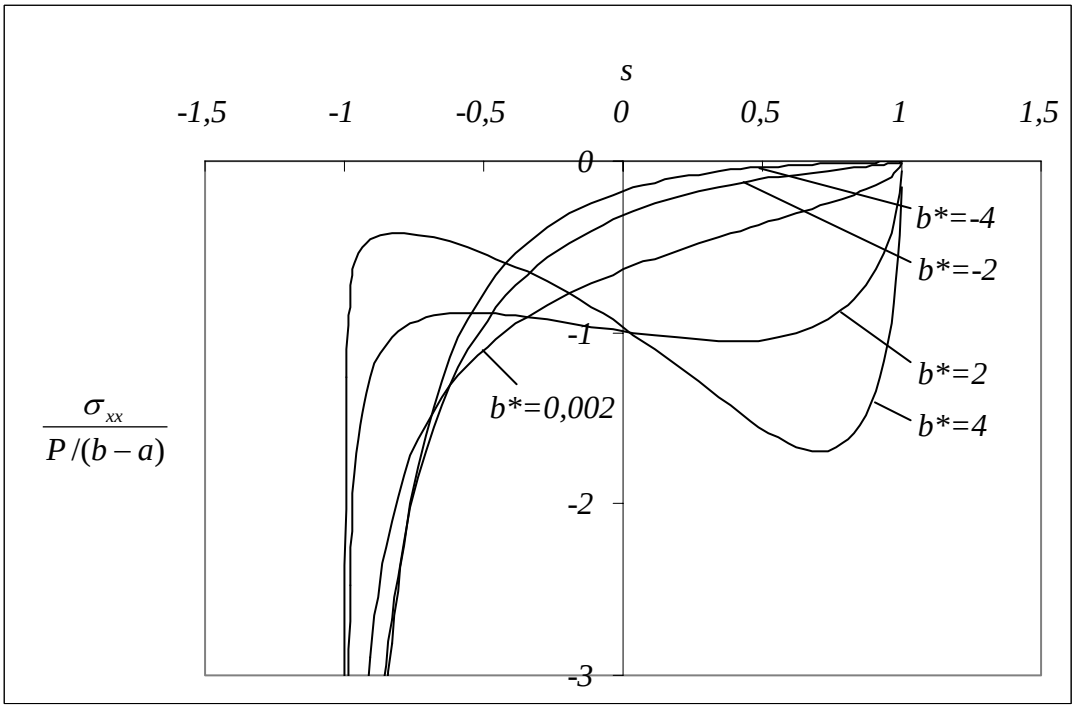

Figure 51: Normalized stress distribution for various values of the nonhomogeneity constant $b^* = \gamma b$. ($\eta = 0$ and $a^* = \gamma a = 0$)

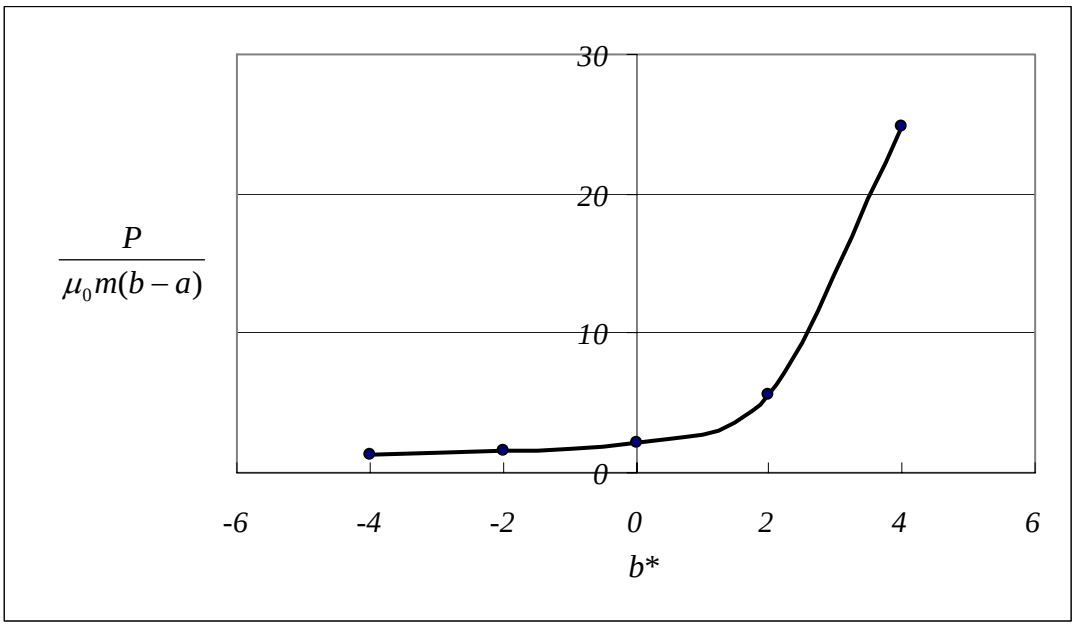

Figure 52: Variation of the normalized force with respect to normalized nonhomogeneity parameter $b^* = \gamma b$. ($\eta = 0$ and $a^* = \gamma a = 0$)

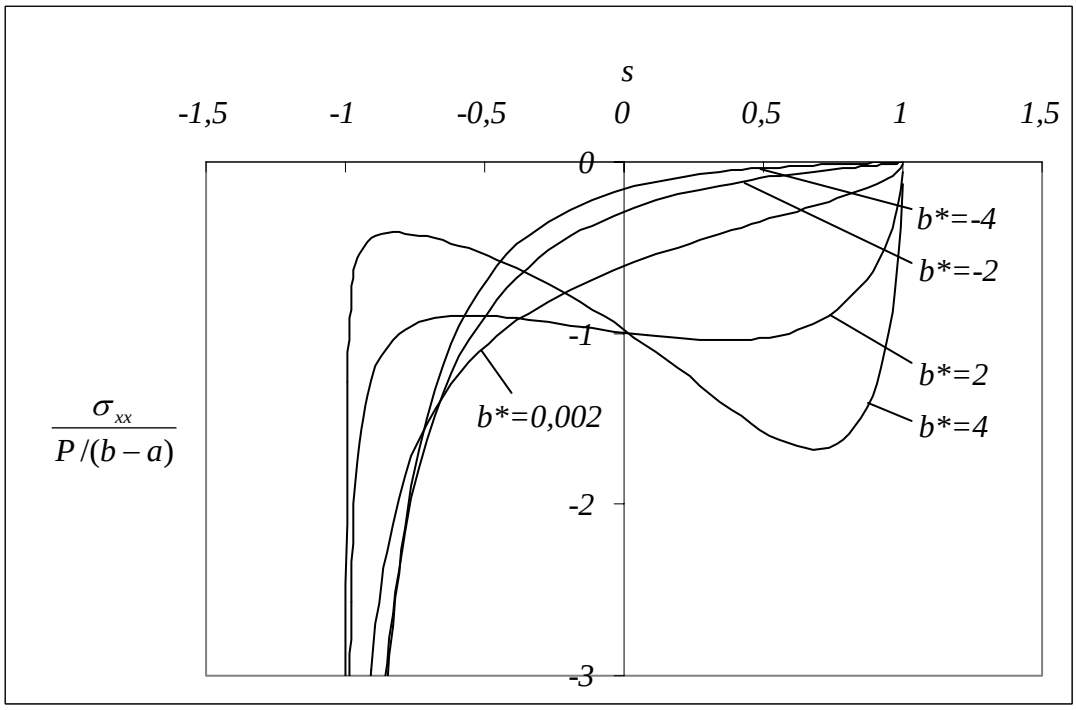

Figure 53: Normalized stress distribution for various values of the nonhomogeneity constant $b^* = \gamma b$. ($\eta = 0{,}2$ and $a^* = \gamma a = 0$)

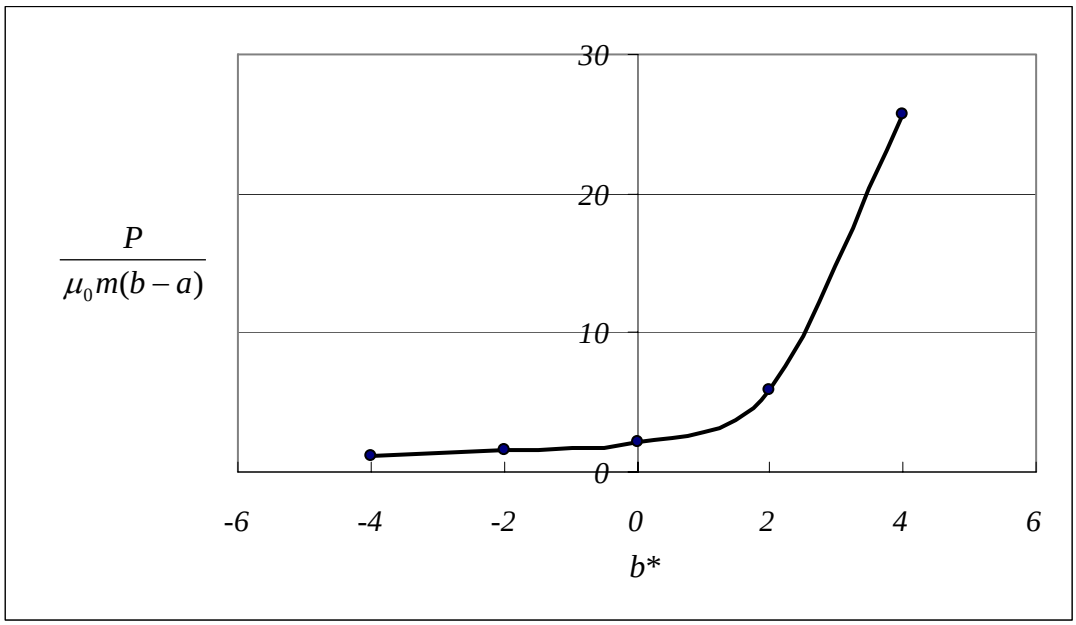

Figure 54: Variation of the normalized force with respect to normalized nonhomogeneity parameter $b^* = \gamma b$. ($\eta = 0{,}2$ and $a^* = \gamma a = 0$)

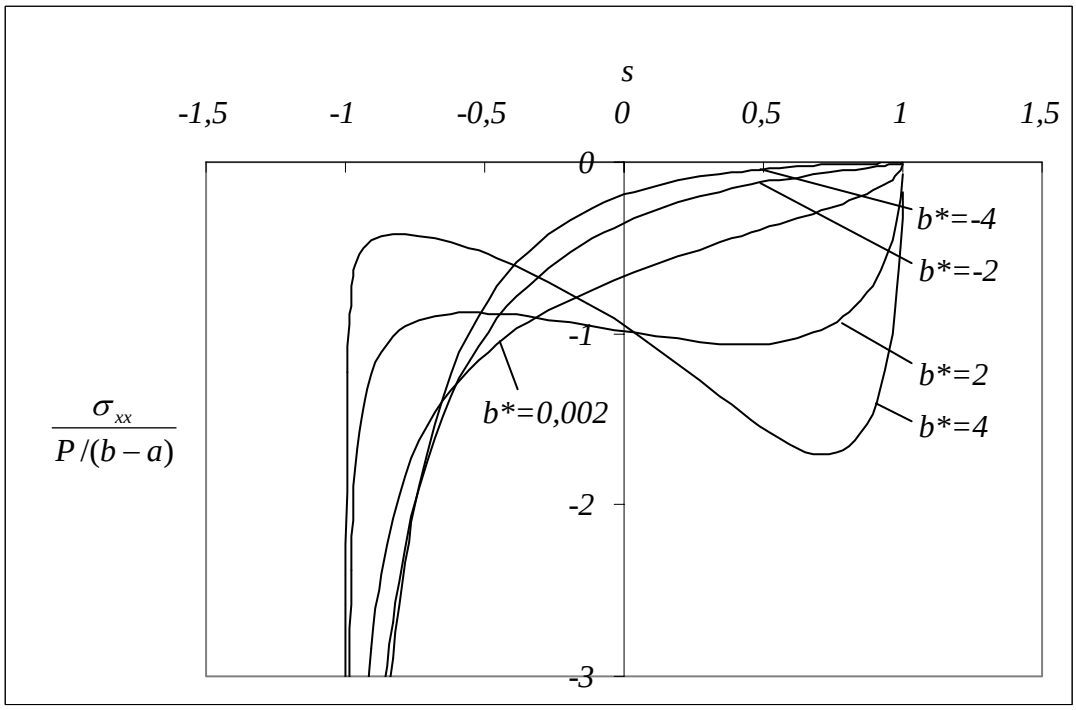

Figure 55: Normalized stress distribution for various values of the nonhomogeneity constant $b^* = \gamma b$. (η= - 0,2 and $a^* = \gamma a$ =0)

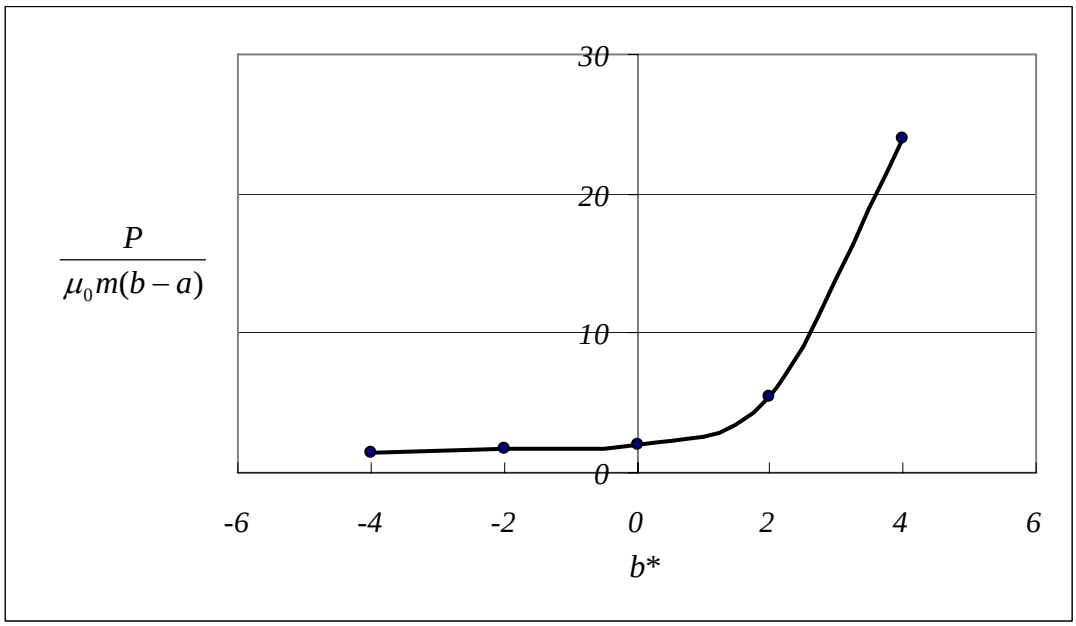

Figure 56: Variation of the normalized force with respect to normalized nonhomogeneity parameter $b^* = \gamma b$. (η= - 0,2 and $a^* = \gamma a$ =0)

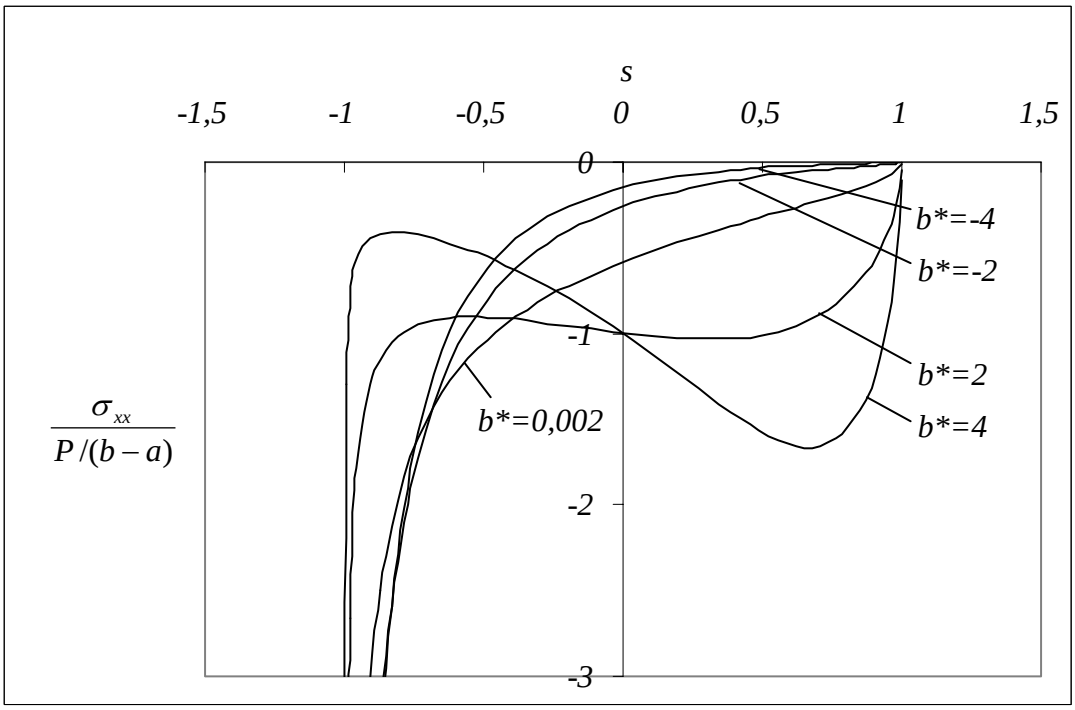

Figure 57: Normalized stress distribution for various values of the nonhomogeneity constant $b^* = \gamma b$. (η= 0,4 and $a^* = \gamma a$ =0)

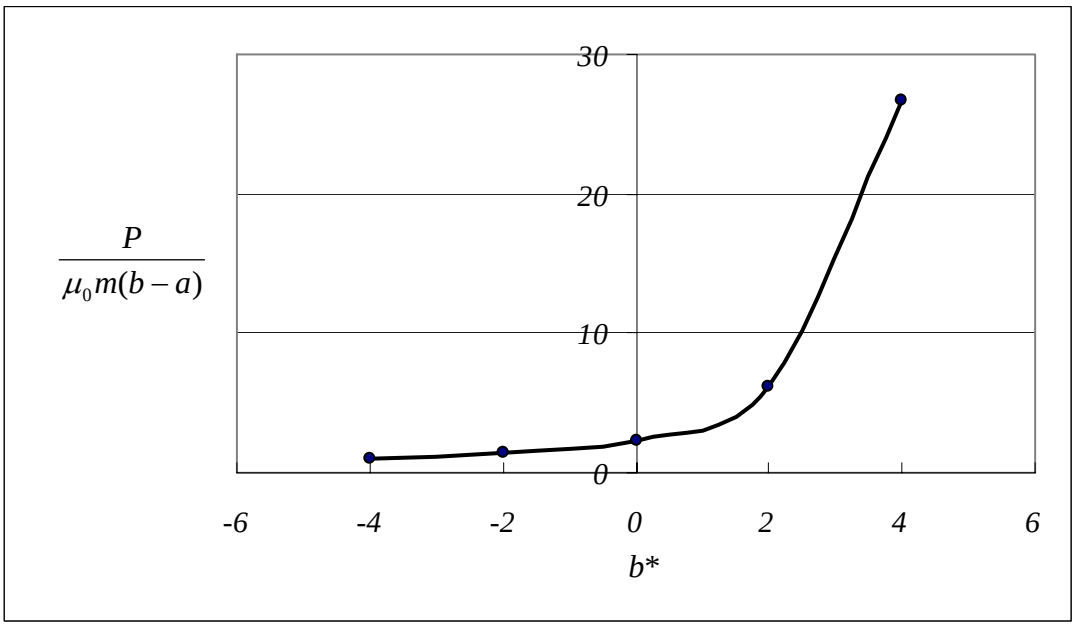

Figure 58: Variation of the normalized force with respect to normalized nonhomogeneity parameter $b^* = \gamma b$. (η= 0,4 and $a^* = \gamma a$ =0)

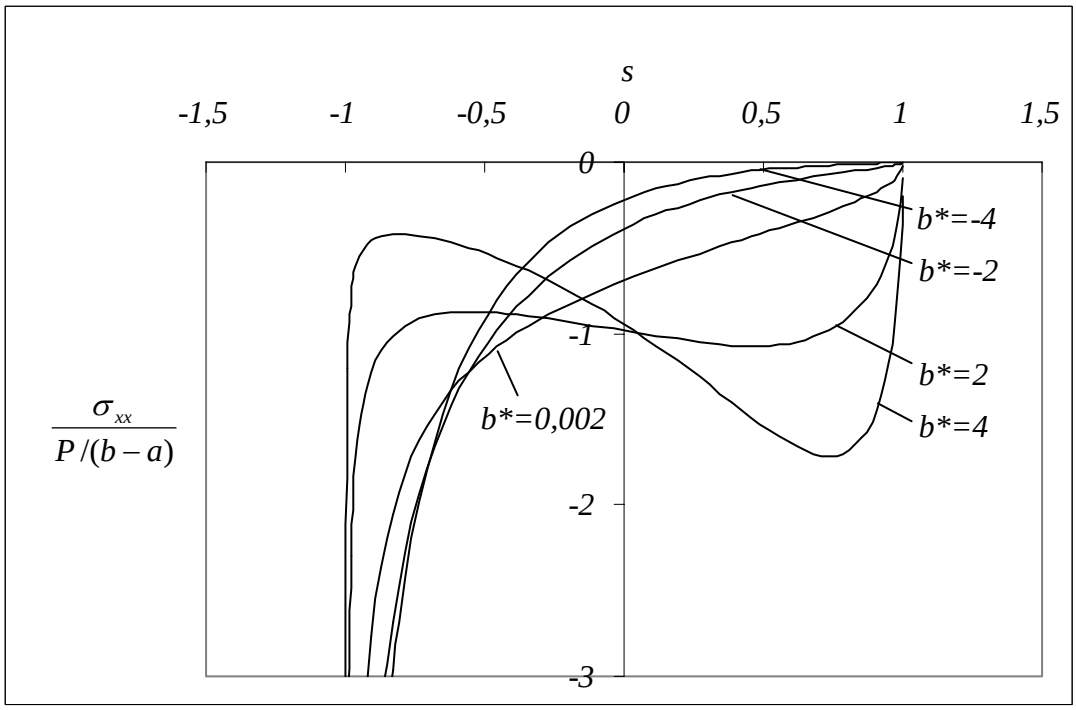

Figure 59: Normalized stress distribution for various values of the nonhomogeneity constant $b^* = \gamma b$. (η= - 0,4 and $a^* = \gamma a$ =0)

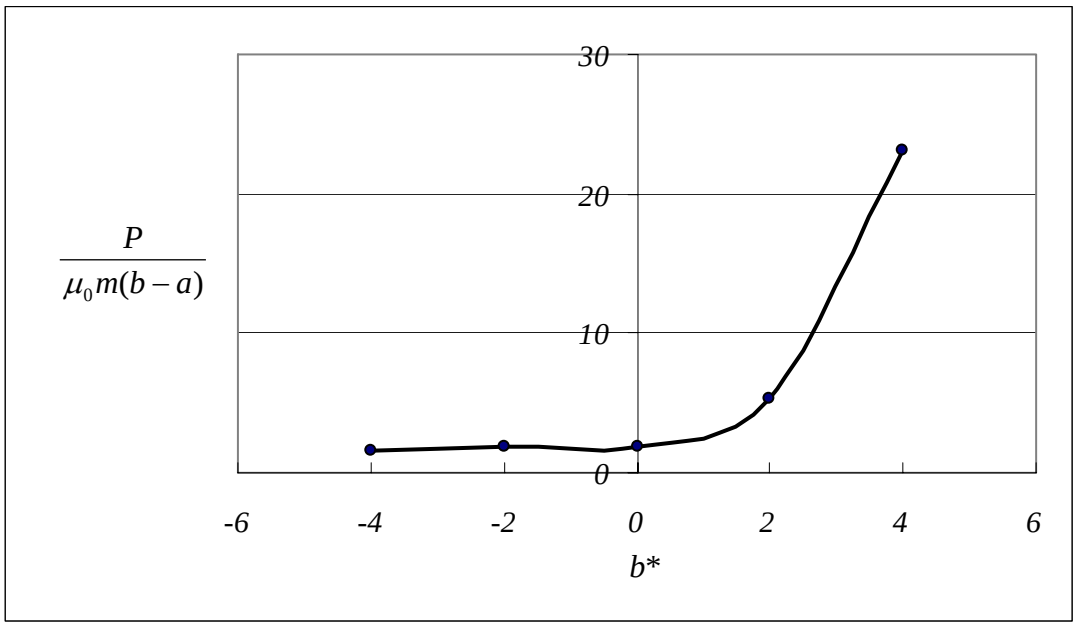

Figure 60: Variation of the normalized force with respect to normalized nonhomogeneity parameter $b^* = \gamma b$. (η= - 0,4 and $a^* = \gamma a$ =0)

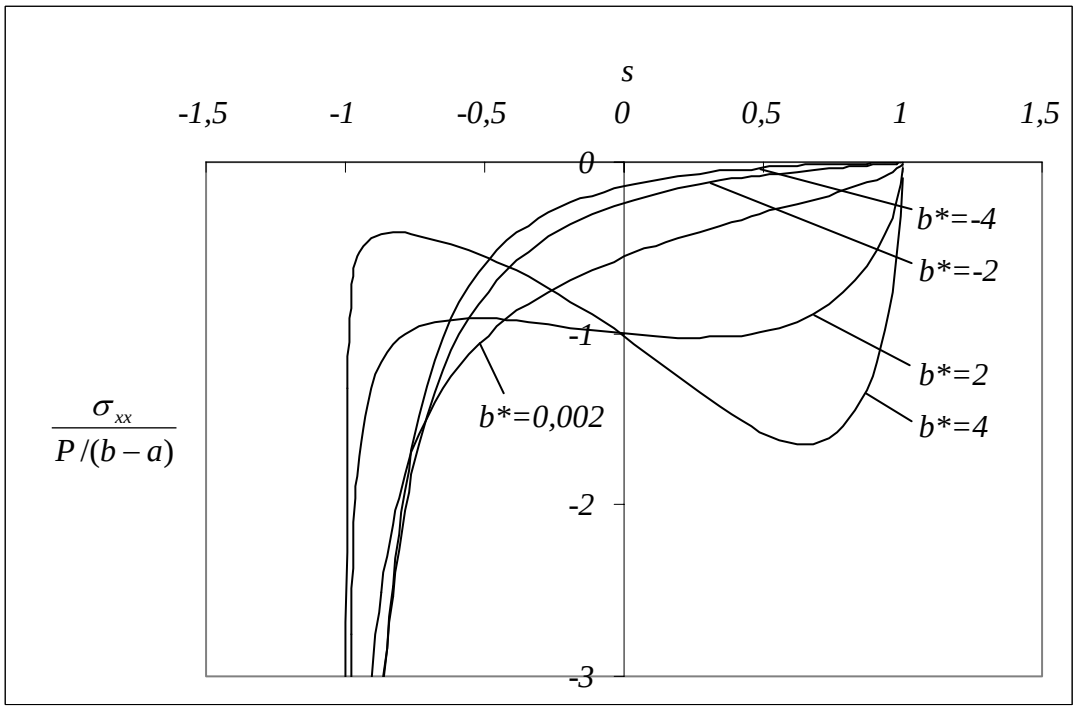

Figure 61: Normalized stress distribution for various values of the nonhomogeneity constant $b^* = \gamma b$. ($\eta =$ 0,6 and $a^* = \gamma a = 0$)

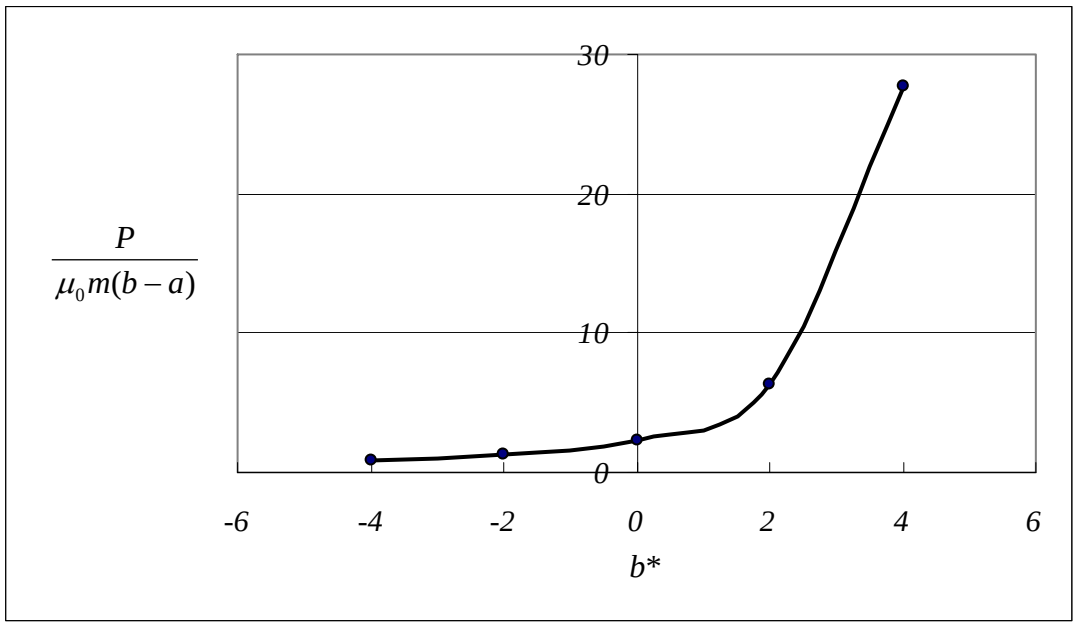

Figure 62: Variation of the normalized force with respect to normalized nonhomogeneity parameter $b^* = \gamma b$. ($\eta =$ 0,6 and $a^* = \gamma a = 0$)

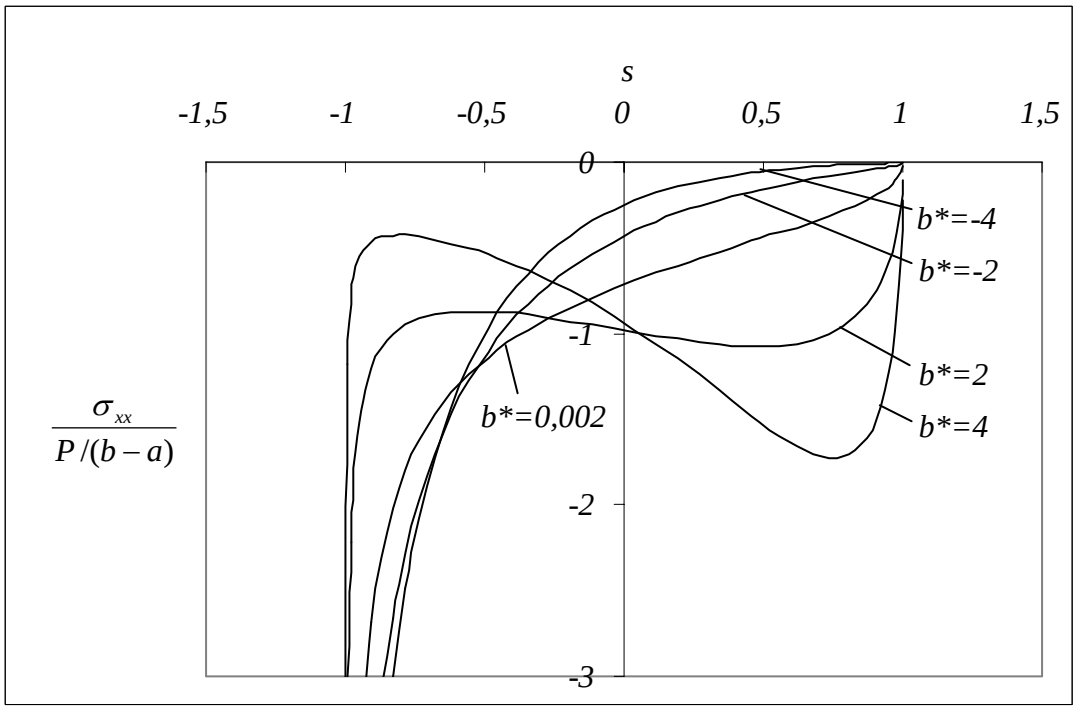

Figure 63: Normalized stress distribution for various values of the nonhomogeneity constant $b^* = \gamma b$. (η= - 0,6 and $a^* = \gamma a$ =0)

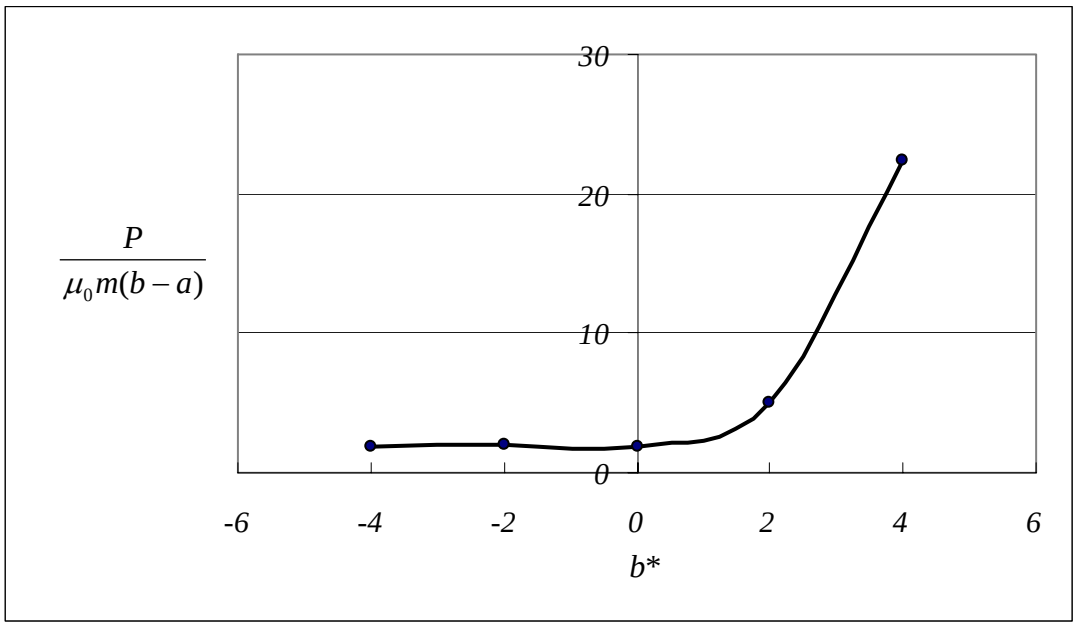

Figure 64: Variation of the normalized force with respect to normalized nonhomogeneity parameter $b^* = \gamma b$. (η= - 0,6 and $a^* = \gamma a$ =0)

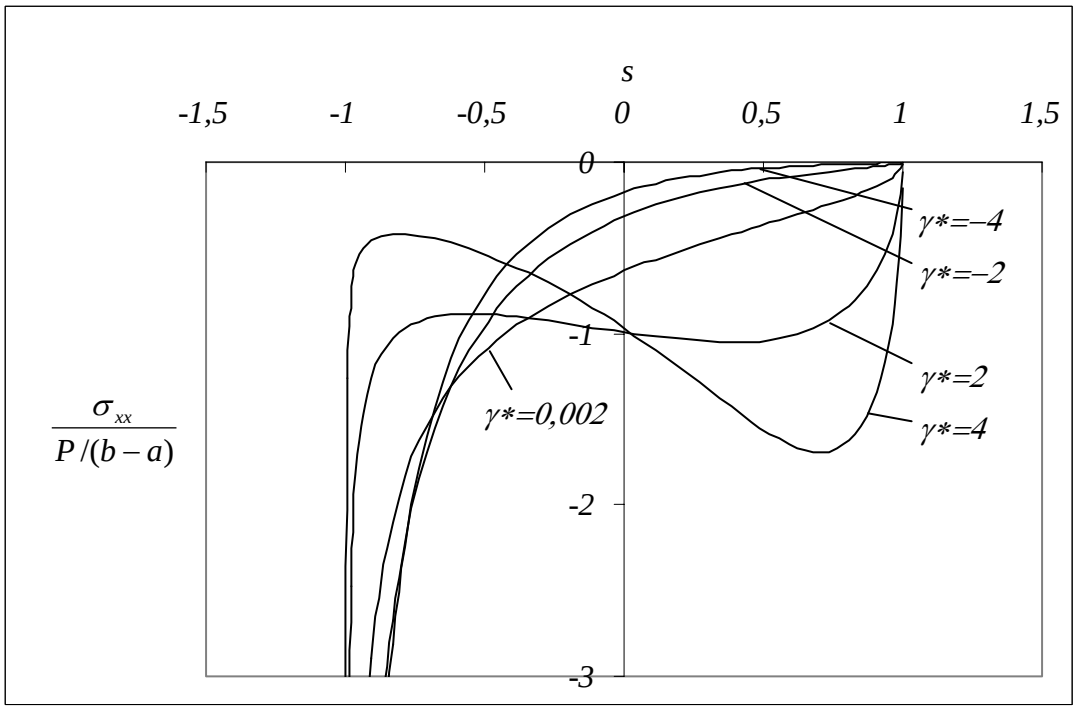

Figure 65: Normalized stress distribution for various values of the nonhomogeneity constant γ^* (η= 0 and γ^{**} =0)

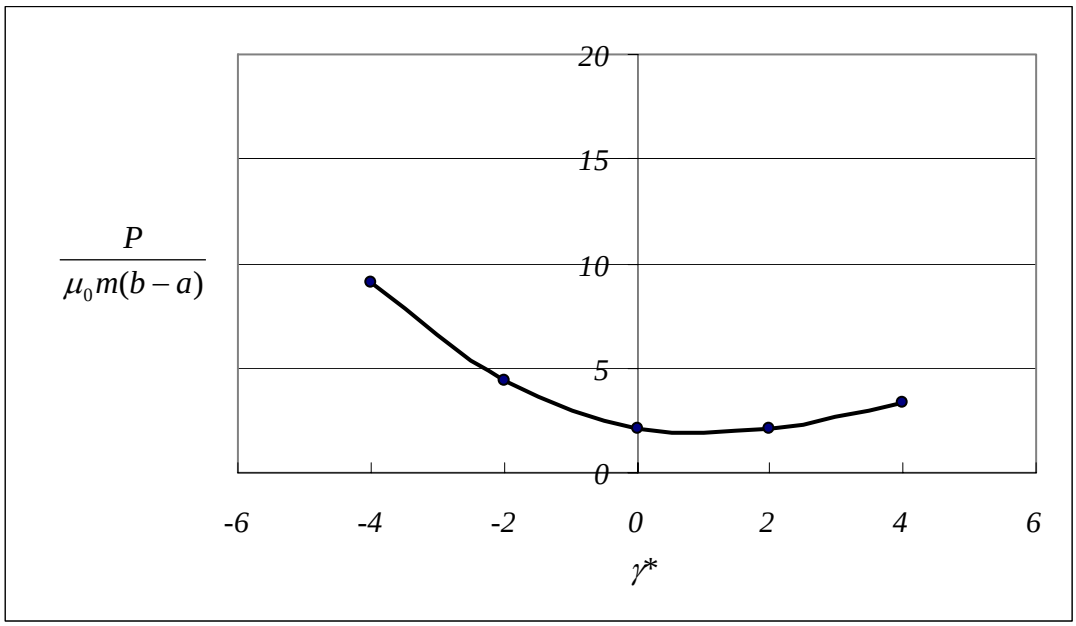

Figure 66: Variation of the normalized force with respect to normalized nonhomogeneity parameter γ^*. (η= 0 and γ^{**} =0)

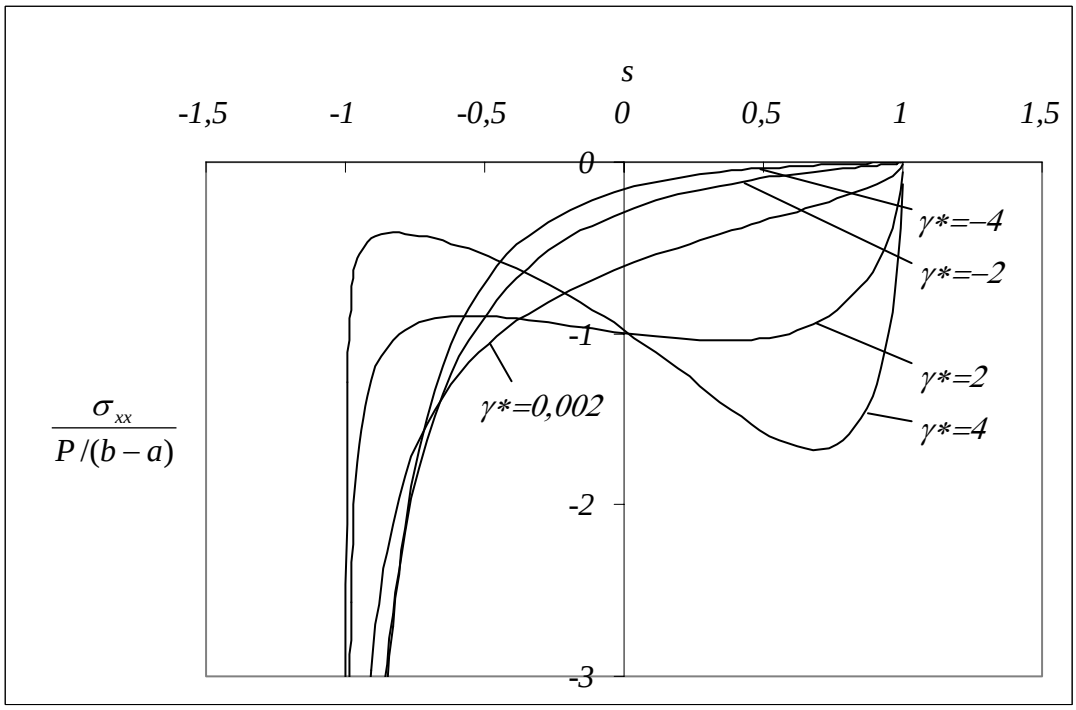

Figure 67: Normalized stress distribution for various values of the nonhomogeneity constant γ^* (η= 0,2 and γ^{**} =0)

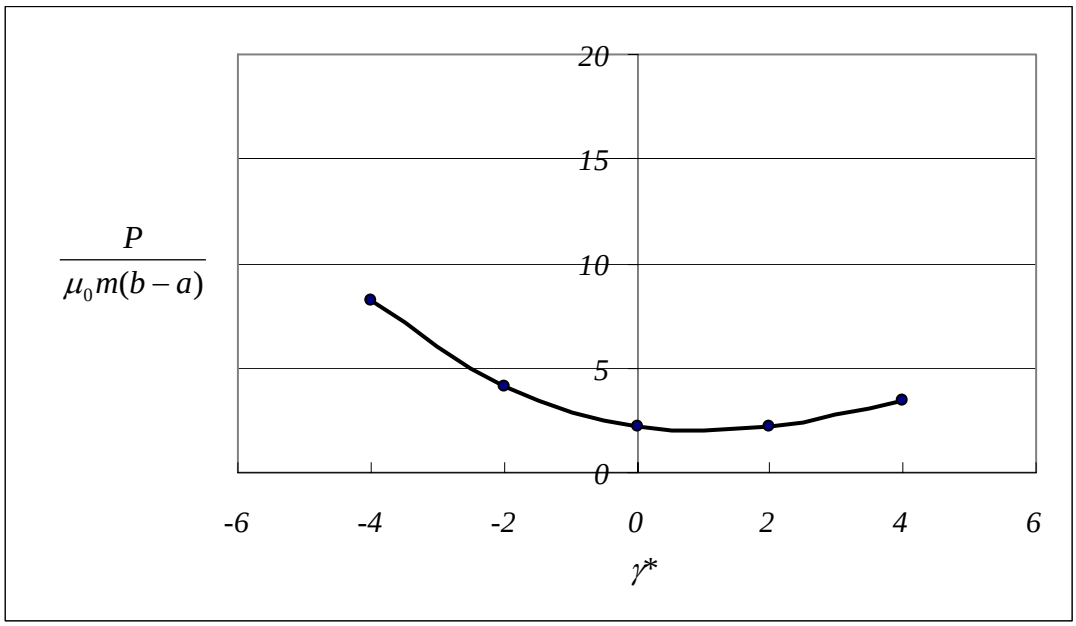

Figure 68: Variation of the normalized force with respect to normalized nonhomogeneity parameter γ^*. (η= 0,2 and γ^{**} =0)

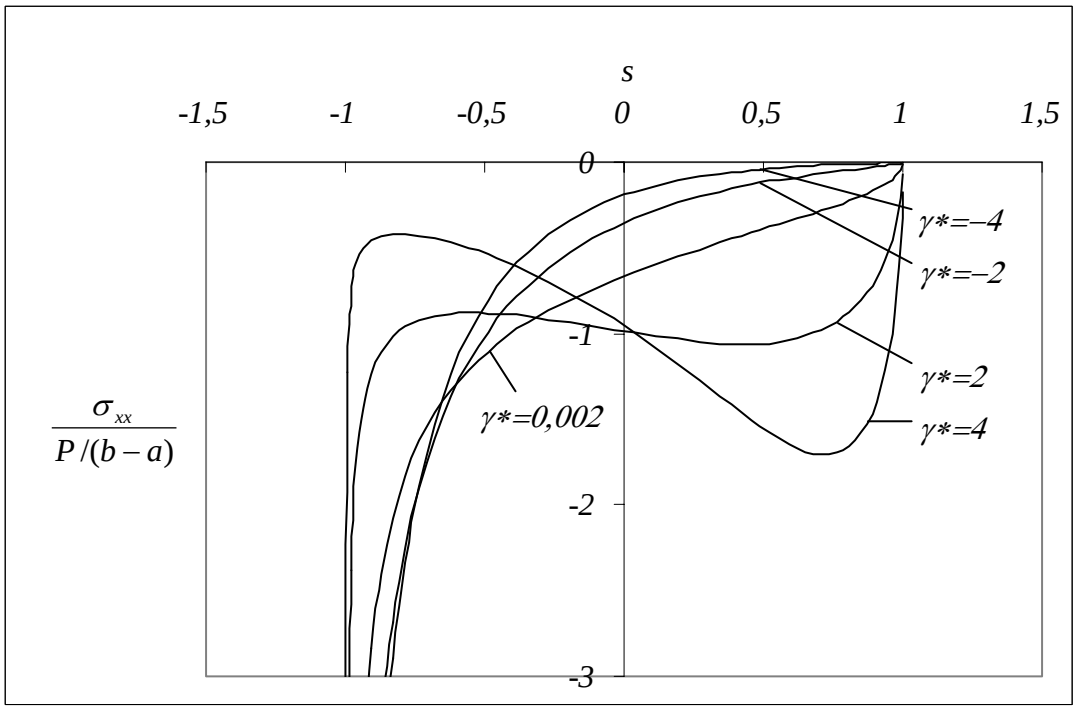

Figure 69: Normalized stress distribution for various values of the nonhomogeneity constant γ^* (η= - 0,2 and γ^{**} =0)

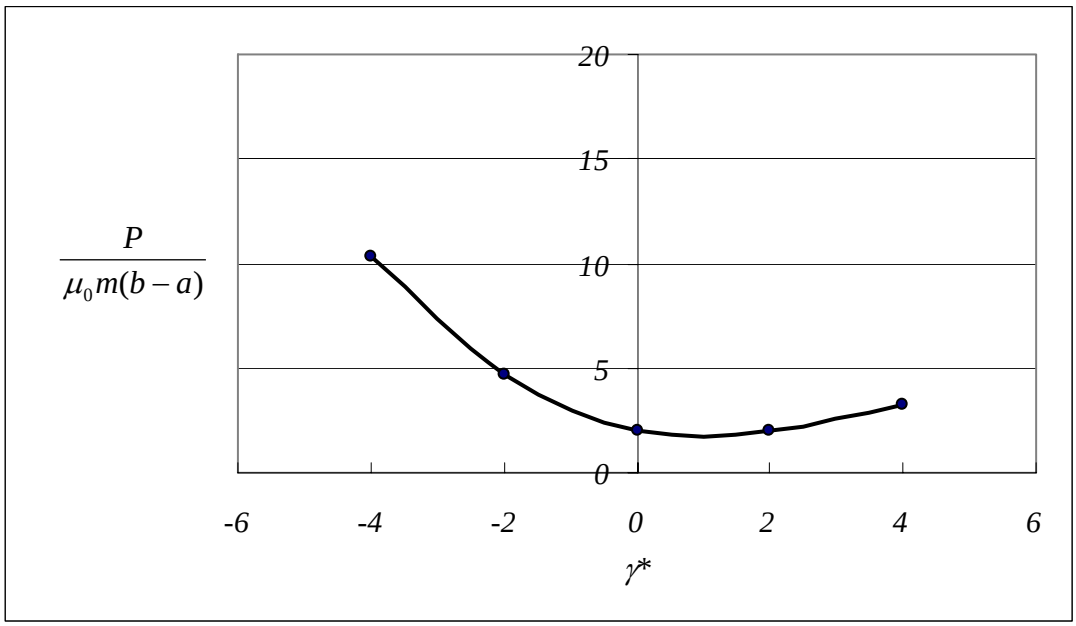

Figure 70: Variation of the normalized force with respect to normalized nonhomogeneity parameter γ^*. (η= - 0,2 and γ^{**} =0)

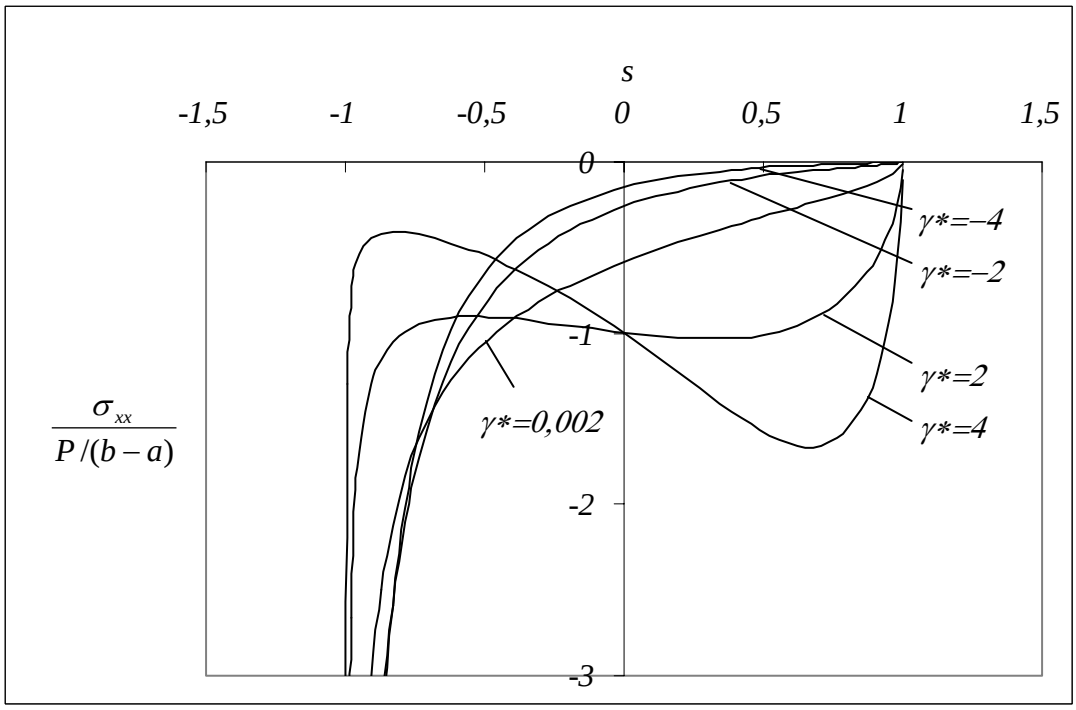

Figure 71: Normalized stress distribution for various values of the nonhomogeneity constant γ^* (η= 0,4 and γ^{**} =0)

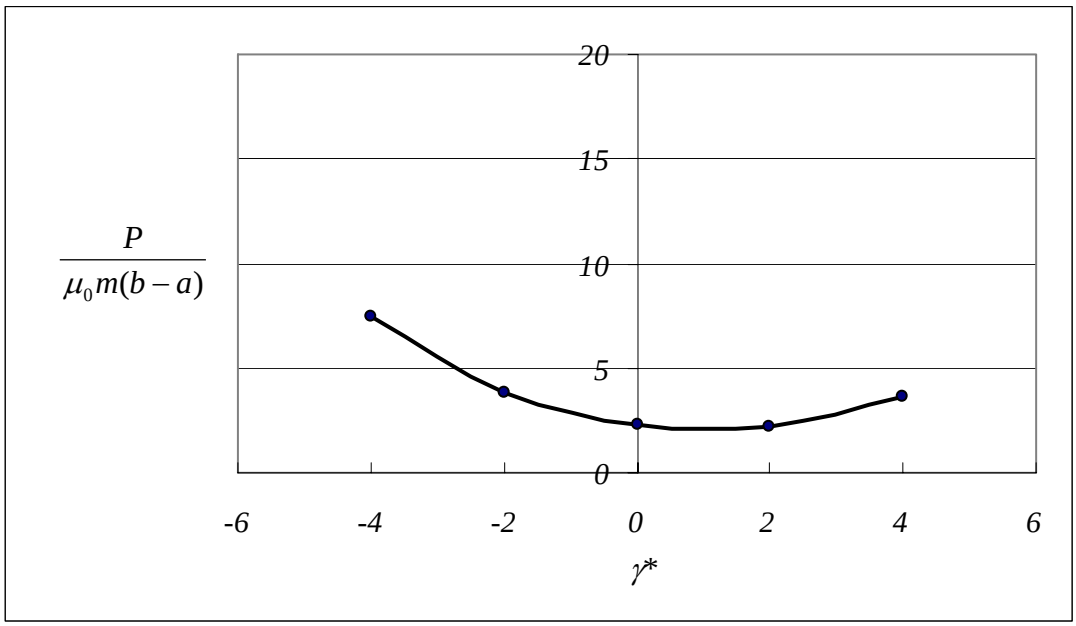

Figure 72: Variation of the normalized force with respect to normalized nonhomogeneity parameter γ^*. (η= 0,4 and γ^{**} =0)

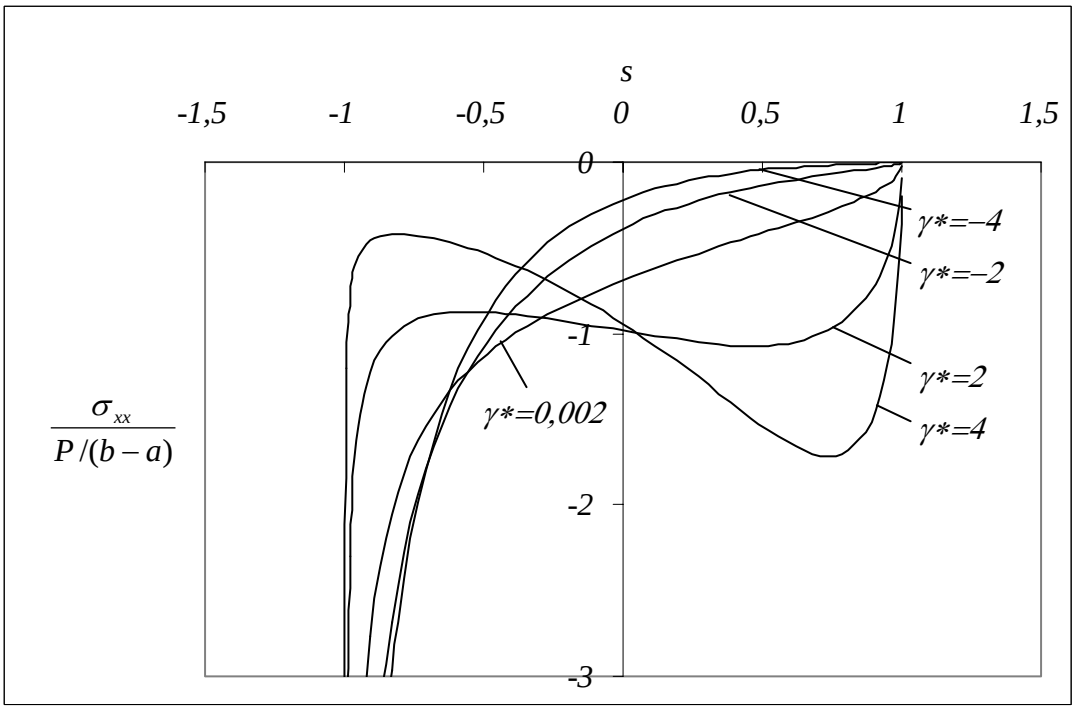

Figure 73: Normalized stress distribution for various values of the nonhomogeneity constant γ^* (η= - 0,4 and γ^{**} =0)

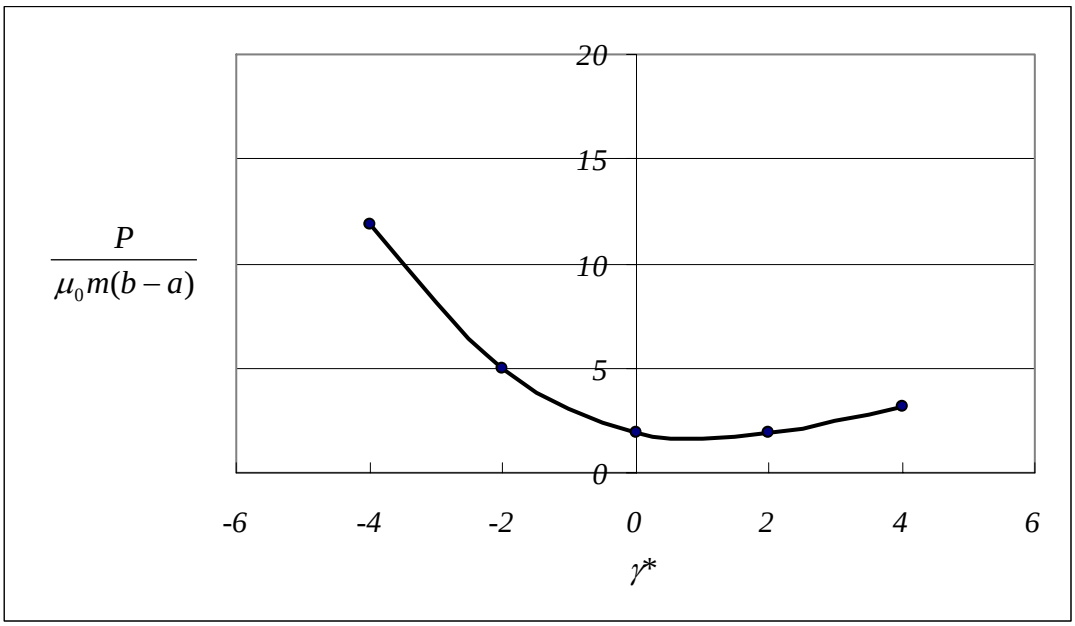

Figure 74: Variation of the normalized force with respect to normalized nonhomogeneity parameter γ^*. (η= - 0,4 and γ^{**} =0)

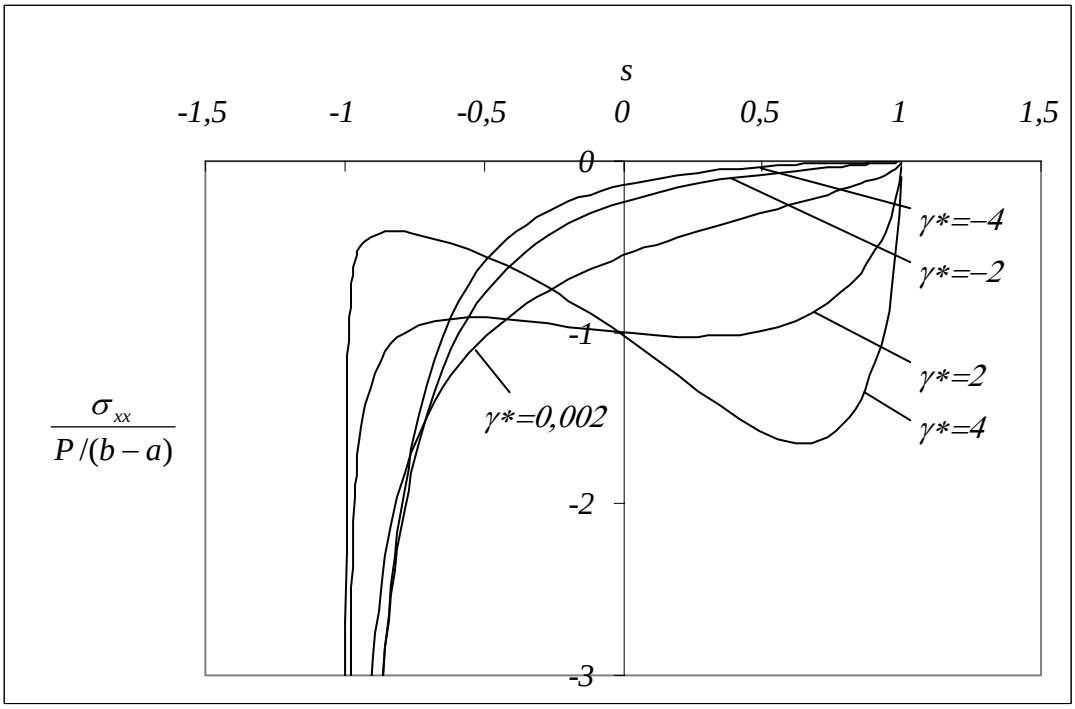

Figure 75: Normalized stress distribution for various values of the nonhomogeneity constant γ^* (η= 0,6 and γ^{**} =0)

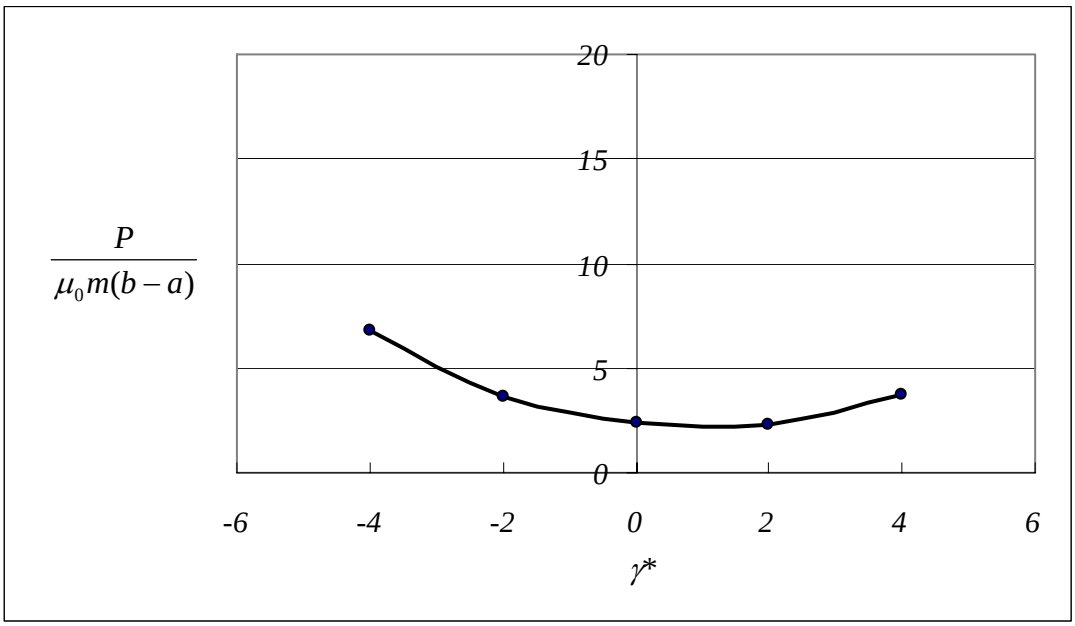

Figure 76: Variation of the normalized force with respect to normalized nonhomogeneity parameter γ^*. (η= 0,6 and γ^{**} =0)

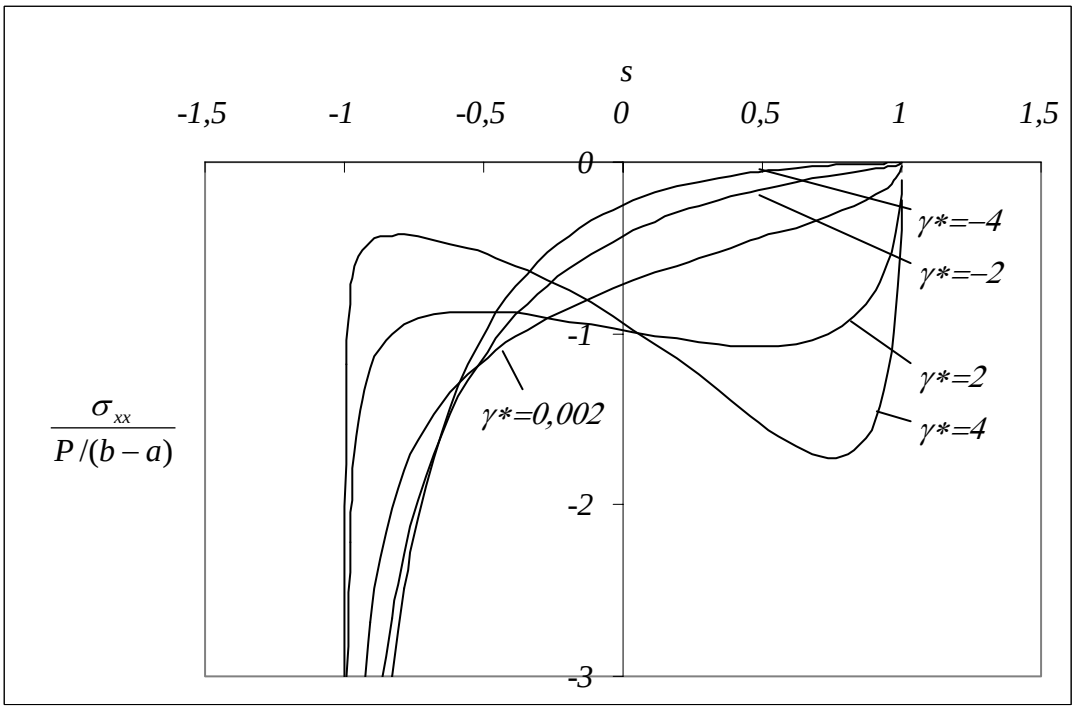

Figure 77: Normalized stress distribution for various values of the nonhomogeneity constant γ^* (η= - 0,6 and γ^{**} =0)

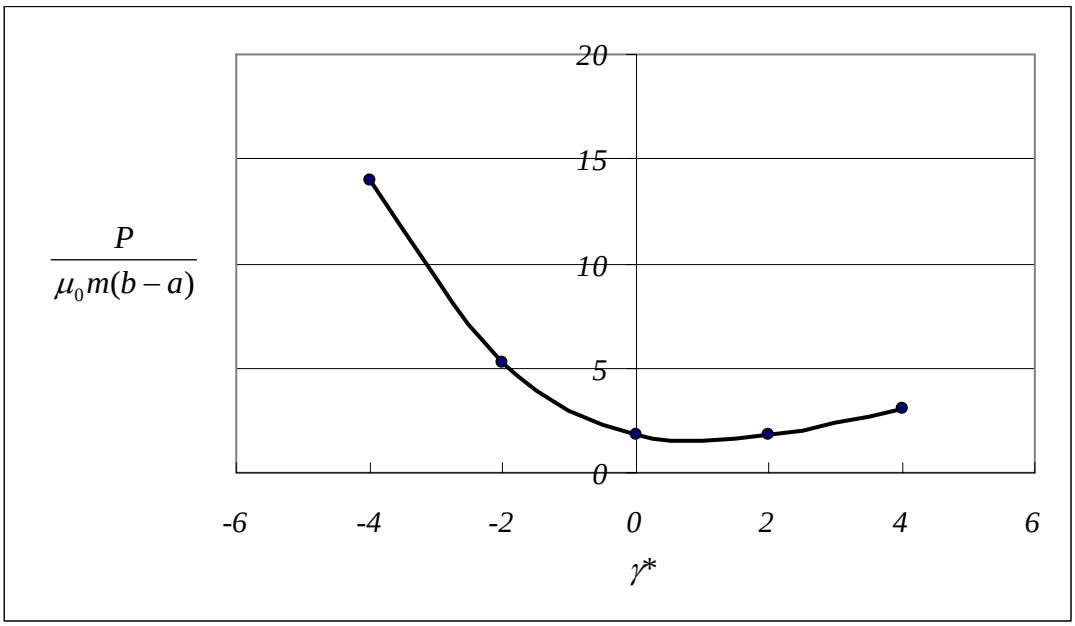

Figure 78: Variation of the normalized force with respect to normalized nonhomogeneity parameter γ^*. (η= - 0,6 and γ^{**} =0)

4.5.Parametric Studies for the Circular Stamp

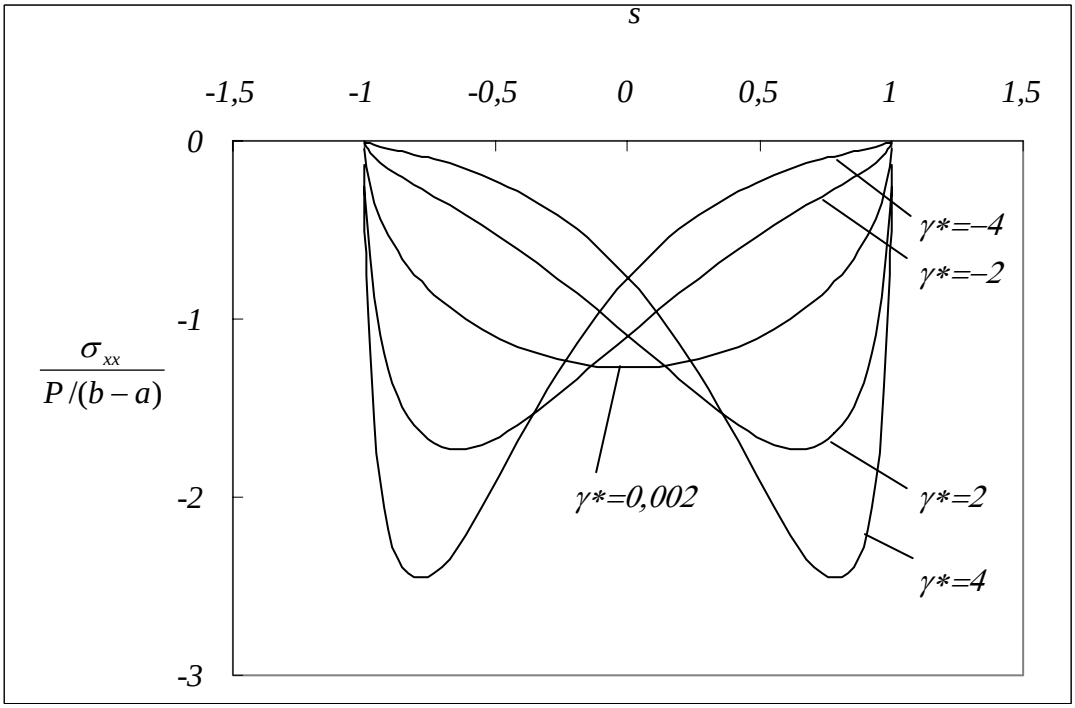

Figure 79: Normalized stress distribution for various values of the nonhomogeneity constant γ^*.(η= 0 and γ^{**} =0, *a/R* = -0,05 , *b/R* = 0,05)

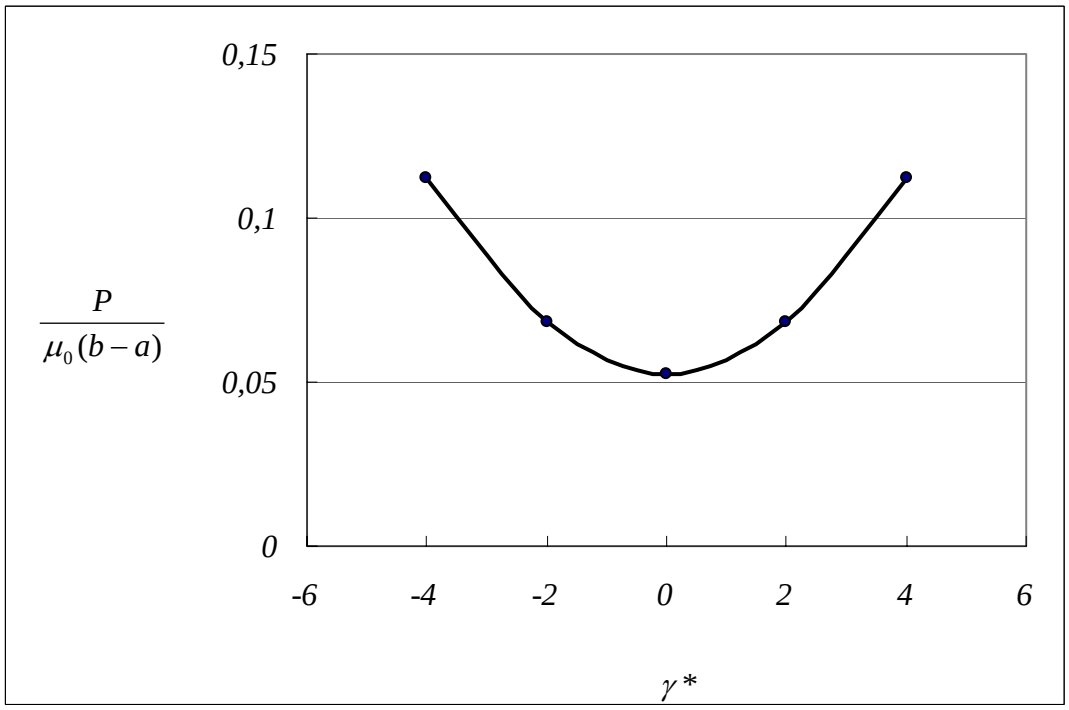

Figure 80: Variation of the normalized force with respect to normalized nonhomogeneity parameter γ^*. (η= 0 and γ^{**} =0, *a/R* = -0,05 , *b/R* = 0,05)

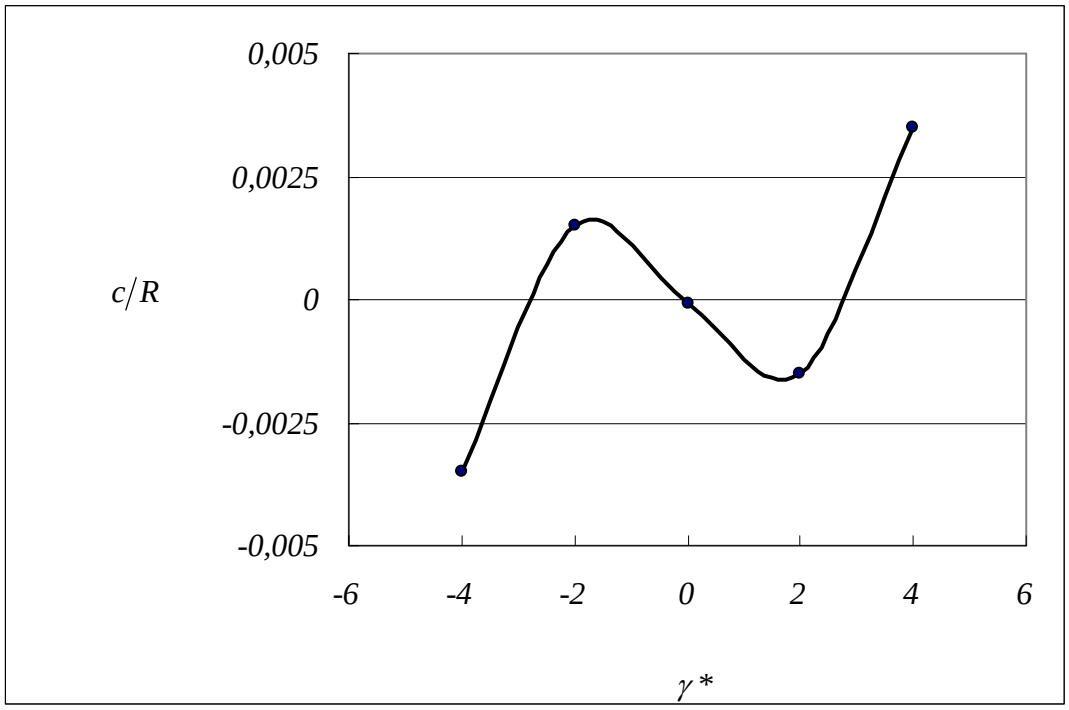

Figure 81: Variation of the location of the centerline with respect to normalized nonhomogeneity parameter γ^*. (η= 0 and γ^{**} =0, *a/R* = -0,05 , *b/R* = 0,05)

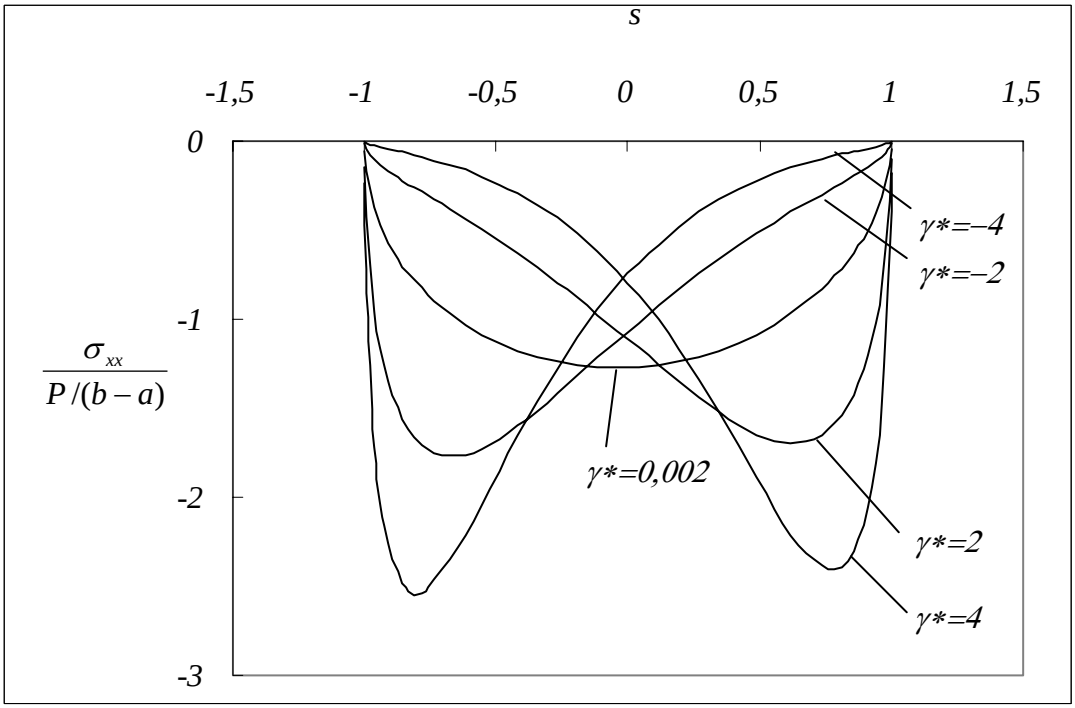

Figure 82: Normalized stress distribution for various values of the nonhomogeneity constant γ^*.(η= 0,2 and γ^{**} =0, *a/R* = -0,05 , *b/R* = 0,05)

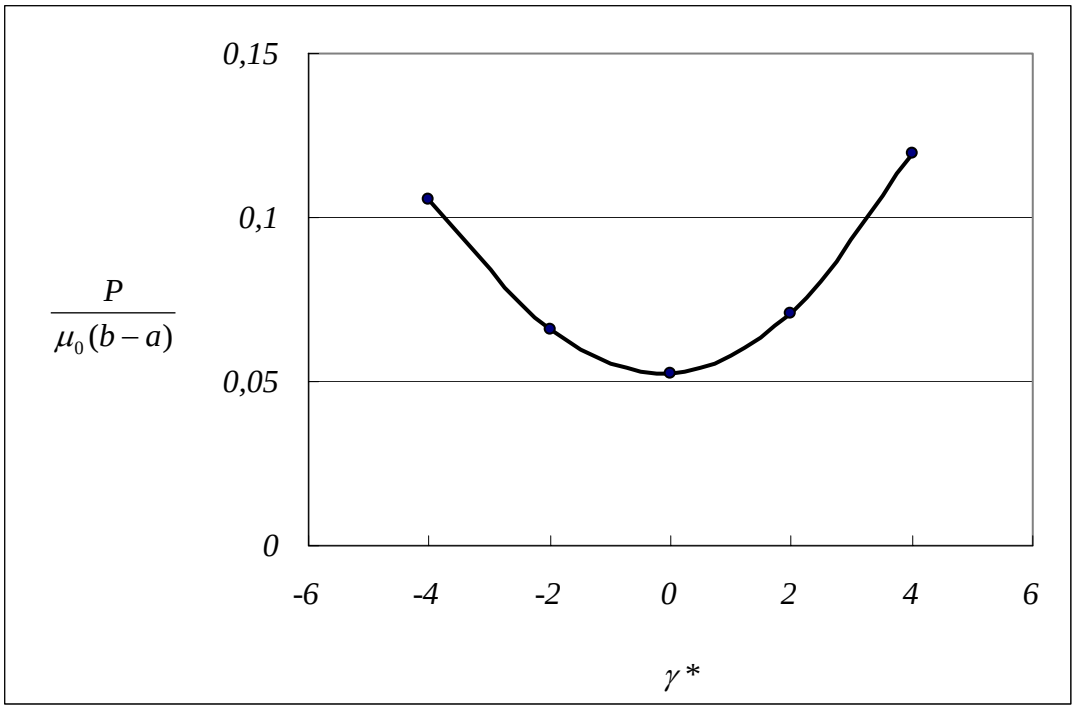

Figure 83: Variation of the normalized force with respect to normalized nonhomogeneity parameter γ^*. (η= 0,2 and γ^{**} =0, a/R = -0,05 , b/R = 0,05)

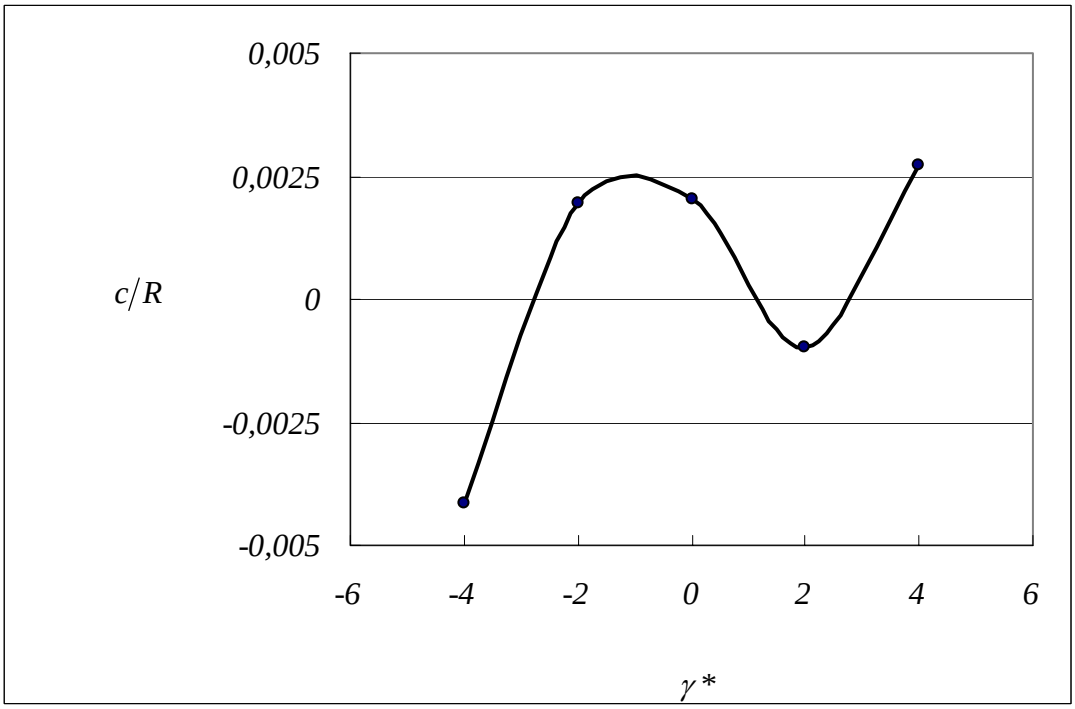

Figure 84: Variation of the location of the centerline with respect to normalized nonhomogeneity parameter γ^*. (η= 0,2 and γ^{**} =0, a/R = -0,05 , b/R = 0,05)

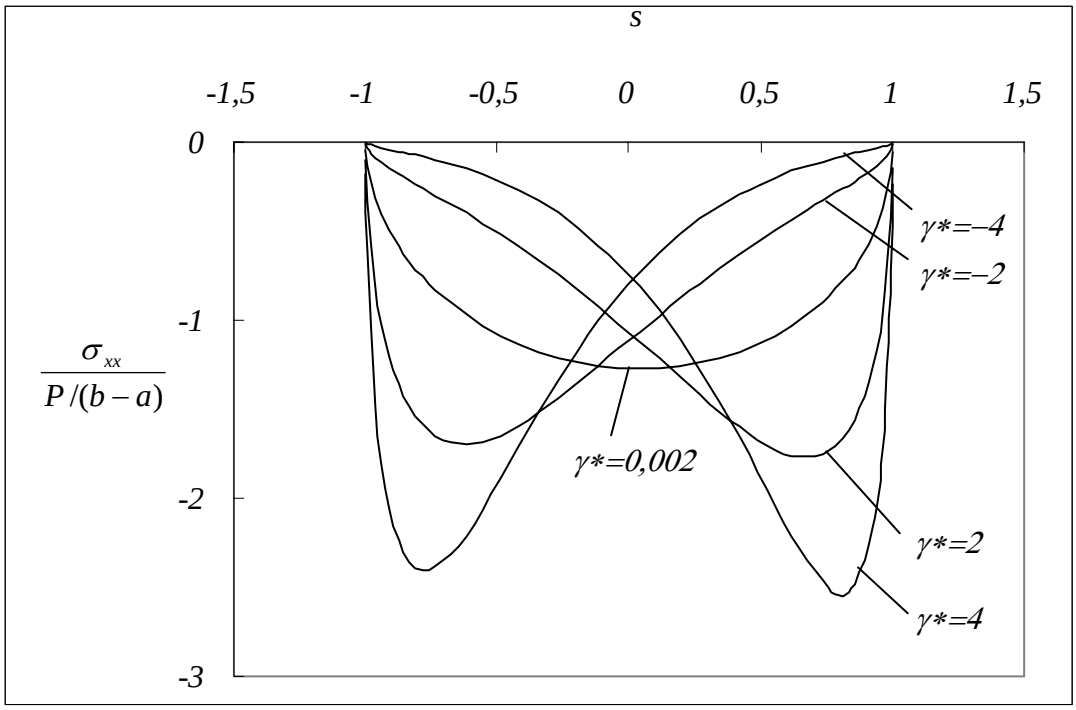

Figure 85: Normalized stress distribution for various values of the nonhomogeneity constant γ^*.(η= - 0,2 and γ^{**} =0, *a/R* = -0,05 , *b/R* = 0,05)

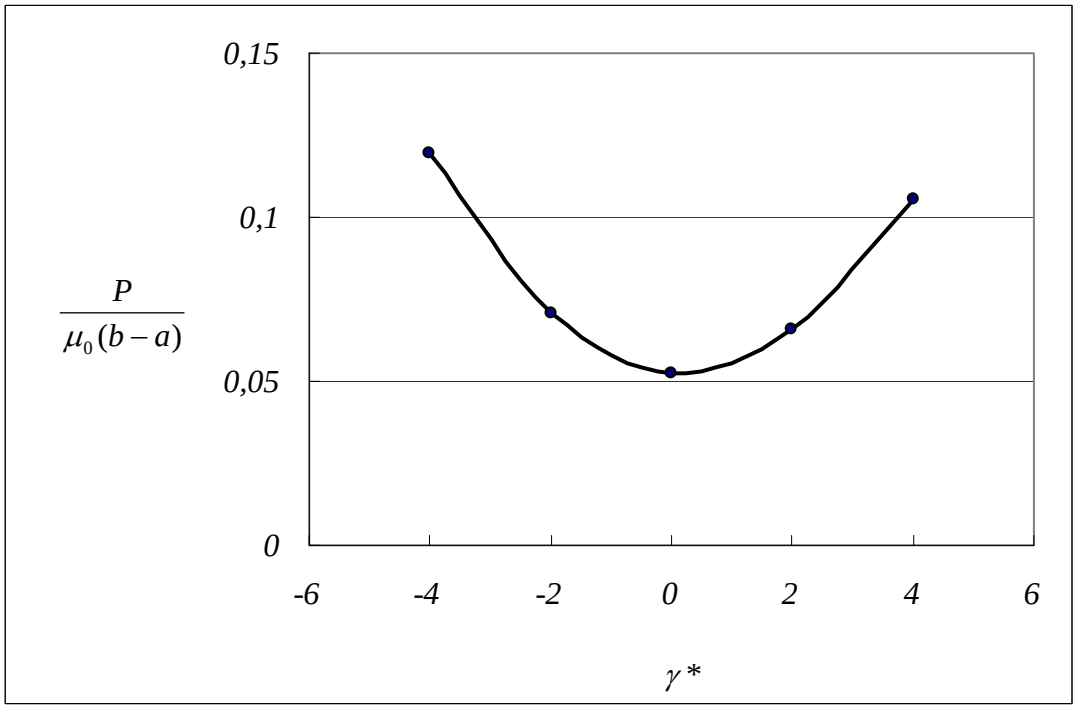

Figure 86: Variation of the normalized force with respect to normalized nonhomogeneity parameter γ^*. (η= - 0,2 and γ^{**} =0, *a/R* = -0,05 , *b/R* = 0,05)

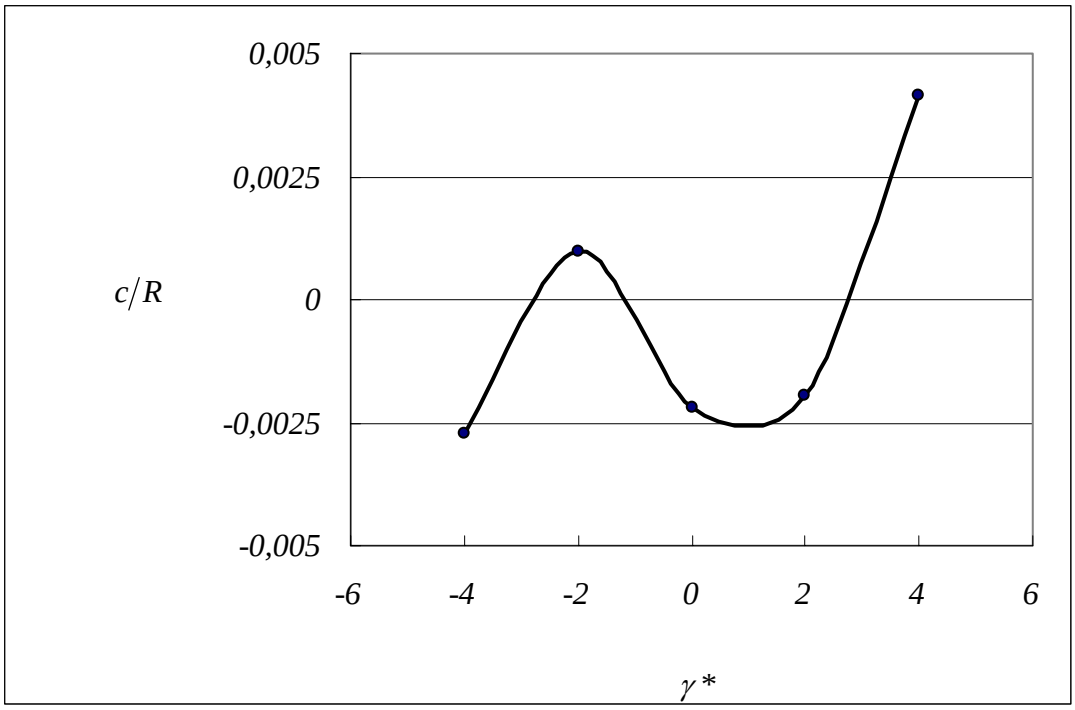

Figure 87: Variation of the location of the centerline with respect to normalized nonhomogeneity parameter γ^*. (η= - 0,2 and γ^{**} =0, a/R = -0,05 , b/R = 0,05)

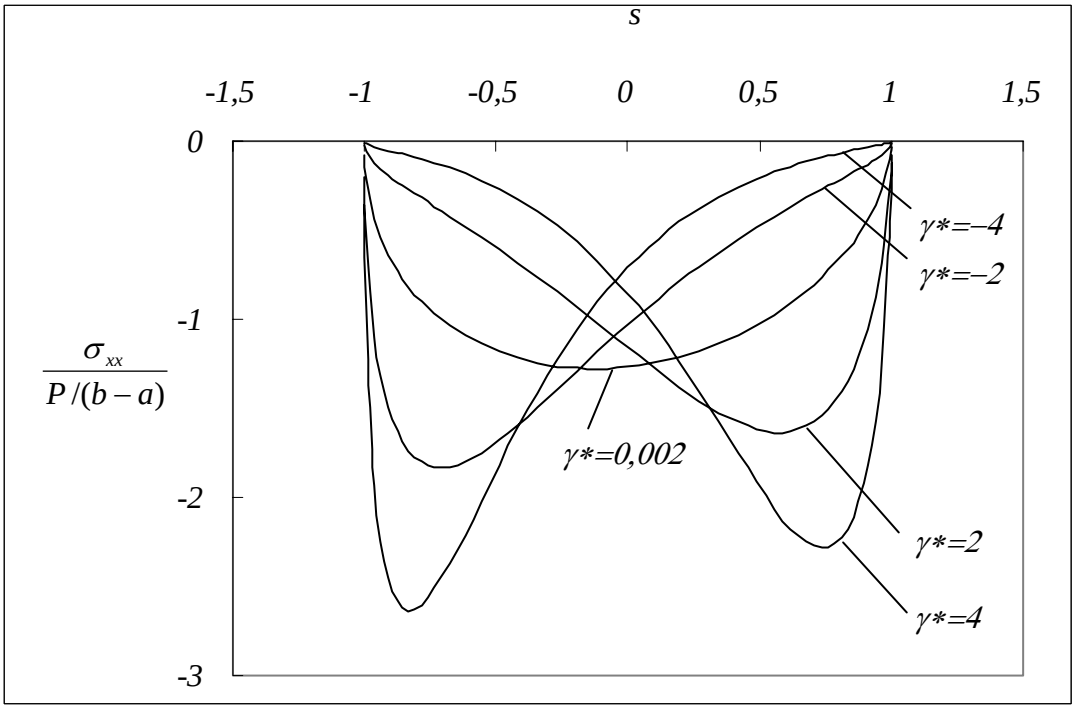

Figure 88: Normalized stress distribution for various values of the nonhomogeneity constant γ^*.(η= 0,6 and γ^{**} =0, a/R = -0,05 , b/R = 0,05)

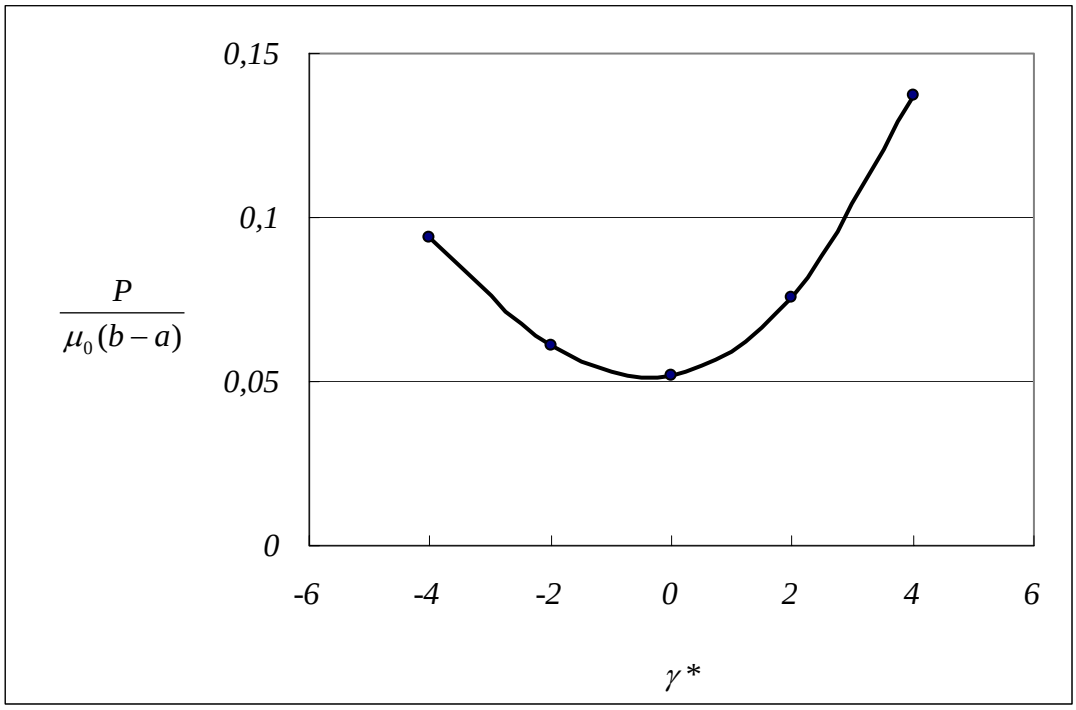

Figure 89: Variation of the normalized force with respect to normalized nonhomogeneity parameter γ^*. (η= 0,6 and γ^{**} =0, a/R = -0,05 , b/R = 0,05)

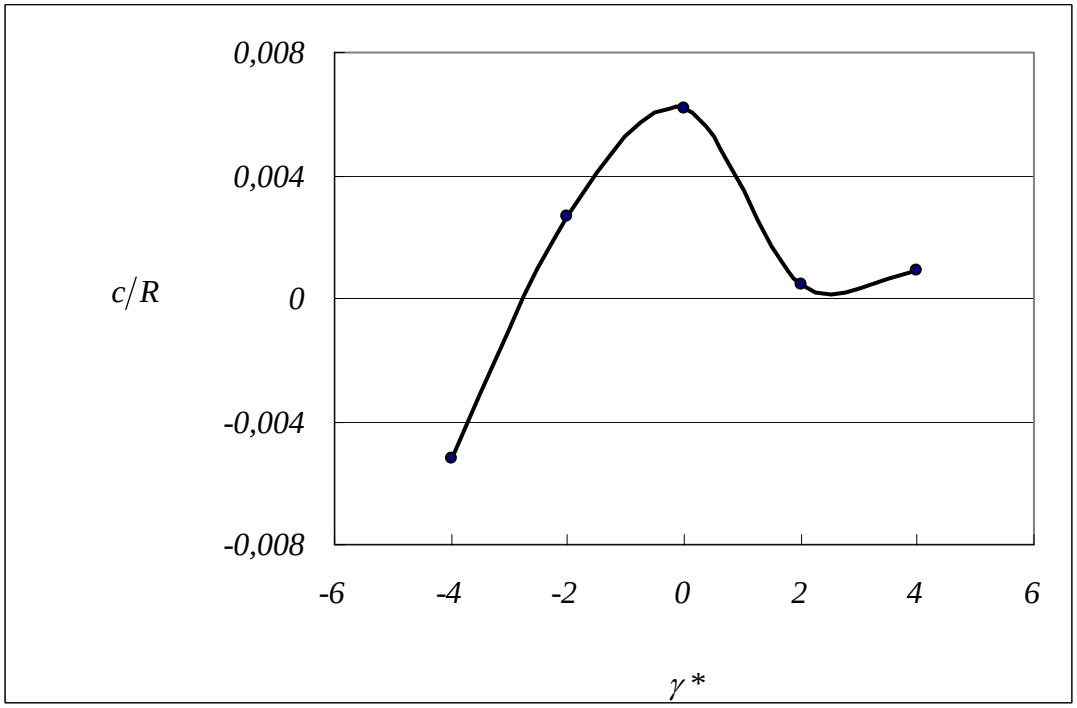

Figure 90: Variation of the location of the centerline with respect to normalized nonhomogeneity parameter γ^*. (η= 0,6 and γ^{**} =0, a/R = -0,05 , b/R = 0,05)

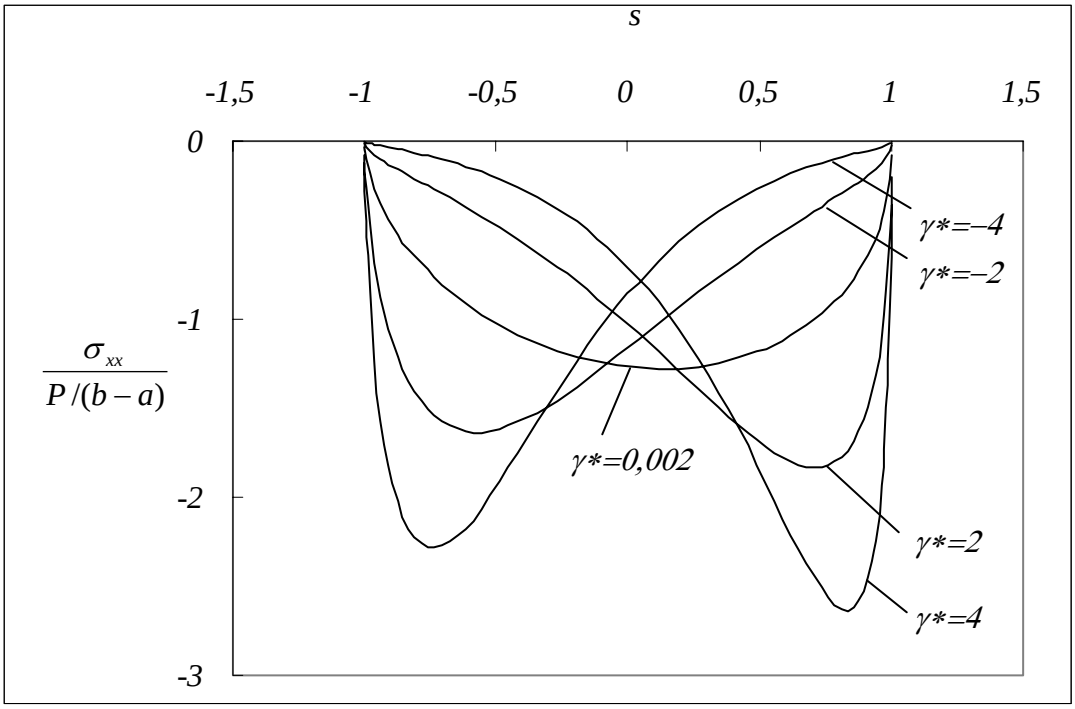

Figure 91: Normalized stress distribution for various values of the nonhomogeneity constant γ^*.(η= - 0,6 and γ^{**} =0, *a/R* = -0,05 , *b/R* = 0,05)

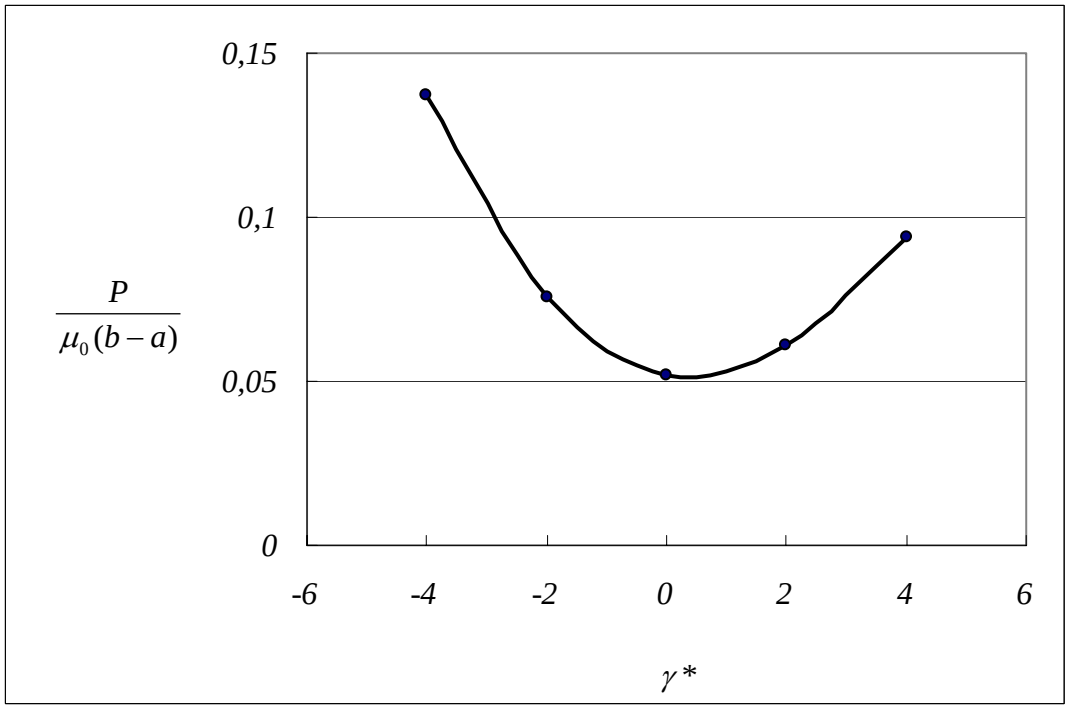

Figure 92: Variation of the normalized force with respect to normalized nonhomogeneity parameter γ^*. (η= - 0,6 and γ^{**} =0, *a/R* = -0,05 , *b/R* = 0,05)

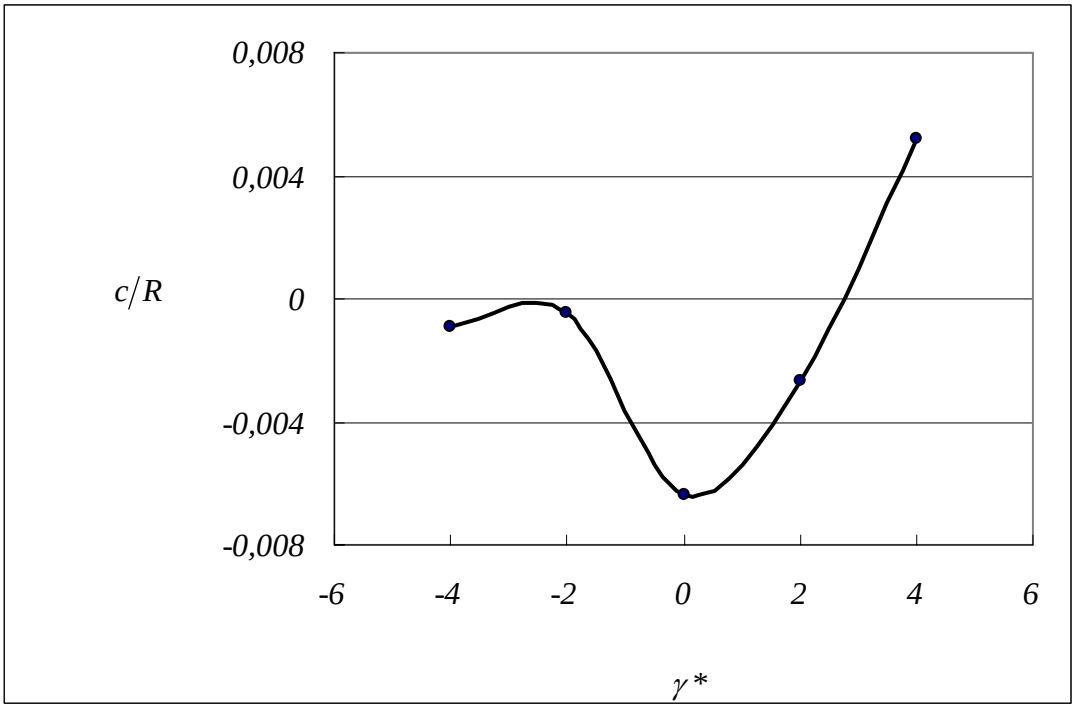

Figure 93: Variation of the location of the centerline with respect to normalized nonhomogeneity parameter γ^*. (η= - 0,6 and γ^{**} =0, a/R = -0,05 , b/R = 0,05)

CHAPTER V

CONCLUSIONS AND FUTURE WORK

5.1. Concluding Remarks

Detailed parametric analyses of the contact mechanics problems considered in this study are given in Chapter 4. In section 4.1, in order to check the accuracy of the results obtained using the developed computer program, some comparisons are given. In this set of results, the nonhomogeneity constant is taken as sufficiently small $\left(\gamma^{*}=0.002\right)$ and the stamp is assumed to be centrally located $\left(\gamma^{**}=0\right)$. Actually, for the homogeneous medium the location of the sliding stamp is irrelevant. The results for $\gamma^{*}=0.002$ are compared to those obtained using the closed form expressions for the homogeneous half–plane which are given in Sections 3.2, 3.4 and 3.6. Figure 7 shows the contact stress distribution at the surface for the flat stamp for various values of the coefficient of friction.

The results generated by our computer program are very close to the results obtained using the closed form solution. Figure 8 shows contact stress distribution for a triangular stamp, and a good agreement is observed between our results and the closed form solution for the triangular stanp problem. Table 1 gives the required contact forces for the data given in Figure 8. Again, the results are very close. The small difference in the results can be attributed to the fact that the nonhomogeneity constant is not exactly zero for the results generated using the computer program. A smaller nonhomogeneity constant is expected yield a better accuracy. The reader can find the comparisons for the circular stamp in Figure 9 and in Tables 2 and 3.

Again, it is seen that there is a close agreement between the results obtained using the two different methods.

The accuracy of the results for a nonzero nonhomogeneity constant is tested by comparing the results to those obtained using a finite element model of the contact mechanics problem. The finite element model is developed by Yıldırım [30] using the commercial finite element software ANSYS. Figures 10 and 11 show the close agreement for the results obtained for the flat stamp problem for both positive and negative nonhomogeneity constants. The agreement of the results for the triangular stamp problem are shown in Figures 12 and 13. The way of generation of the results using the finite element model is different from the analytical approach. In the triangular stamp problem for example, in the finite element solution the applied force has to be specified first. The extent of the contact region $(b-a)$ is determined after post-processing. In the analytical solution however there is no need to specify the contact force as an input to the problem. We also note that some convergence problems are observed in the finite element solution for the triangular stamp problem especially for large values of the angle θ. Figures 14 and 15 show the comparisons for the circular stamp problem. In the finite element solution of the circular stamp problem, the contact force and the location of the centerline are specified first and the extent of the contact region, $(b-a)/R$ is determined after post–processing. In the analytical approach however, the centerline location and the required contact force are the outputs of the numerical solution for a given contact length. The best agreement seemed to occur in the circular stamp problem. In the flat and triangular stamp problems, there are stress singularities at the sharp corners. In the analytical approach, the strengths of the singularity are determined and embedded in the solution. Finite element model also captures the singular behavior at the ends, but the strengths of the singularity are not embedded. This may be a reason for the comparatively larger deviation of the results for the flat and triangular stamp problems. But, for all practical intents and purposes, the results are sufficiently close for all cases. Another drawback in the finite element model is that, it is not possible to give an exactly continuous variation to the elastic properties as in the analytical approach. The elastic properties can be specified for each element

and the smoothness of the variation of the elastic properties depends on the element size. Tables 4–6 give the values of the normalized force and centerline location for the triangular and circular stamp problems considered in section Section 4.2.

5.1.1. Comments on the Results Obtained for the Flat Stamp

In section 4.3 parametric studies are given for the flat stamp problem. The results given in this section can be grouped according to the location of the stamp. In Figures 16–22, the stress distributions are given for $\gamma b = 0$. For a nonzero nonhomogeneity constant, this implies that the right corner of the flat stamp is at the origin. In Figures 23–29, the results are given for $\gamma a = 0$ which implies that, for a nonzero value of the nonhomogeneity constant left corner of the stamp is at the origin. In Figures 30–36, the results are given for $\gamma^{**} = 0$. In this case the flat stamp is centrally located. In each group, each figure corresponds to a different value of the friction coefficient. Positive, negative and zero friction coefficients are considered. A negative friction coefficient indicates a reversal of direction of the applied tangential force. In our sign convention, a positive friction coefficient implies a tangential force acting in the direction of the positive y – axis as shown in Figure 3. If the friction coefficient is taken as negative the applied tangential force acts in the negative y – direction. A zero friction coefficient is for the frictionless contact. Figure 16 shows the normalized stress distribution versus the normalized position parameter s for the flat stamp for $\gamma a = \eta = 0$. The results are given for three different nonhomogeneity constants. It is seen that for $\gamma a = -0.002$ the stress distribution is almost symmetric which is an expected result. The distortion in the stress distribution for nonzero values of the nonhomogeneity constant can be seen in the other curves. The minimum pressure seemed to be lower in the laterally nonhomogeneous medium. There is also symmetry with respect to the nonhomogeneity constant. Note that the curves $a^* = -2$ and $a^* = 2$ are aymmetric about $s = 0$. The effect of friction for $\gamma b = 0$ can be seen in the other figures, i.e. in Figures 17–22. In Figures 17 and 18, we see that reversing the direction of the applied force does not significantly effect the stress distribution for $\eta = 0.2$. For

higher values of the friction coefficient the effect is more pronounced (see for example, Figures 21 and 22 which are given for $\eta = 0.6$ and $\eta = -0.6$, respectively). But in all the cases, the shear modulus gradient is the prevailing factor effecting the contact stress distribution. The stress distributions for a flat stamp whose left corner is at the origin $(\gamma a = 0)$ is given in Figures 23–29. For a centrally located stamp $(\gamma^{**} = 0)$, we can see the results in Figures 30–36. Similar trends can also be observed in these figures.

In summary, in the flat stamp problem we observe that the contact stress distribution is distorted to take the shape of the shear modulus variation. For example in Figure 30, for a shear modulus increasing in y – direction the contact stress distribution is in the shape of the exponential function with a positive exponent (see the curve for $\gamma^* = 2$). If the shear modulus is decreasing in y – direction the contact stress distribution takes the shape of an exponential function with a negative exponent (see the curve for $\gamma^* = -2$). This trend is observed in all the cases.

5.1.2. Comments on the Results Obtained for the Triangular Stamp

The results for the triangular stamp problem are given in Figures 37–78. These results can also be divided into three main groups. Figures 37–50 give the results for a triangular stamp whose smooth end is at the origin after contact, i.e. $\gamma b = 0$. The results for a triangular stamp whose sharp corner is at the origin $(\gamma a = 0)$ are given in Figures 51–64. Figures 65–78 give the results for a triangular stamp whose end points are symmetric after contact $(\gamma^{**} = 0)$.

On each page the normalized contact stress distribution versus normalized position parameter s and the corresponding contact force versus the relevant nonhomogeneity parameter plots are given. Figures 37 and 38 show the contact stress and normalized force distribution for $\gamma b = \eta = 0$. In this case we see that at $y = a$ $(s = -1)$ there is an elastic stress singularity and at $y = b$ $(s = 1)$ the contact stress is zero due to smooth contact. Hence, there is no symmetry in the stress

distribution even for $\eta = \gamma a = 0$. The effect of the nonhomogeneity constant on the contact stress distribution is very significant and can be seen in Figure 37. The required contact force for the curves given in Figure 37 are not same. In Figure 38, we observe that required contact forces increases considerably as $a^* = \gamma a$ increases. Since, a is negative in this case, a positive value for a^* implies a negative γ, hence a decreasing shear modulus in the direction of the positive y – axis. The competing effects of the value of the friction coefficient, direction of the applied frictional force and the nonhomogeneity constant for $\gamma b = 0$ can be observed in Figures 39–50. In all cases contact stress distributions are similar. Again, nonhomogeneity constant is the most important factor effecting the distribution of the contact stresses. In all the cases, the required contact force increases as a^* increases.

The normalized contact stress and normalized contact force distributions for a triangular stamp whose sharp corner is at origin $(\gamma a = 0)$ are given in Figures 51–64. Similar results are obtained in this case, but interestingly this time normalized contact force is increasing for increasing shear modulus (see for example, Figures 52, 54, 56, 58, 60, 62). So, effect of the location of the stamp on the contact stress distribution is significant for the triangular stamp case. Similar results are given for a centrally located triangular stamp in Figures 65–78. The behavior of the variation of the normalized contact force is different from the two cases described above. As can be seen in Figures 66, 68, 70, 72, 74, 76 and 78 the normalized force generally makes a minimum near $\gamma^* = 0$ and it increases in both positive and negative γ^* directions (a positive γ^* implies a positive value for γ and vice versa).

The main conclusion of this section is that the contact stress distribution again mimics the shear modulus variation, such that the it adapts to the variation of the shear modulus. This can be clearly seen in the Figures.

5.1.3. Comments on the Results Obtained for the Circular Stamp

The results related to the circular stamp problem are given in Figures 79–93. The computation time required for the solution of the circular stamp problem is much more than the time required for the flat stamp or triangular stamp problems. So, in this case parametric studies are carried out for a centrally located circular stamp. In all cases, It is assumed that after indentation $a/R = -0.05$ and $b/R = 0.05$. For each case, the location of the centerline and the required normalized contact force are computed. Figure 79 shows the contact stress distribution for frictionless contact. The symmetry is distorted for the laterally nonhomogenous medium as expected. But, the behavior is symmetric with respect to the nonhomogeneity parameter γ^*, which is expected for frictionless contact. Here, we observe that even though that maximum pressure in the contact is larger for the nonhomogeneous medium, the absolute value of the pressure is significantly smaller in some parts of the contact when compared to the homogeneous case. Figure 80 shows the variation of the normalized contact force, which is symmetric about $\gamma^* = 0$ and increases in both positive and negative γ^* directions. There is a skew – symmetry for the location of the centerline c/R about $\gamma^* = 0$ as can be seen in Figure 81. For a medium with a shear modulus increasing in y – direction, centerline shifts to the right, while for a medium with a shear modulus decreasing in y – direction centerline shifts to the left. The other figures (i.e., Figures 82–93) are for nonzero friction coefficients and they depict the increasing effect of the coefficient of friction on the stress distribution, normalized force and centerline location. In these figures, we observe that perfect symmetry (or skew – symmetry in the case of c/R) with respect to γ^* is distorted. The effect of the direction of the tangential force also seems to be significant (see for example Figures 88 and 91).

Let us consider Figure 82, in order to examine the competing effects of the nonhomogenity constant and the friction coefficient on the stress distribution. In this case, we observe that for a nonhomogeneous medium the highest pressure in the contact is larger. But, for $\gamma^* = 2$ and $\gamma^* = 4$, we observe that the pressure near

the trailing end of the contact is significantly reduced. It is known that surface crack inititation due to sliding contact always begins at the trailing end [23, 31]. Hence, a reduction in the pressure around the trailing end can have a positive effect on the fatigue life of a surface. It is obvious that this reduction is a consequence of grading in lateral direction and this point can be further investigated.

5.2. Future Work

In this study, a semi – analytical technique is developed to study the contact mechanics of a laterally graded medium. The results of this study show that elastic gradation in lateral direction can have a significant influence on the contact stress distribution at the surface. So, it is shown that in order to have more realistic models on the contact mechanics of nonhomogeneous media lateral nonhomogeneity has to be taken into account. The model considered in this study can be further used to study the subsurface stresses in the semi – infinite medium. This requires that asymptotic analyses be made for all stress components. When the subsurface stresses are calculated the integrals have to be handled very carefully in order not to lose accuracy due to singular terms. In this study it is seen that, a lateral nonhomogeneity can significantly reduce the pressure near the trailing end of a sliding contact. This point can be further investigated to clarify the effect of the lateral nonhomogeneity. In order to study this effect, coupled crack and contact problem in a laterally nonhomogeneous medium can be formulated and the behavior of a surface crack can be examined.

There are a number of other research areas related to the contact mechanics of nonhomogeneous media. In order to study the effects of nonhomogeneities in both depth and lateral directions, a mathematical model containing variations in elastic properties in both directions can be developed. An analysis of this sort will reveal the behavior of a surface which is graded in two directions. Another important subject that can be further studied is the contact mechanics of coated nonhomogenous surfaces. The coating thickness may have an important effect on the contact stress distribution. This subject is studied by Güler [22]. But, the

approach in this study can be extended to include the effect of intentional or natural lateral nonhomogeneities for coated surfaces.

In the contact mechanics problem considered in this study, Columb's friction model is assumed to hold. But, this is only valid when the applied tangential force is sufficiently large. When the applied tangential force is small, only some portion of the contact slips while there is stick in the other portion. This is the so – called partial slip contact problem in solid mechanics and it has not been studied for a nonhomogeneous medium. The analysis of partial slip contact in materials having nonhomogeneities in depth and/or lateral directions will be an important contribution to the literature. Crack propagation due to repeated microslip commonly occurs in practical applications. The analysis of this problem requires the solution of the partial slip contact mechanics problem. Analysis of crack growth under repeated microslip in FGMs can be another area of future study. In all the fields of study mentioned above, both analytical and computational (using FEM or BEM) studies are required in order to have a better understanding of the contact mechanics of nonhomogeneous media.

REFERENCES

[1] Selvadurai, A.P.S. and Lan, Q., 1998, "Axisymmetric Mixed Boundary Value Problems for an Elastic Halfspace with a Periodic Nonhomogeneity," *International Journal of Solids and Structures*, Vol. 35, pp. 1813 – 1826.

[2] Hertz, H., 1882, "On the Contact of Elastic Solids," *J. Reine und Angewandte Mathematik*, Vol. 92, pp. 156 – 171. (in German).

[3] Barber, J.R. and Ciavarella, M., 2000, "Contact Mechanics," *International Journal of Solids and Structures*, Vol. 27, pp. 29 – 43.

[4] Erdoğan, F., 1994, "Fracture Problems in Functionally Graded Materials," *Turkish Journal of Engineering and Environmental Sciences*, Vol. 18, pp. 185 – 210.

[5] Selvadurai, A.P.S., 1996, "The Settlement of a Rigid Circular Foundation Resting on a Half – Space Exhibiting a Near Surface Elastic Non-Homogeneity," *International Journal for Numerical and Analytical Methods in Geomechanics*, Vol. 20, pp. 351 – 364.

[6] Gibson, R.E., 1967, "Some Results Concerning Displacements and Stresses in a Nonhomogeneous Elastic Half – Plane," *Geotechnique*, Vol. 17, pp. 58 – 67.

[7] Calladine, C.R. and Greenwood, J.A., 1978, "Line and Point Loads on a Nonhomogeneous Incompressible Elastic Half – Space," *Quarterly Journal of Mechanics and Applied Mathematics*, Vol. 31, pp. 507 – 529.

[8] Awojobi, A.O. and Gibson, R.E., 1973, "Plane Strain and Axially Symmetric Problems of a Linearly Homogeneous Elastic Half – Space," *Quarterly Journal of Mechanics and Applied Mathematics*, Vol. 26, pp. 285 – 302.

[9] Gibson, R.E. and Sills, G.C., 1975, "Settlement of a Strip on a Non-Homogeneous Orthotropic Incompressible Elastic Half – Space," *Quarterly Journal of Mechanics and Applied Mathematics*, Vol. 28, pp. 233 – 243.

[10] Brown, P.T. and Gibson, R.E., 1972, "Surface Settlement of a Deep Elastic Stratum whose Modulus Increases Linearly with Depth," *Canadian Geotechnical Journal*, Vol.9, pp. 467 – 476.

[11] Kassir, M.K "Boussinesq Problems for Nonhomogeneous Solids," *ASCE Journal of Engineering Mechanics*, Vol. 98, pp. 457 – 471.

[12] Bakırtaş, I., 1980, "The Problem of a Rigid Punch on a Non – Homogeneous Elastic Half – Space," *International Journal of Engineering Science*, Vol. 18, pp. 597 – 610.

[13] Fabrikant, V.I. and Sankar, T.S., 1984, "On Contact Problems in an Inhomogeneous Half – Space," *International Journal of Solids and Structures*, Vol. 20, pp. 159 – 166.

[14] Selvadurai, A.P.S., Singh, B.M. and Vrbik, J., 1986, "A Reissner – Sagoci Problem for a Nonhomogeneous Solid," *Journal of Elasticity*, Vol. 16, pp. 383 – 391.

[15] Suresh, S. and Mortensen, A., 1998, *Fundamentals of Functionally Graded Materials: Processing and Thermomechanical Behavior of Graded Metals and Metal – Ceramic Composites*, IOM Communications, London, UK.

[16] Miyamoto, M., Kaysser, W.A., Rabin, B.H., Kawasaki, A. and Ford, R. G., eds., 1999, *Functionally Graded Materials: Design, Processing and Applications*, Kluwer Academic Publishers, MA, USA.

[17] Suresh, S., Olsson, M., Giannakopoulos, A.E., Padture, N.P. and Jitcharoen, J., 1999, "Engineering the Resistance to Sliding Contact Damage Through Controlled Gradients in Elastic Properties at Contact Surfaces," *Acta Materialia*, Vol. 47, pp. 3915 – 3926.

[18] Giannakopoulos, A.E. and Suresh, S., 1997, "Indentation of Solids with Gradients in Elastic Properties: Part I. Point force," *International Journal of Solids and Structures*, Vol. 34, pp. 2357 – 2392.

[19] Giannakopoulos, A.E. and Suresh, S., 1997, "Indentation of Solids with Gradients in Elastic Properties: Part II. Axisymmetric Indetors," *International Journal of Solids and Structures*, Vol. 34, pp. 2393 – 2428.

[20] Giannakopoulos, A.E., 2000, "Indentation of Graded Substrates," *Thin Solid Films*, Vol. 332, pp. 172 – 179.

[21] Giannakopoulos, A.E. and Pallot, P., 2000, "Two – Dimensional Contact Analysis of Elastic Graded Materials," *Journal of the Mechanics and Physics of Solids*, Vol. 48, pp. 1597 – 1631.

[22] Güler, M.A., 2000, *Contact Mechanics of FGM Coatings*, Ph.D. Dissertation, Lehigh University, Bethlehem, Pennsylvania, USA.

[23] Dağ, S., 2001, *Crack and Contact Problems in Graded Materials*, Ph.D. Dissertation, Lehigh University, Bethlehem, Pennsylvania, USA.

[24] Dağ, S. and Erdoğan, F., 2002, "A Surface Crack in a Graded Medium Loaded by a Sliding Rigid Stamp," *Engineering Fracture Mechanics*, Vol. 69, pp. 1729 – 1751.

[25] Erdoğan, F. and Dağ, S., 2001, *Cracking of a Graded Half – Plane due to Sliding Contact*, Project Report, US Air Force Office of Scientific Research, Grant F49620-98-1-0028.

[26] Yanovskaya, T.B., 2002, "Asymptotic ray theory for seismic surface waves in laterally inhomogeneous media," *Studia Geophysica Et Geodaetica*, Vol. 46, pp. 267 – 282.

[27] Kamiyama, M. and Satoh, T., 2002, "Seismic response analysis of laterally inhomogeneous ground with emphasis on strains," *Soil Dynamics and Earthquake Engineering*, Vol. 22, 877 – 884.

[28] Singh, B.M., Rokne, J.G. and Dhaliwal, R.S., 1981, "A contact problem for a nonhomogeneous half – space," *International Journal of Engineering Science*, Vol. 19, pp. 427 – 433.

[29] Erdoğan, F., 1978, "Mixed Boundary Value Problems in Mechanics," *Mechanics Today*, Vol. 4, Nemat – Nasser, S., ed., Pergamon Press, New York, USA, pp. 1 – 84.

[30] Yıldırım, B., 2003, Department of Mechanical Engineering, Osmangazi University, Eskişehir, Turkey, Private Communication.

[31] Hills, D.A. and Nowell, D., 1994, *Mechanics of Fretting Fatigue*, Kluwer Academic Publishers, Dordrecht, The Netherlands.

APPENDIX A

SOME USEFUL INTEGRALS

In this section, the expressions that are used to evaluate the integrals involving the asymptotic expansions of the integrands of the kernels are given. The integrals that we want to evaluate are in the following form:

$$C_n = \int_A^\infty \frac{1}{\rho^n} \cos(\rho u)\, d\rho \tag{A1}$$

$$S_n = \int_A^\infty \frac{1}{\rho^n} \sin(\rho u)\, d\rho \tag{A2}$$

For $n = 1$, following results are obtained using MAPLE,

$$C_1 = -\mathrm{Ci}(A|u|), \tag{A3}$$

$$S_1 = \mathrm{sign}(u)\left\{\frac{\pi}{2} - \mathrm{Si}(A|u|)\right\}, \tag{A4}$$

where $\mathrm{Ci}(\ )$ and $\mathrm{Si}(\ )$ are cosine and sine integrals, respectively and they are defined as:

$$\mathrm{Ci}(x) = \gamma_0 + \ln(x) + \int_0^x \frac{\cos(\alpha) - 1}{\alpha}\, d\alpha \tag{A5}$$

$$\mathrm{Si}(x)=\int_0^x \frac{\sin(\alpha)}{\alpha}d\alpha \tag{A6}$$

γ_0 is the Euler constant and it is equal to 0.5772156649. For $n>1$, integrating (A1) and (A2) by parts the following general recursive relations can be obtained [23],

$$C_n=-\frac{1}{1-n}\frac{\cos(uA)}{A^{n-1}}+\frac{u}{1-n}S_{n-1},\qquad n>1, \tag{A7}$$

$$S_n=-\frac{1}{1-n}\frac{\sin(uA)}{A^{n-1}}-\frac{u}{1-n}C_{n-1},\qquad n>1. \tag{A8}$$